Supporting Information

Rhodium Catalyst Immobilization in Trialkylamine-functionalized Ionic Liquids as a New Efficient Way to Promote Biphasic Reductive Hydroformylation of Methyl 10-undecenoate

Authors: Camille Galand,[a] Jérémy Ternel,[a] Nicolas Kania,[a] Frédéric Capet,[b] Hervé Bricout,[a] Sébastien Tilloy,[a] Eric Monflier,[a] and Michel Ferreira*[a]

[a] *Univ. Artois, CNRS, Centrale Lille, Univ. Lille, UMR 8181, Unité de Catalyse et Chimie du Solide (UCCS), 62300 Lens, France.*

[b] *Univ. Lille, CNRS, Centrale Lille, Univ. Artois, UMR 8181, UCCS, Unité de Catalyse et Chimie du Solide, Lille, France.*

* Correspondence: michel.ferreira@univ-artois.fr

Number of pages: 56

Number of figures: 84

Number of tables: 10

Table of contents

I) General purpose

All chemicals were purchased from Fisher Scientific or Merck and were used without prior purification. Pinane solvent was provided by SARL SICO-CHEM and POC SARL (France). Hydroformylation experiments were carried out in a 25 mL autoclave (Parr instrument company) equipped with a mechanical stirrer. All reactions involving metal-ionic liquids catalysts were performed under air atmosphere and each run was performed at least twice to ensure reproducibility.

The NMR spectra were recorded at 298K on a Bruker Avance Neo 400 spectrometer operating at 9.4 T field strength (400 MHz for ^{1}H nuclei and 100 MHz for ^{13}C nuclei) equipped with a 5 mm BBFO SmartProbe ($^{1}H/^{19}F/^{31}P$ - ^{109}Ag) and an automatic sample loading system. Chemical shifts are reported in ppm (δ) and were referenced to appropriate internal standards or residual solvent peaks.

The determination of ionic liquids leaching in organic phases was performed using a Shimadzu Nexera XR HPLC system equipped with LC20AD pumps, a SIL-20AC autosampler, and a CTO-20A column oven set at 40 °C. Separation was achieved on a Kinetex C18 100 Å, 5 µm column under isocratic conditions using 100 % acetonitrile at a flow rate of 0.8 mL/min. Detection was carried out with a Photodiode Array Detector (SPD-M20A), and absorbance values were measured at 190 nm. The method duration was 10 minutes, with the ionic liquid eluting at approximately 2 min 30 s. A calibration curve for each ionic liquid analyzed is prepared in acetonitrile. The ionic liquid with unknown leaching is collected at the end of the reaction and subsequently injected for analysis.

Rhodium concentrations were determined through inductively coupled plasma optical emission spectroscopy experiments using a Thermo Scientific iCAP 7000 Plus Series ICP-OES. Samples composed of an aliquot of the organic phase were digested before ICP experiments in nitric acid via microwave mineralization using a MARS 6 microwave digestion system.

Differential Scanning Calorimetry (DSC) was performed to investigate the phase transitions of ionic liquids using a Mettler DSC 5+ instrument under a nitrogen flow of 50 mL/min. The thermal program consisted of 2 cycles, each including a heating from -20 °C to 150 °C followed by a cooling from 150 °C to -20 °C, all at a rate of 5 °C/min. The first cycle was used to erase the sample's previous thermal history and establish a consistent thermal baseline, enabling reliable comparison of measurements between different samples.

Thermogravimetric Analysis (TGA) was performed to assess the thermal stability and decomposition behavior of the ionic liquids using a Mettler TGA 3+ instrument under a nitrogen flow of 50 mL/min. The thermal program consisted of a single heating ramp from ambient temperature to 250 °C at a rate of 5 °C/min.

Transmission Electron Microscopy (TEM) was performed on a Tecnai microscope (200 kV). Samples were cryo-prepared using an ultramicrotome. Sample of ionic liquids with rhodium were first frozen in liquid nitrogen and subsequently sectioned at –120 °C with a 35° diamond knife, yielding ultrathin sections of approximately 50 nm thickness and then deposited onto the carbon coated copper grid.

Crystals of the ionic liquids were obtained by slow evaporation of dichloromethane, with subsequent induction of nucleation using an external seed. Single-crystal X-ray diffraction measurements were carried out at 120 K for [PEDMim][PF_6] and [PEMim][PF_6], and at 100 K for [PEEtOHim][PF_6]. Data collection was performed using a Bruker DUO diffractometer equipped with a Photon III C14 detector for the first two compounds, and a Bruker D8 Venture

diffractometer with a Photon IV C16 detector for the third. MoKα radiation (λ = 0.71073 Å) was employed for all measurements. The structures were solved using SHELXT and refined by least-squares on F² with SHELXL. Hydrogen atoms were positioned geometrically and refined using a riding model on their parent atoms, except for the one bonded to O1 in [PEEtOHim][PF_6], which were located from a difference Fourier map.

CCDC 2506183-2506185 contain the supplementary crystallographic data for this paper. These data can be obtained free of charge from The Cambridge Crystallographic Data Centre via www.ccdc.cam.ac.uk/structures.

II) Catalytic tests and recycling

In a typical catalytic experiment, Rh(acac)$(CO)_2$ (6.0 mg, 23 µmol, 1 equiv.), ligand (75 equiv.), methyl 10-undecenoate (1.15 g, 1.325 mL, 5.9 mmol, 250 equiv.), and heptane (10 mL) were added in a 25 mL stainless-steel autoclave (Parr instrument company) equipped with a mechanical stirrer. The reactor was sealed, the reaction mixture was stirred and the reactor was heated at the desired temperature. Then, the reactor was pressurized with CO and H_2 at the desired pressure. After the appropriate reaction time (usually 6h), the reactor was cooled to room temperature and depressurized. The lighter layer was isolated by decantation. After removing heptane by evaporation, the obtained mixture was then analyzed by ^{1}H NMR spectroscopy who gives access, after integration of the characteristic signals for each type of compound, to the exact overall composition of the medium in terms of residual methyl 10-undecenoate and reaction products[1]. So, conversion, yields, and l/b ratios were determined easily. The heavier ionic liquid layer which contains the catalytic system can then be used for further run after addition of a fresh new mixture of methyl 10-undecenoate and heptane.

Recycling experiments were carried out as follows: a sample was taken after 6 h of reaction, and the autoclave was opened after 24 h under CO/H_2. The upper organic phase (heptane) containing the reaction products was collected, followed by the addition of a fresh heptane phase containing methyl undecenoate, and the system was repressurized.

III) NMR characterization of ligands derivates

1) 1-(2-piperid-1-yl-ethyl)-3-ethanolimidazolium chloride [PEEtOHim][Cl]

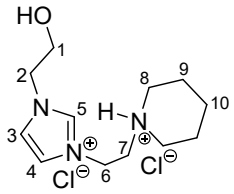

[1] El Mouat, A., Becquet, C., Ternel, J., Ferreira, M., Bricout, H., Monflier, E., Lahcini, M., and Tilloy, S. (2022). Promising Recyclable Ionic Liquid-Soluble Catalytic System for Reductive Hydroformylation. *ACS Sustainable Chemistry & Engineering*, *10*(34), 11310-11319.
[2] Sheldrick, G.M. (2015). Acta Cryst. A71, 3-8.
[3] Sheldrick, G.M. (2015). Acta Cryst. C71, 3-8.

^{1}H NMR (DMSO-d6, 400 MHz, 25 °C, δ(ppm)): 11.18 (s, 1H, NH), 9.36 (s, 1H, N-CH-N), 7.89 (t, 1H, *J = 1,7 Hz*, CH), 7.78 (t, 1H, *J = 1,7 Hz*, CH), 5.28 (s, 1H, OH), 4.73 (t, 2H, *J = 6,1 Hz*, CH_2), 4.22 (t, 2H, *J = 4,8 Hz*, CH_2-OH), 3.74 (t, 2H, *J = 4,8 Hz*, CH_2), 3.62 (q, 2H, *J = 5,8 et 5.2 Hz*, CH_2), 3.48 (d, 2H, *J = 11,2 Hz*, CH_2), 2.95 (q, 2H, *J = 11 et 9,4 Hz*, CH_2), 1.93-1.33 (m, 6H, cycle CH_2). **^{13}C NMR (DMSO-d6, 100 MHz, 25 °C, δ(ppm)):** 137.2 (C5), 123.1 (C4), 122.1 (C3), 59.2 (C2), 54.3 (C7), 52.2 (C1), 52.0 (C8), 42.8 (C6), 21.8 (C9), 21.2 (C10).

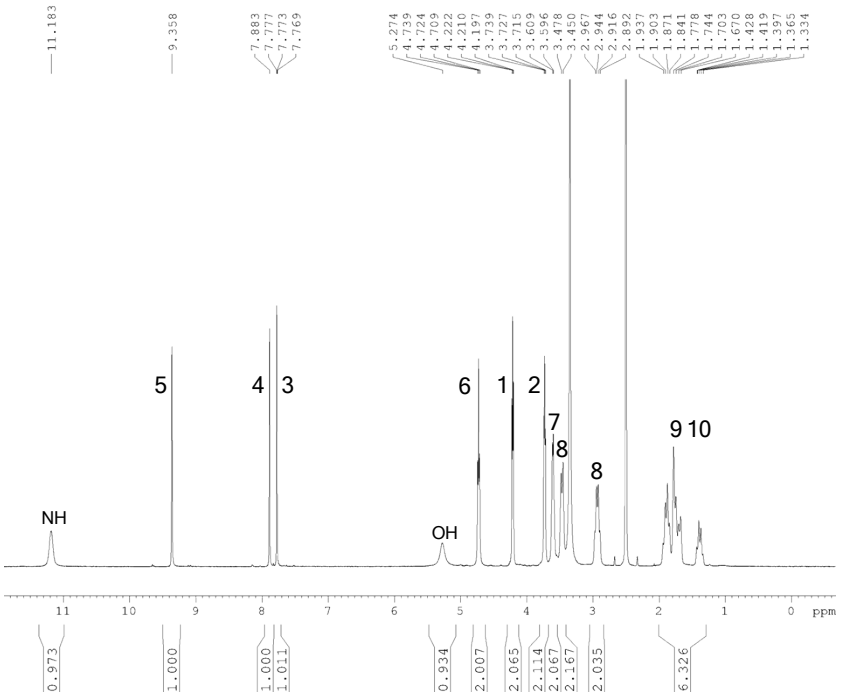

Figure S1. ^{1}H NMR spectrum of 1-(2-piperid-1-yl-ethyl)-3-ethanolimidazolium chloride **[PEEtOHim][Cl]** (400 MHz, DMSO-d6, 25 °C)

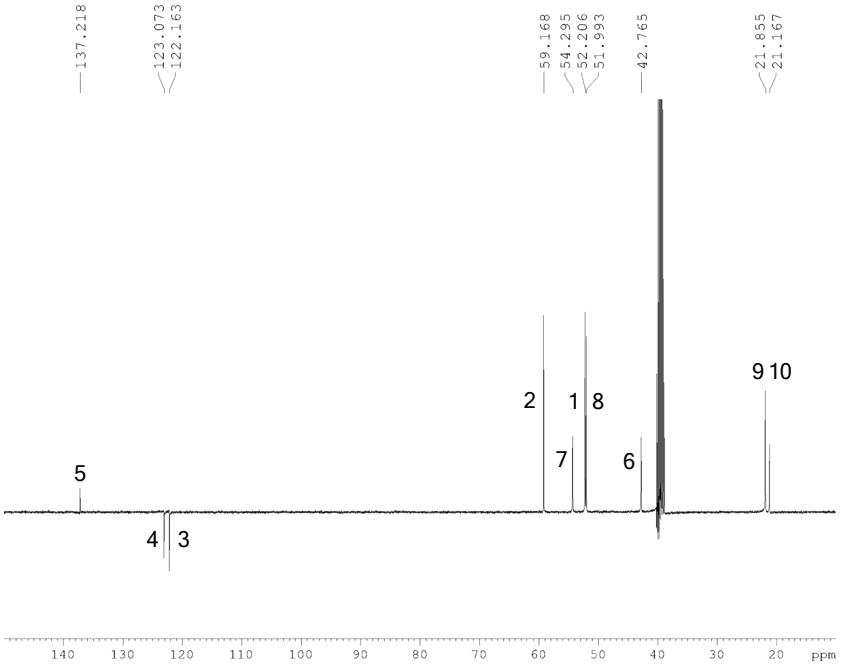

Figure S2. ^{13}C-JMOD NMR spectrum of 1-(2-piperid-1-yl-ethyl)-3-ethanolimidazolium chloride **[PEEtOHim][Cl]** (100 MHz, DMSO-d6, 25 °C)

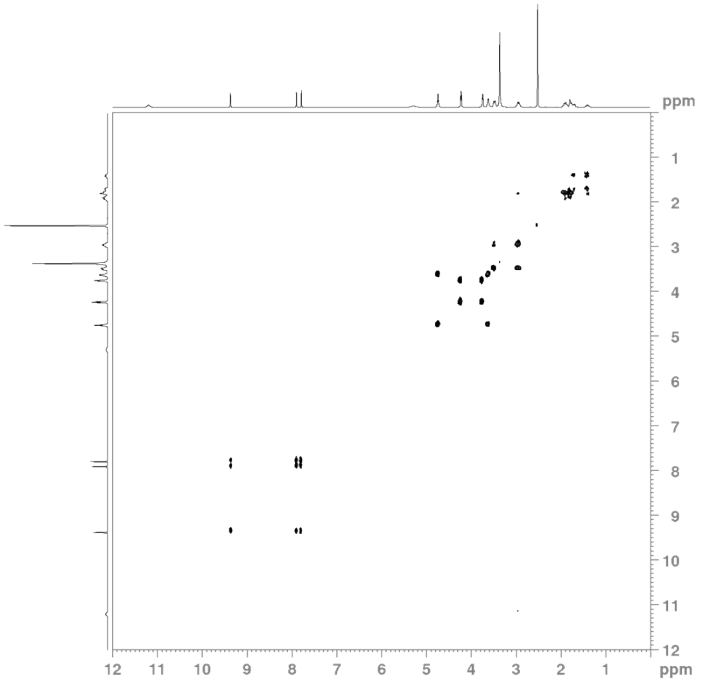

Figure S3. COSY NMR spectrum of 1-(2-piperid-1-yl-ethyl)-3-ethanolimidazolium chloride **[PEEtOHim][Cl]** (400 MHz, DMSO-d6, 25 °C)

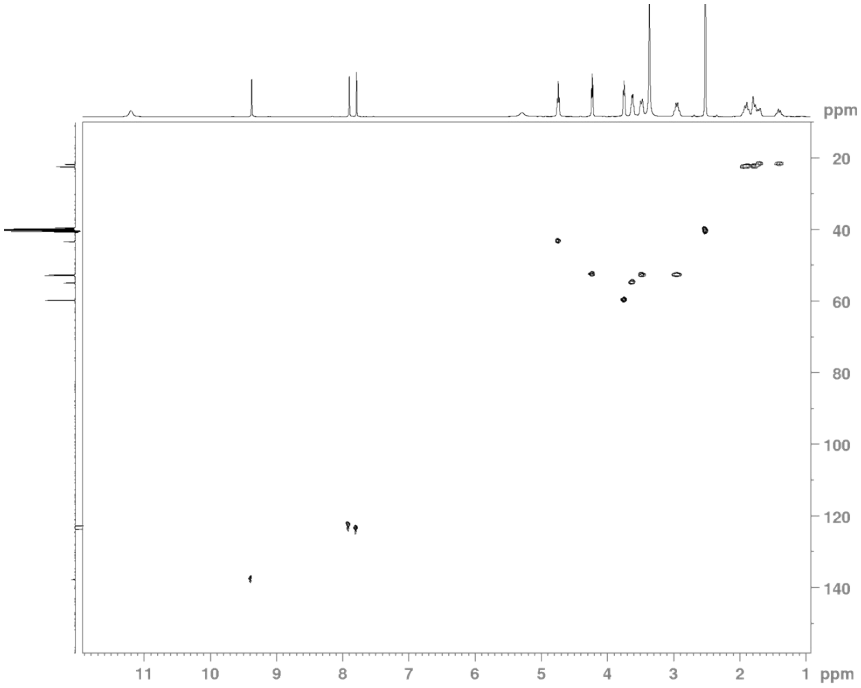

Figure S4. HSQC spectrum of 1-(2-piperid-1-yl-ethyl)-3-ethanolimidazolium chloride **[PEEtOHim][Cl]** (400 MHz, DMSO-d6, 25 °C)

2) 1-(2-piperid-1-yl-ethyl)-3-ethanolimidazolium hexafluorophosphate [PEEtOHim][PF_6]

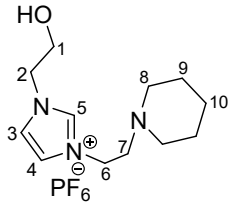

^{1}H NMR (DMSO-d6, 400 MHz, 25 °C, δ(ppm)): 9.06 (s, 1H, N-CH-N), 7.74 (t, 1H, *J = 1,7 Hz*, CH), 7.72 (t, 1H, *J = 1,7 Hz*, CH), 5.17 (s, 1H, OH), 4.28 (t, 2H, *J = 5,8 Hz*, CH_2), 4.24 (t, 2H, *J = 4,8 Hz*, CH_2-OH), 3.74 (q, 2H, *J = 5,2 et 5.0 Hz*, CH_2), 2.63 (t, 2H, *J = 6 Hz*, CH_2), 2.38 (m, 4H, CH_2), 1.50-1.37 (m, 6H, cycle CH_2). **^{13}C NMR (DMSO-d6, 100 MHz, 25 °C, δ(ppm)):** 136.9 (C5), 122.9 (C4), 122.8 (C3), 59.8 (C2), 57.7 (C7), 54.2 (C8), 52.1 (C1), 46.6 (C6), 25.9 (C9), 24.3 (C10).

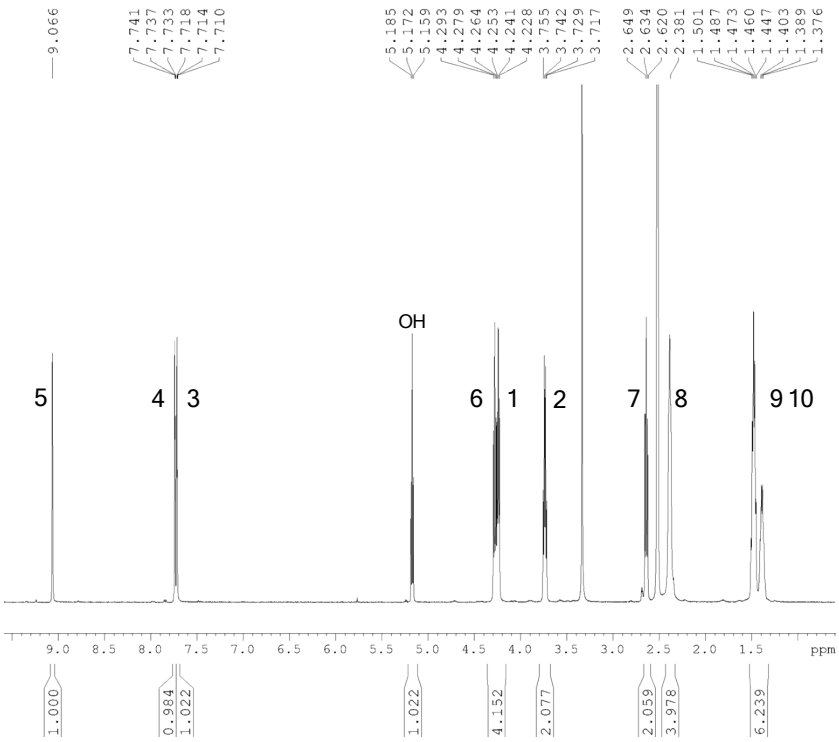

Figure S5. ^{1}H NMR spectrum of 1-(2-piperid-1-yl-ethyl)-3-ethanolimidazolium hexafluorophosphate **[PEEtOHim][PF_6]** (400 MHz, DMSO-d6, 25 °C)

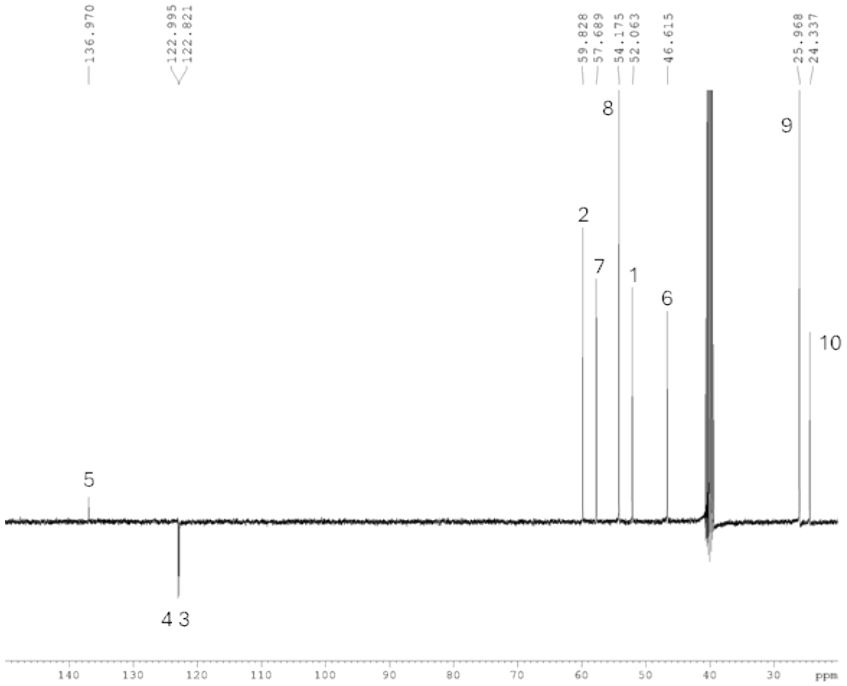

Figure S6. ^{13}C-JMOD NMR spectrum of 1-(2-piperid-1-yl-ethyl)-3-ethanolimidazolium hexafluorophosphate **[PEEtOHim][PF_6]** (100 MHz, DMSO-d6, 25 °C)

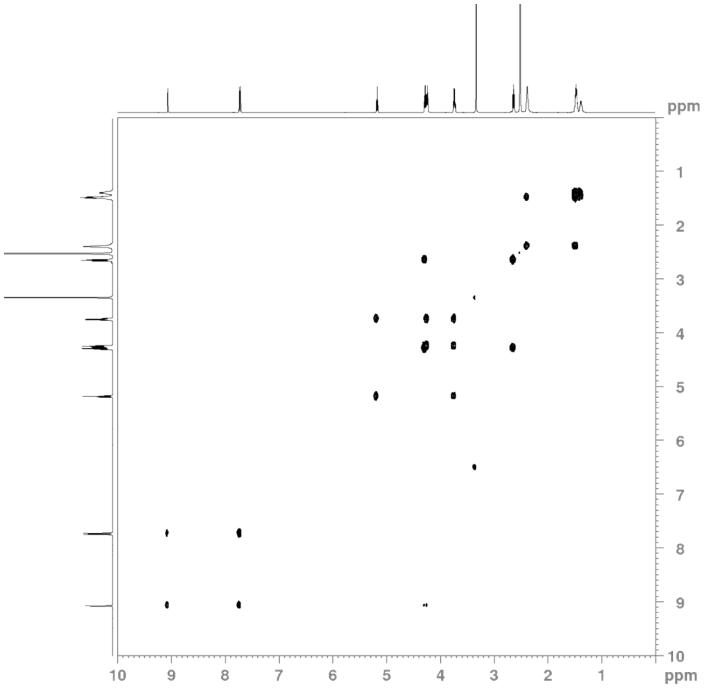

Figure S7. COSY spectrum of 1-(2-piperid-1-yl-ethyl)-3-ethanolimidazolium hexafluorophosphate **[PEEtOHim][PF_6]** (400 MHz, DMSO-d6, 25 °C)

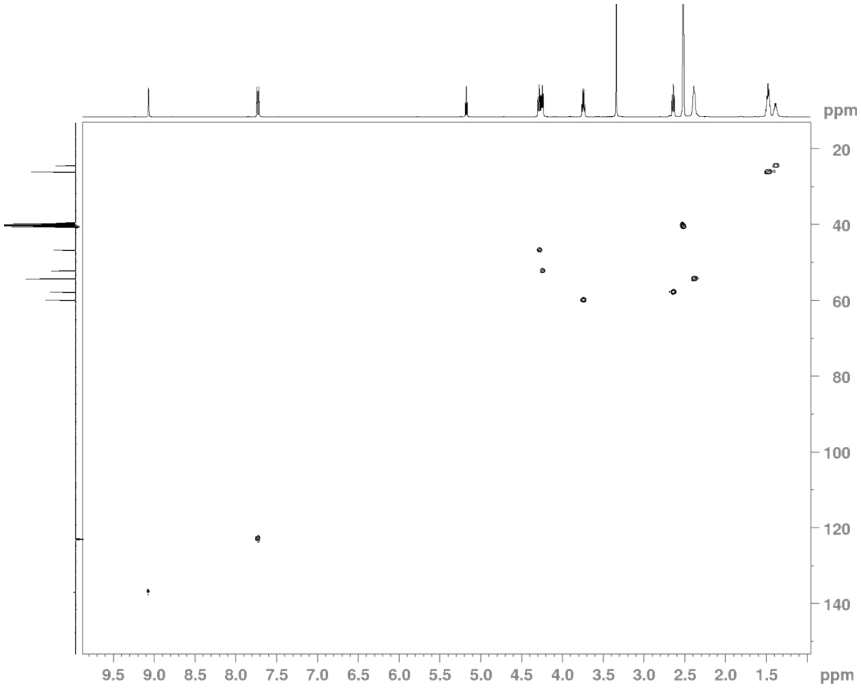

Figure S8. HSQC NMR spectrum of 1-(2-piperid-1-yl-ethyl)-3-ethanolimidazolium hexafluorophosphate **[PEEtOHim][PF_6]** (400 MHz, DMSO-d6, 25 °C)

3) 1-(2-piperid-1-yl-ethyl)-3-methylimidazolium chloride [PEMim][Cl]

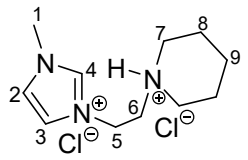

^{1}H NMR (DMSO-d6, 400 MHz, 25 °C, δ(ppm)): 11.43 (s, 1H, NH), 9.37 (s, 1H, N-CH-N), 7.89 (t, 1H, *J = 1,7 Hz*, CH), 7.74 (t, 1H, *J = 1,7 Hz*, CH), 4.74 (t, 2H, *J = 6,4 Hz*, CH_2), 3.85 (s, 3H, CH_3), 3.58 (q, 2H, *J = 5.9 et 5,4 Hz*, CH_2), 3.44 (d, 2H, *J = 11,6 Hz*, CH_2), 2.93 (q, 2H, *J = 11,6 et 9,3 Hz*, CH_2), 1.96-1.34 (m, 6H, CH_2 cycle). **^{13}C NMR (DMSO-d6, 100 MHz, 25 °C, δ(ppm)):** 138.1 (C4), 124.2 (C2), 122.7 (C3), 54.8 (C6), 52.7 (C7), 43.3 (C5), 36.3 (C1), 22.4 (C8), 21.7 (C9).

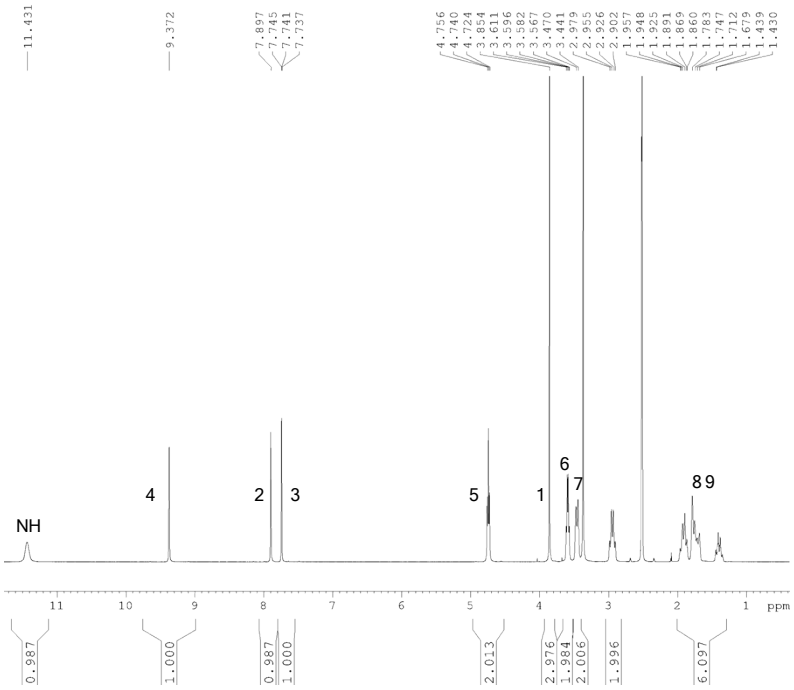

Figure S9. ^{1}H NMR spectrum of 1-(2-piperid-1-yl-ethyl)-3-methylimidazolium chloride **[PEMim][Cl]** (400 MHz, DMSO-d6, 25 °C)

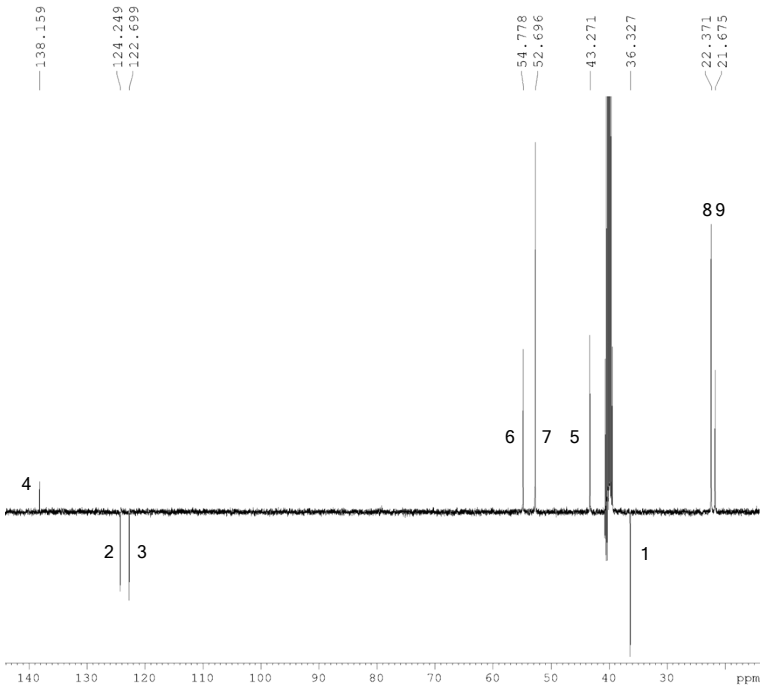

Figure S10. ^{13}C-JMOD NMR spectrum of 1-(2-piperid-1-yl-ethyl)-3-methylimidazolium chloride **[PEMim][Cl]** (100 MHz, DMSO-d6, 25 °C)

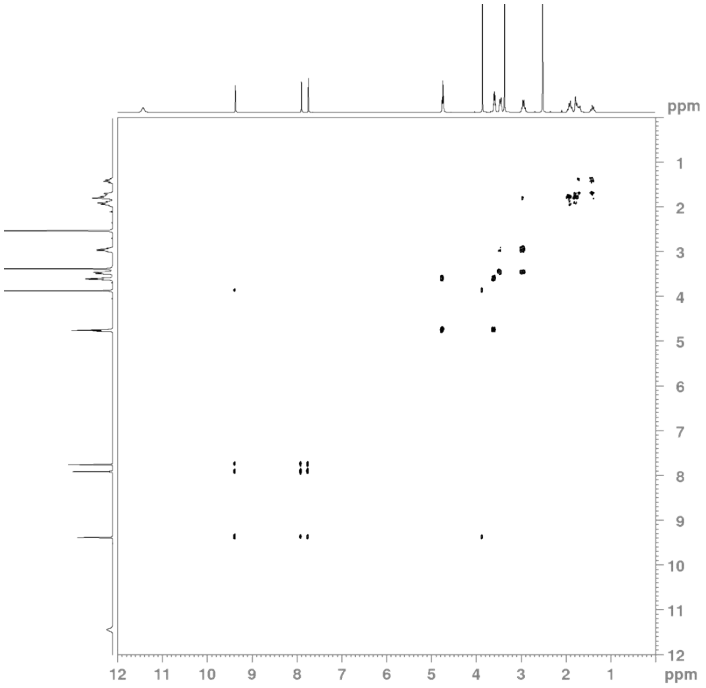

Figure S11. COSY NMR spectrum of 1-(2-piperid-1-yl-ethyl)-3-methylimidazolium chloride **[PEMim][Cl]** (400 MHz, DMSO-d6, 25 °C)

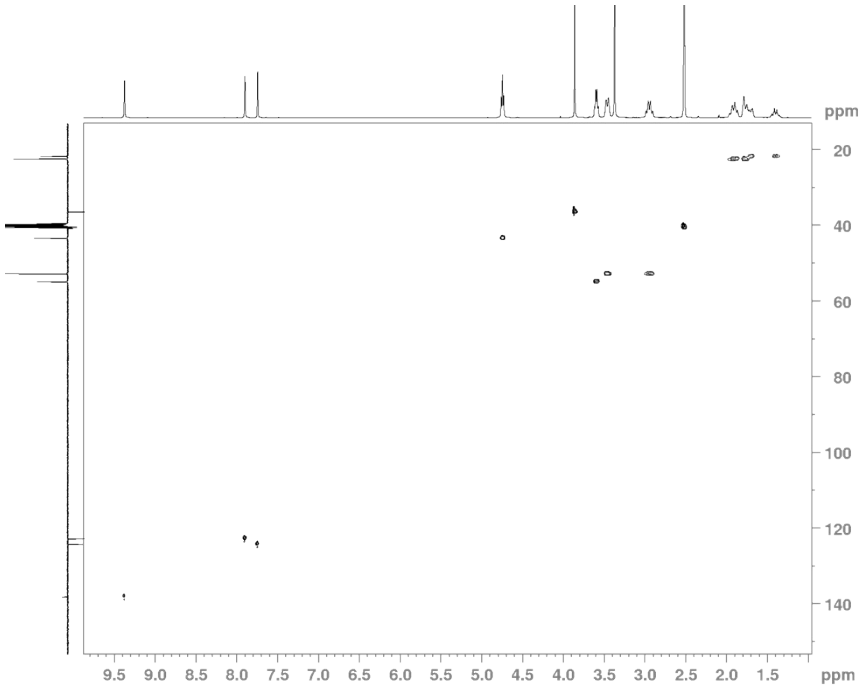

Figure S12. HSQC NMR spectrum of 1-(2-piperid-1-yl-ethyl)-3-methylimidazolium chloride **[PEMim][Cl]** (400 MHz, DMSO-d6, 25 °C)

4) 1-(2-piperid-1-yl-ethyl)-3-methylimidazolium hexafluorophosphate [PEMim][PF_6]

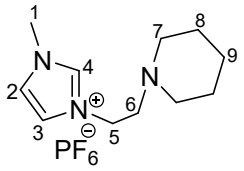

^{1}H NMR (DMSO-d6, 400 MHz, 25 °C, δ(ppm)): 9.03 (s, 1H, N-CH-N), 7.73 (t, 1H, *J = 1.7 Hz*, CH), 7.67 (t, 1H, *J = 1,7 Hz*, CH), 4.26 (t, 2H, *J = 5.9 Hz*, CH_2), 3.88 (s, 3H, CH_3), 2.64 (t, 2H, *J = 5.9 Hz*, CH_2), 2.38 (m, 4H, CH_2), 1.51-1.37 (m, 6H, CH_2 cycle). **^{13}C NMR (DMSO-d6, 100 MHz, 25 °C, δ(ppm)):** 137.1 (C4), 123.6 (C2), 123.2 (C3), 57.7 (C6), 54.2 (C7), 46.6 (C5), 36.2 (C1), 25.9 (C8), 24.3 (C9).

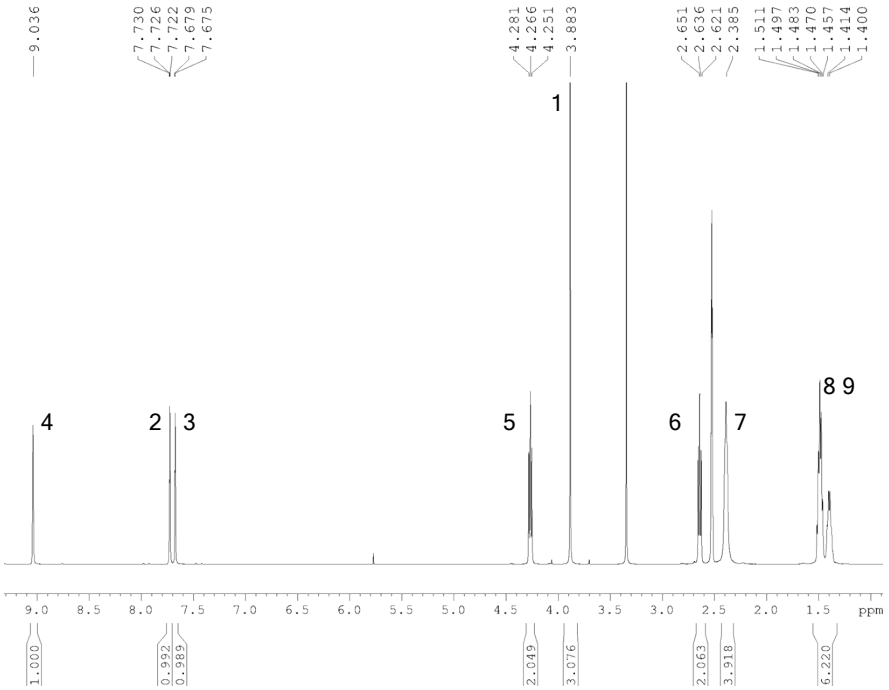

Figure S13. ^{1}H NMR spectrum of 1-(2-piperid-1-yl-ethyl)-3-methylimidazolium hexafluorophosphate **[PEMim][PF_6]** (400 MHz, DMSO-d6, 25 °C)

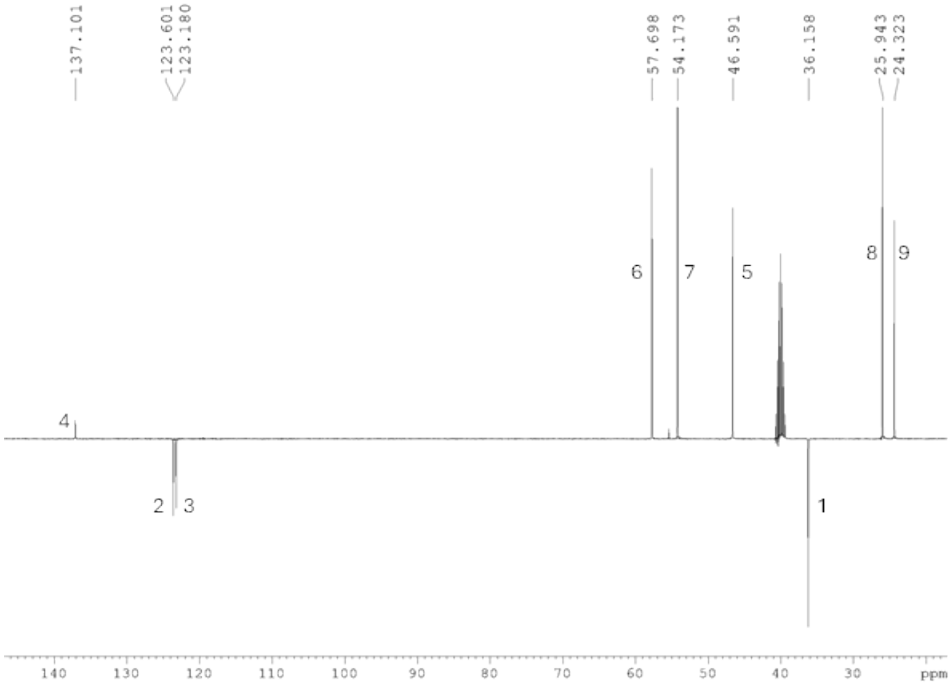

Figure S14. ^{13}C-JMOD NMR spectrum of 1-(2-piperid-1-yl-ethyl)-3-methylimidazolium hexafluorophosphate **[PEMim][PF_6]** (100 MHz, DMSO-d6, 25 °C)

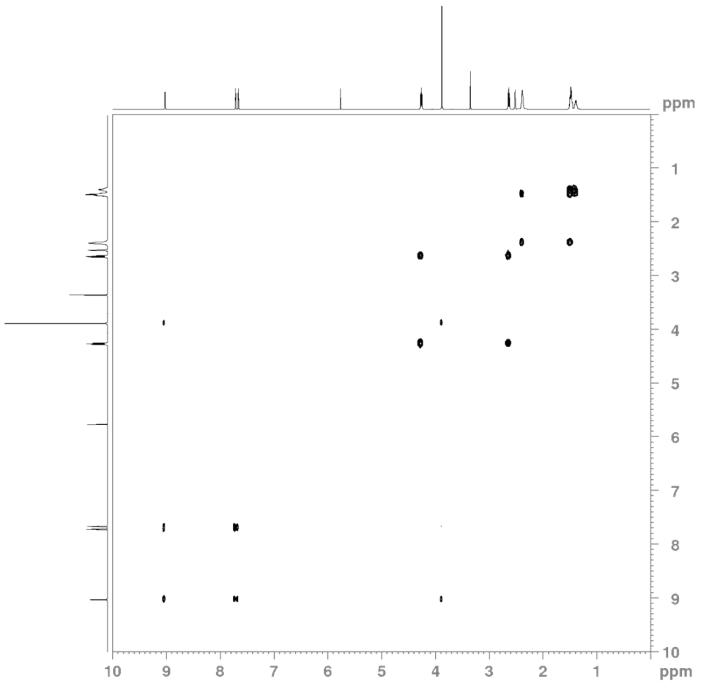

Figure S15. COSY spectrum of 1-(2-piperid-1-yl-ethyl)-3-methylimidazolium hexafluorophosphate **[PEMim][PF_6]** (400 MHz, DMSO-d6, 25 °C)

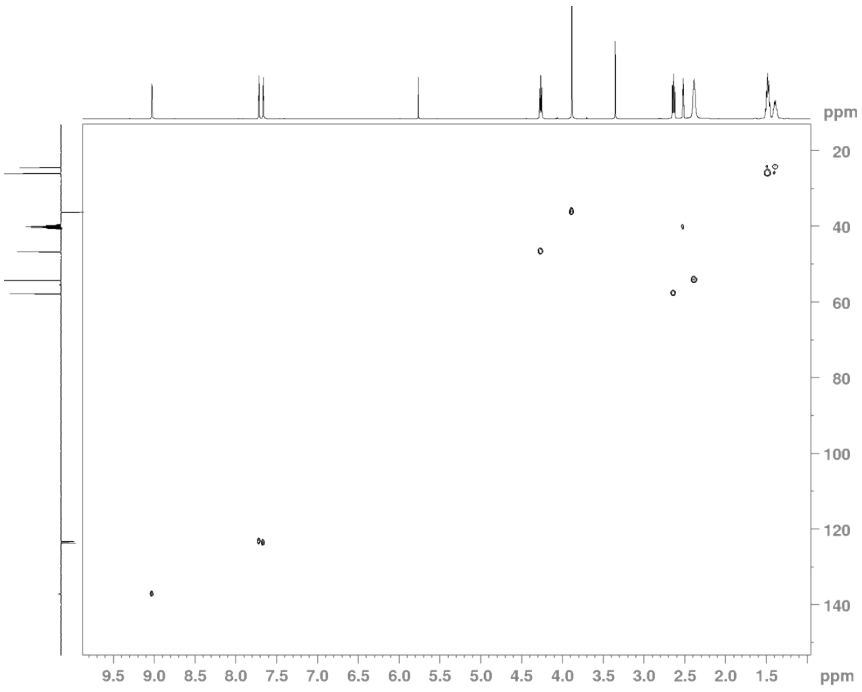

Figure S16. HSQC NMR spectrum of 1-(2-piperid-1-yl-ethyl)-3-methylimidazolium hexafluorophosphate **[PEMim][PF_6]** (400 MHz, DMSO-d6, 25 °C)

5) 1-(2-piperid-1-yl-ethyl)-3-methylimidazolium tetrafluoroborate [PEMim][BF_4]

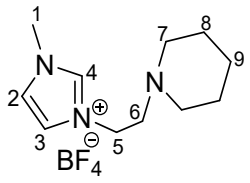

^{1}H NMR ($CDCl_3$, 400 MHz, 25 °C, δ(ppm)): 9.02 (s, 1H, N-CH-N), 7.72 (t, 1H, *J = 1.7 Hz*, CH), 7.67 (t, 1H, *J = 1,7 Hz*, CH), 4.25 (t, 2H, *J = 5.9 Hz*, CH_2), 3.87 (s, 3H, CH_3), 2.63 (t, 2H, *J = 5.9 Hz*, CH_2), 2.37 (m, 4H, CH_2), 1.652-1.508 (m, 6H, CH_2 cycle). **^{13}C NMR (DMSO-d6, 100 MHz, 25 °C, δ(ppm)):** 137.1 (C4), 123.6 (C2), 123.2 (C3), 57.7 (C6), 54.2 (C7), 46.5 (C5), 36.2 (C1), 25.9 (C8), 24.3 (C9).

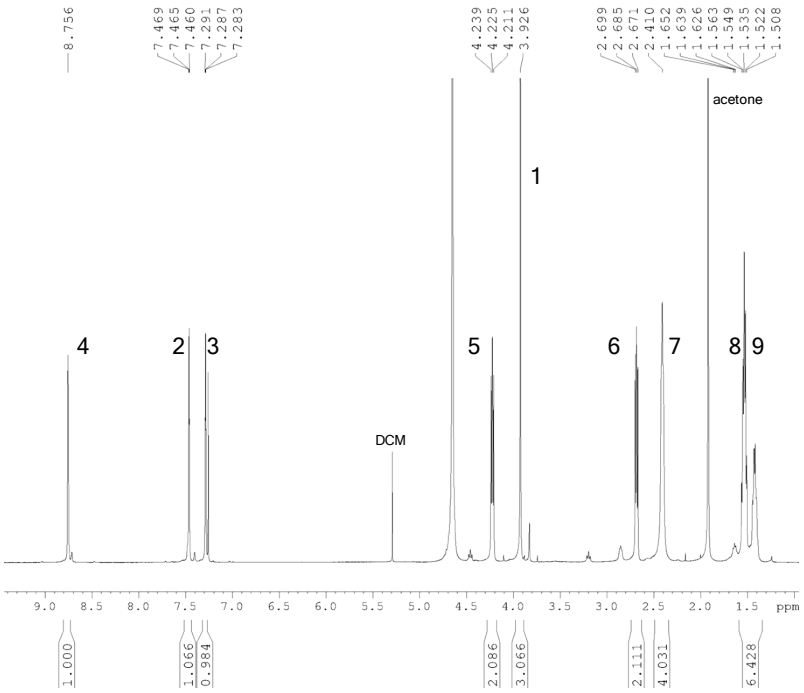

Figure S17. ^{1}H NMR spectrum of 1-(2-piperid-1-yl-ethyl)-3-methylimidazolium tetrafluoroborate **[PEMim][BF_4]** (400 MHz, DMSO-d6, 25 °C)

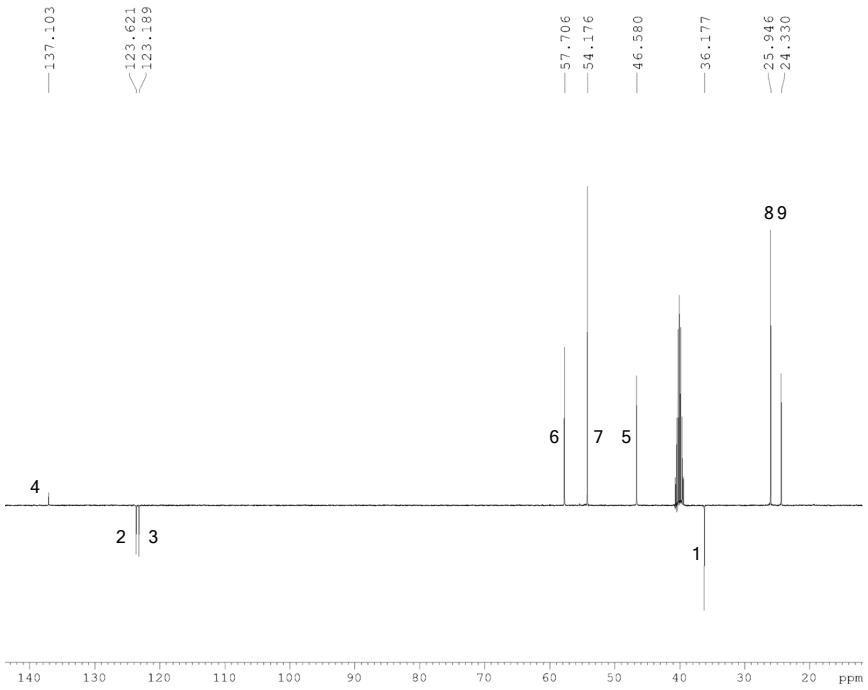

Figure S18. ^{13}C-JMOD NMR spectrum of 1-(2-piperid-1-yl-ethyl)-3-methylimidazolium tetrafluoroborate **[PEMim][BF$_4$]** (100 MHz, DMSO-d6, 25 °C)

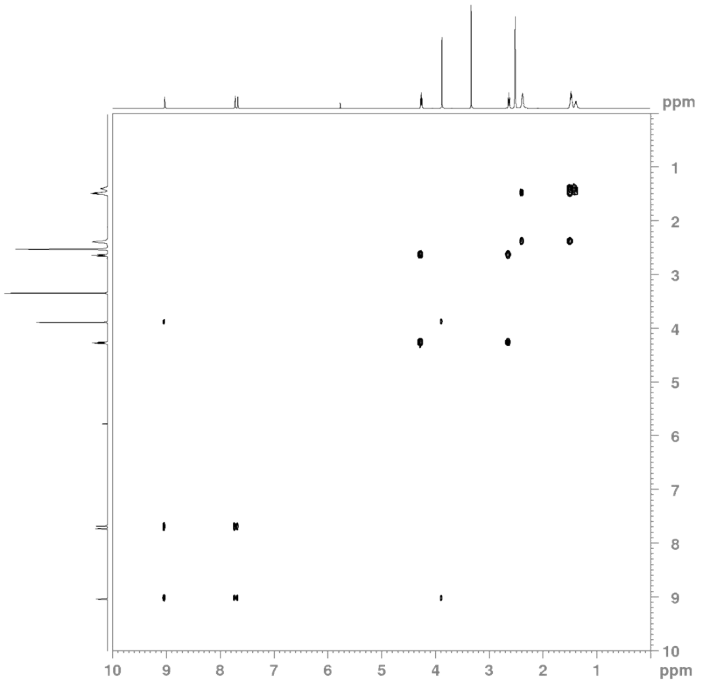

Figure S19. COSY NMR spectrum of 1-(2-piperid-1-yl-ethyl)-3-methylimidazolium tetrafluoroborate **[PEMim][BF$_4$]** (400 MHz, DMSO-d6, 25 °C)

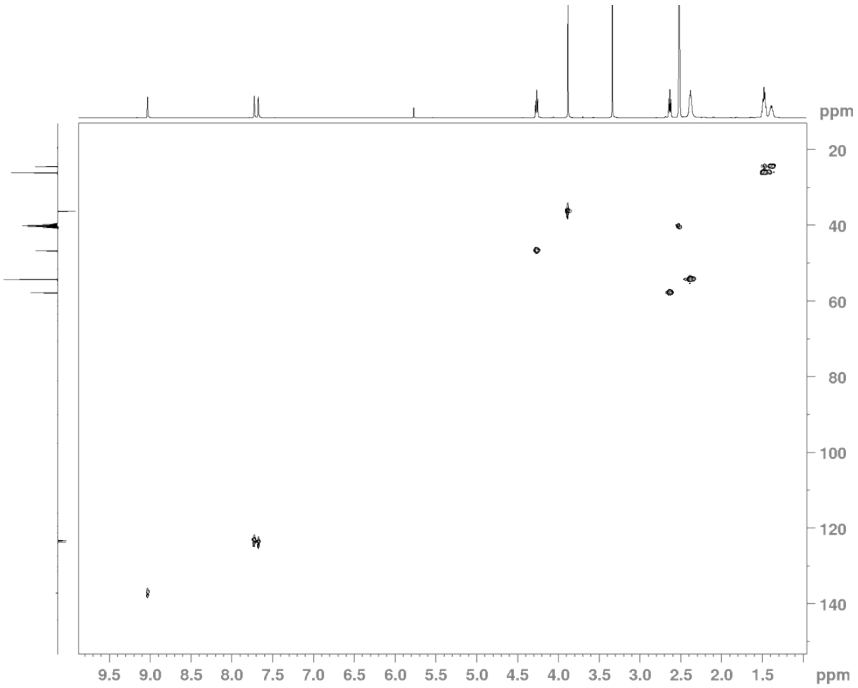

Figure S20. HSQC NMR spectrum of 1-(2-piperid-1-yl-ethyl)-3-methylimidazolium tetrafluoroborate **[PEMim][BF_4]** (400 MHz, DMSO-d6, 25 °C)

6) 1-(2-piperid-1-yl-ethyl)-3-methylimidazolium bis(trifluoromethylsulfonyl)imide [PEMim][Tf_2N]

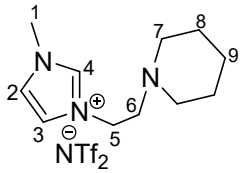

^{1}H NMR (DMSO-d6, 400 MHz, 25 °C, δ(ppm)): 9.03 (s, 1H, N-CH-N), 7.71 (t, 1H, *J = 1.7 Hz*, CH), 7.66 (t, 1H, *J = 1,7 Hz*, CH), 4.26 (t, 2H, *J = 5.9 Hz*, CH_2), 3.88 (s, 3H, CH_3), 2.63 (t, 2H, *J = 5.9 Hz*, CH_2), 2.38 (m, 4H, CH_2), 1.51-1.37 (m, 6H, CH_2 cycle). **^{13}C NMR (DMSO-d6, 100 MHz, 25 °C, δ(ppm)):** 137.1 (C4), 124.8 (CF_3), 123.6 (C2), 123.2 (C3), 121.5 (CF_3), 118.4 (CF_3), 115.2 (CF_3), 57.7 (C6), 54.2 (C7), 46.6 (C5), 36.2 (C1), 25.9 (C8), 24.3 (C9).

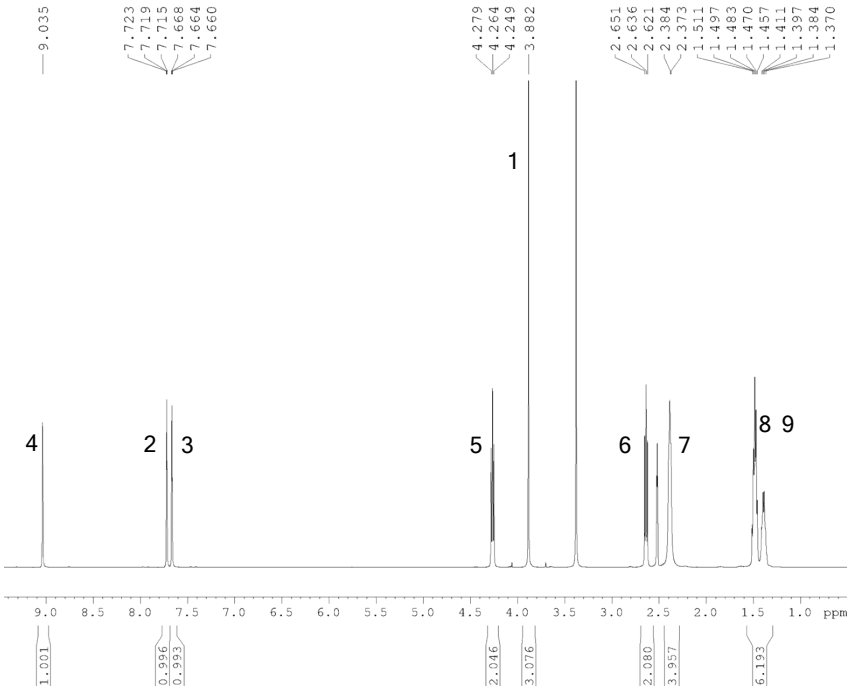

Figure S21. ^{1}H NMR spectrum of 1-(2-piperid-1-yl-ethyl)-3-methylimidazolium bis(trifluoromethylsulfonyl)imide **[PEMim][Tf$_2$N]** (400 MHz, DMSO-d6, 25 °C)

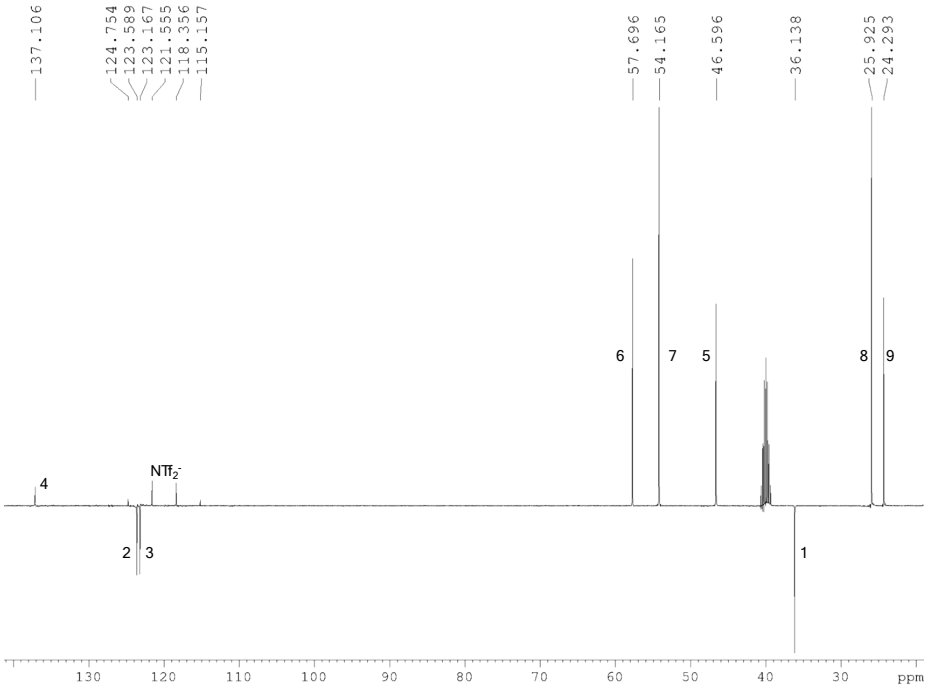

Figure S22. ^{13}C-JMOD NMR spectrum of 1-(2-piperid-1-yl-ethyl)-3-methylimidazolium bis(trifluoromethylsulfonyl)imide **[PEMim][Tf$_2$N]** (100 MHz, DMSO-d6, 25 °C)

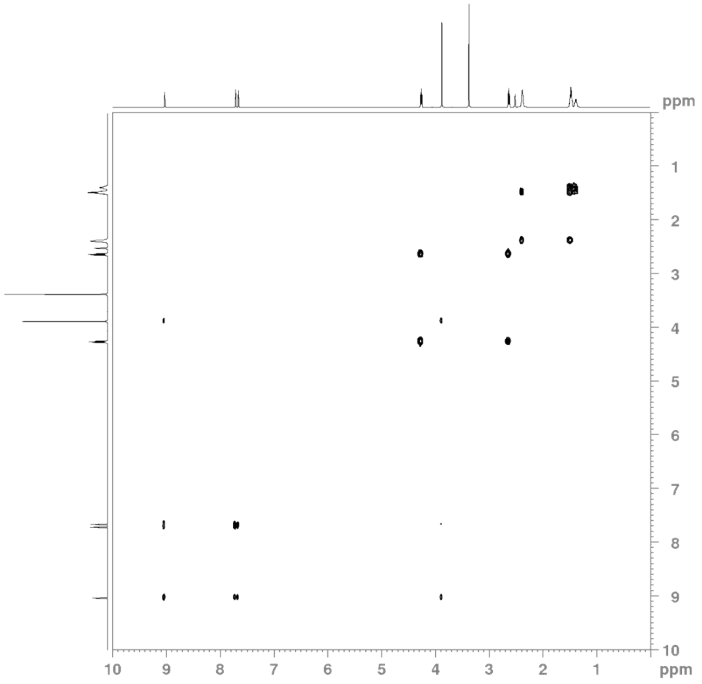

Figure S23. COSY NMR spectrum of 1-(2-piperid-1-yl-ethyl)-3-methylimidazolium bis(trifluoromethylsulfonyl)imide **[PEMim][Tf_2N]** (400 MHz, DMSO-d6, 25 °C)

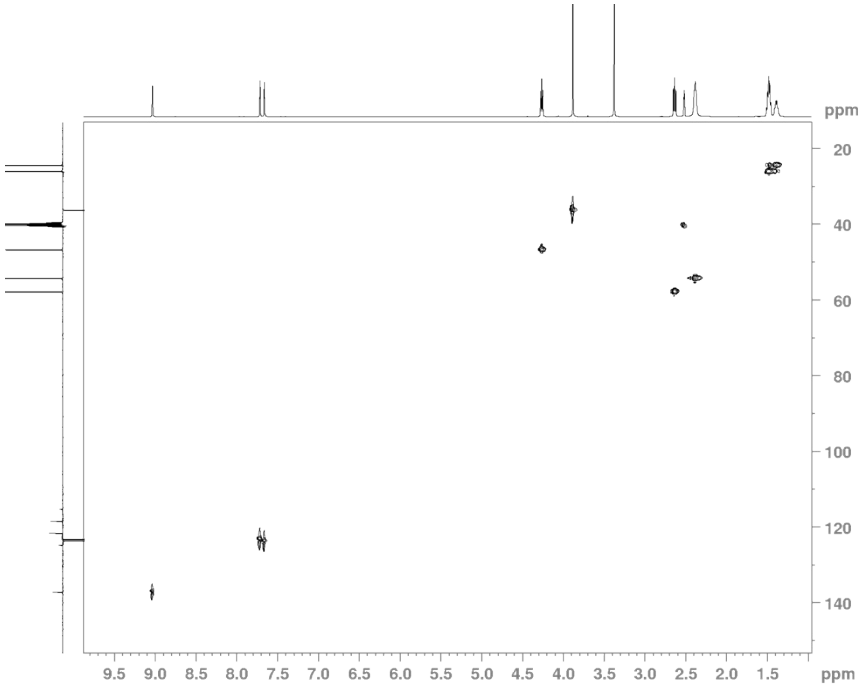

Figure S24. HSQC NMR spectrum of 1-(2-piperid-1-yl-ethyl)-3-methylimidazolium bis(trifluoromethylsulfonyl)imide **[PEMim][Tf_2N]** (400 MHz, DMSO-d6, 25 °C)

7) 1-(2-piperid-1-yl-ethyl)-3-methylimidazolium dicyanamide [PEMim][$(CN)_2N$]

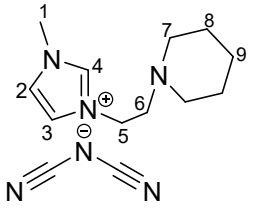

^{1}H NMR (DMSO-d6, 400 MHz, 25 °C, δ(ppm)): 9.04 (s, 1H, N-CH-N), 7.72 (t, 1H, *J = 1.7 Hz*, CH), 7.66 (t, 1H, *J = 1,7 Hz*, CH), 4.25 (t, 2H, *J = 5.9 Hz*, CH_2), 3.87 (s, 3H, CH_3), 2.62 (t, 2H, *J = 5.9 Hz,* CH_2), 2.36 (m, 4H, CH_2), 1.48-1.36 (m, 6H, CH_2 cycle). **^{13}C NMR (DMSO-d6, 100 MHz, 25 °C, δ(ppm)):** 137.1 (C4), 123.6 (C2), 123.2 (C3), 57.7 (C6), 54.2 (C7), 46.6 (C5), 36.2 (C1), 25.9 (C8), 24.3 (C9).

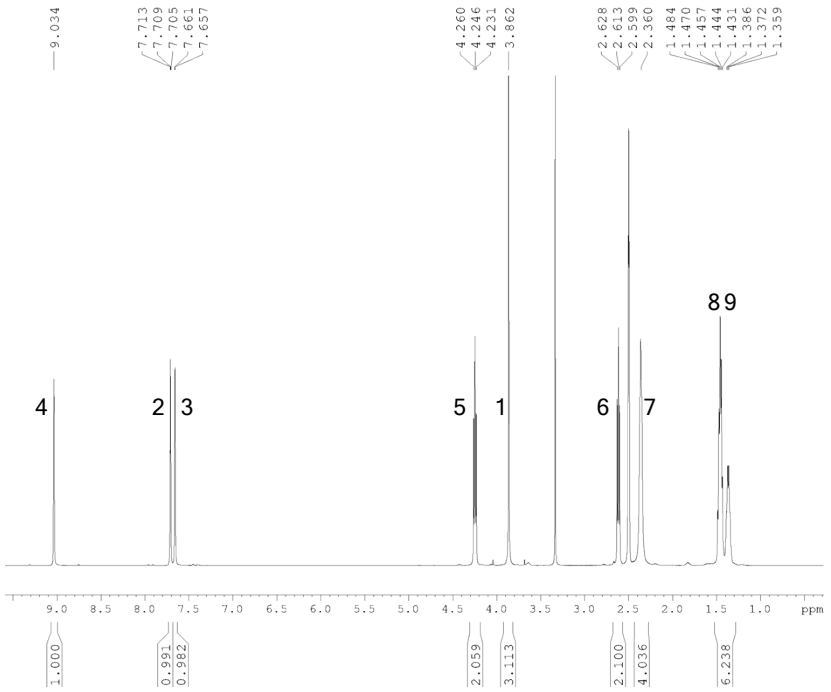

Figure S25. ^{1}H NMR spectrum of 1-(2-piperid-1-yl-ethyl)-3-methylimidazolium dicyanamide **[PEMim][$(CN)_2$N]** (400 MHz, DMSO-d6, 25 °C)

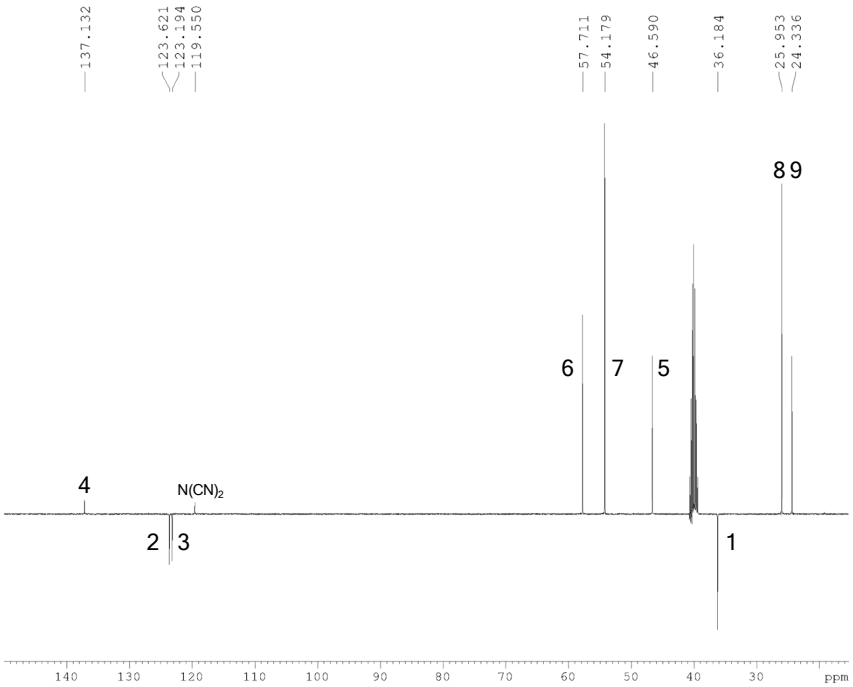

Figure S26. ^{13}C-JMOD NMR spectrum of 1-(2-piperid-1-yl-ethyl)-3-methylimidazolium dicyanamide **[PEMim][(CN)$_2$N]** (100 MHz, DMSO-d6, 25 °C)

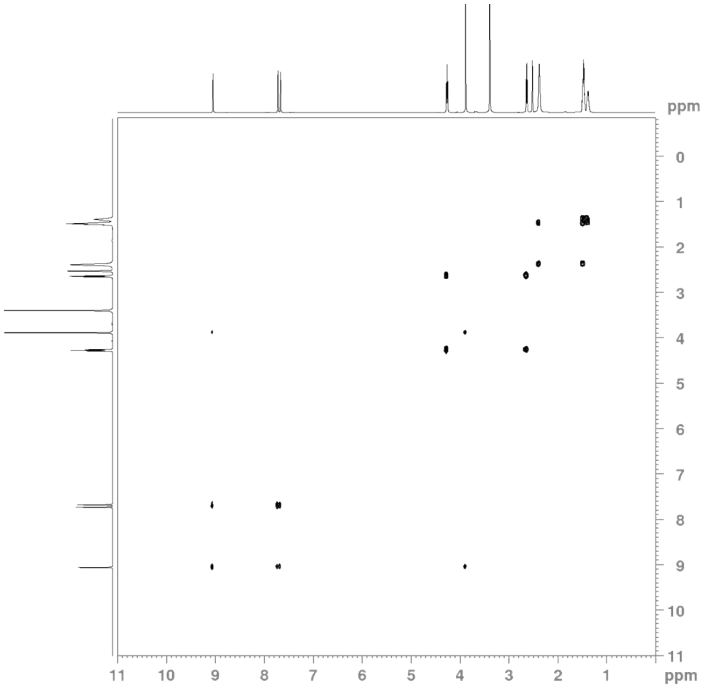

Figure S27. COSY NMR spectrum of 1-(2-piperid-1-yl-ethyl)-3-methylimidazolium dicyanamide **[PEMim][(CN)$_2$N]** (400 MHz, DMSO-d6, 25 °C)

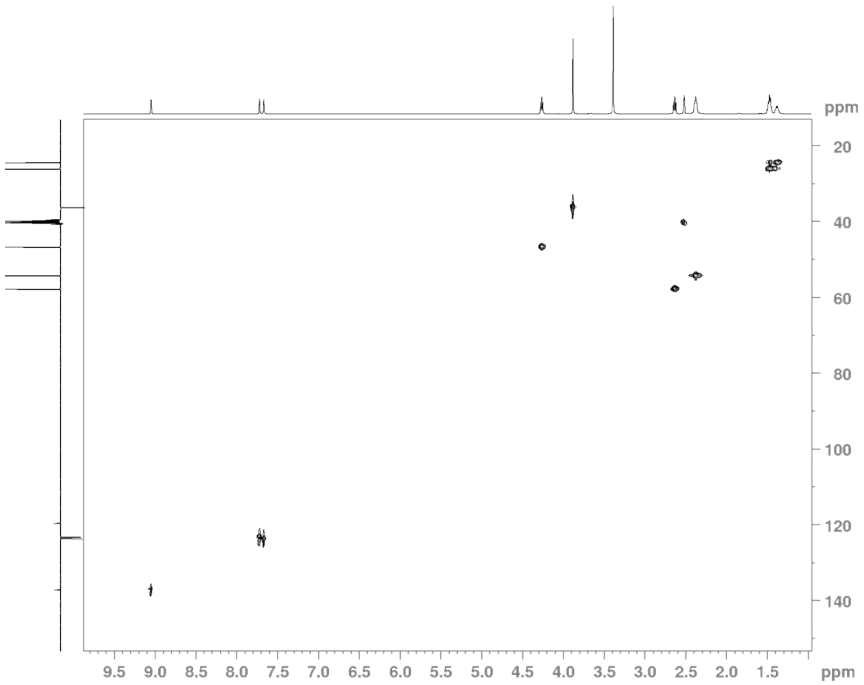

Figure S28. HSQC NMR spectrum of 1-(2-piperid-1-yl-ethyl)-3-methylimidazolium dicyanamide **[PEMim][(CN)$_2$N]** (400 MHz, DMSO-d6, 25 °C)

8) 1-(2-piperid-1-yl-ethyl)-3-methylimidazolium acetate [PEMim][AcO]

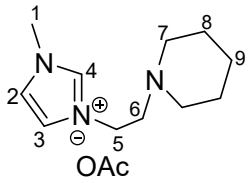

^{1}H NMR (D_2O, 400 MHz, 25 °C, δ(ppm)): 7.42 (t, 1H, *J = 1.7 Hz*, CH), 7.35 (t, 1H, *J = 1,7 Hz*, CH), 4.28 (t, 2H, *J = 7.0 Hz*, CH_2), 3.81 (s, 3H, CH_3), 2.77 (t, 2H, *J = 7.0 Hz,* CH_2), 2.43 (m, 4H, CH_2), 1.51-1.37 (m, 6H, CH_2 cycle). **^{13}C NMR (D_2O, 100 MHz, 25 °C, δ(ppm)):** 181.4 (AcO^-), 136.0 (C4), 123.6 (C2), 122.2 (C3), 57.0 (C6), 53.6 (C7), 45.9 (C5), 35.6 (C1), 24.6 (C8), 23.2 (AcO^-), 23.2 (C9).

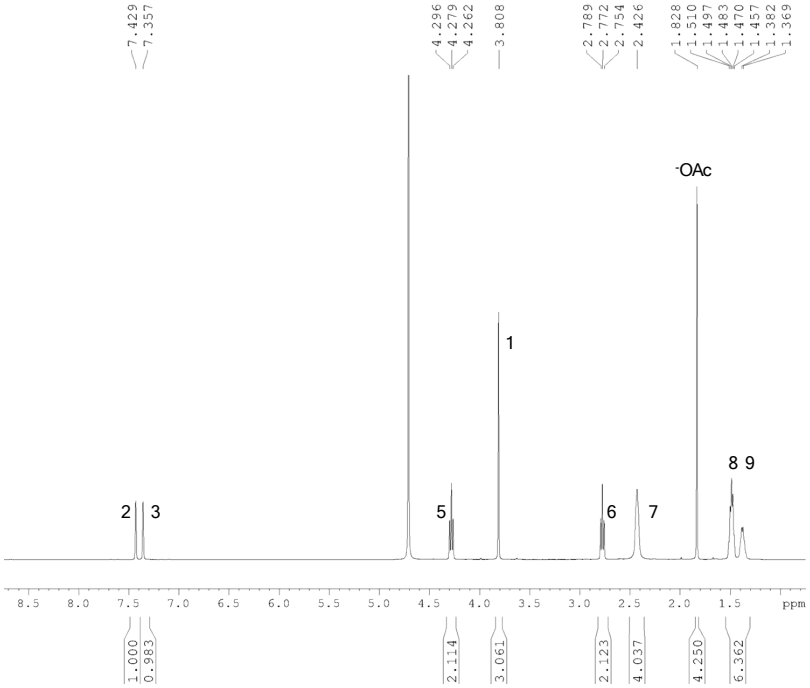

Figure S29. ^{1}H NMR spectrum of 1-(2-piperid-1-yl-ethyl)-3-methylimidazolium acetate **[PEMim][AcO]** (400 MHz, D_2O, 25 °C)

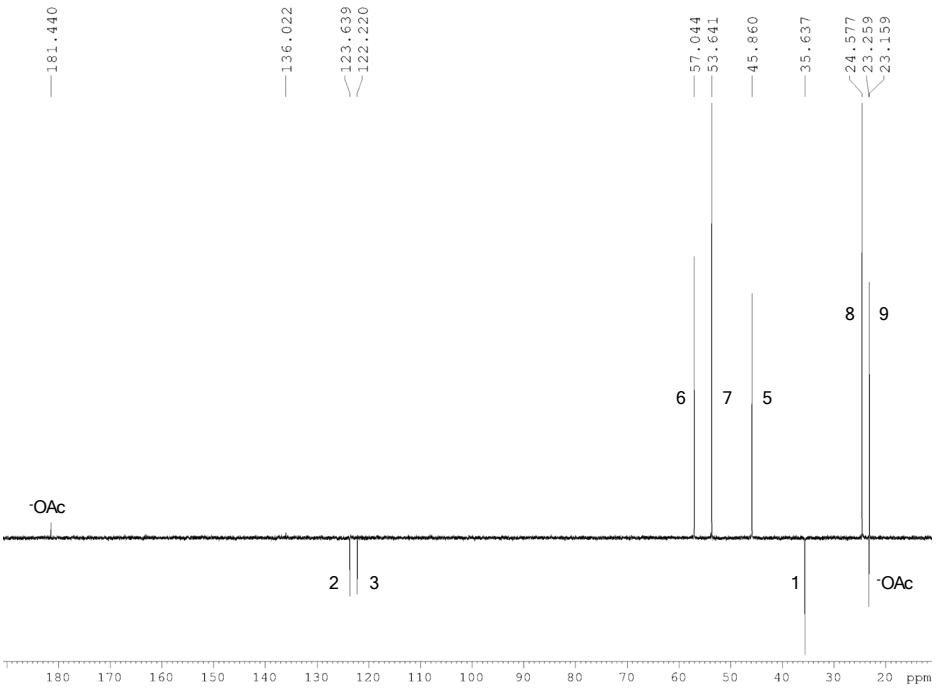

Figure S30. ^{13}C-JMOD NMR spectrum of 1-(2-piperid-1-yl-ethyl)-3-methylimidazolium acetate **[PEMim][AcO]** (100 MHz, D_2O, 25 °C)

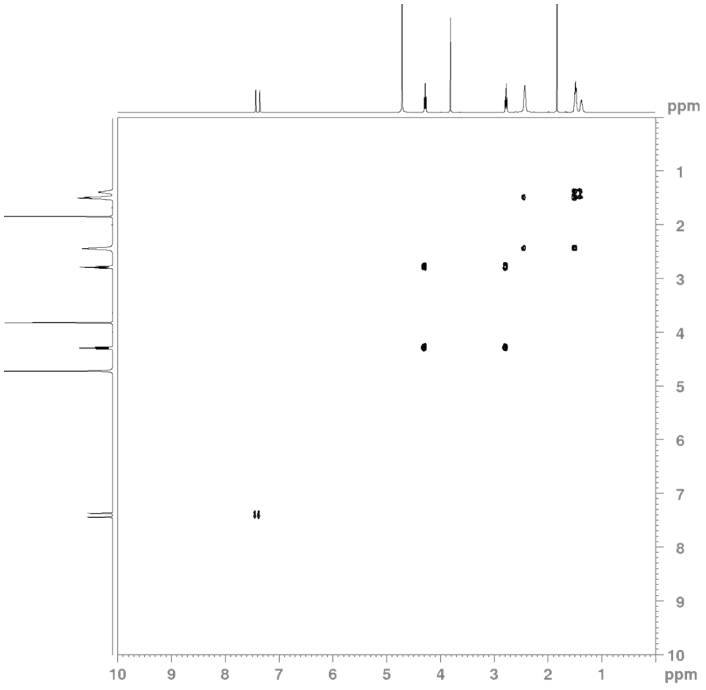

Figure S31. COSY NMR spectrum of 1-(2-piperid-1-yl-ethyl)-3-methylimidazolium acetate **[PEMim][AcO]** (400 MHz, D_2O, 25 °C)

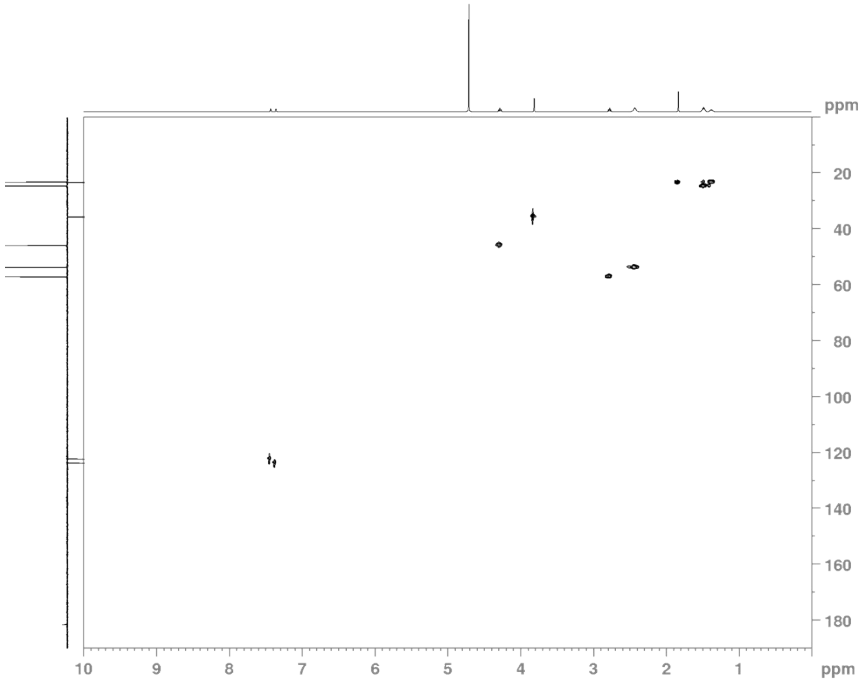

Figure S32. HSQC NMR spectrum of 1-(2-piperid-1-yl-ethyl)-3-methylimidazolium acetate **[PEMim][AcO]** (400 MHz, D_2O, 25 °C)

9) 1-(2-piperid-1-yl-ethyl)-2,3-dimethylimidazolium hexafluorophosphate [PEDMim][PF_6]

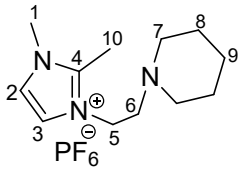

^{1}H NMR (DMSO-d6, 400 MHz, 25 °C, δ(ppm)): 7.60 (d, 1H, *J = 2,1 Hz*, CH), 7.59 (d, 1H, *J = 2.1 Hz*, CH), 4.20 (t, 2H, *J = 5,9 Hz*, CH_2), 3.77 (s, 3H, CH_3), 2.59 (s, 3H, CH_3), 2.56 (t, 2H, *J = 5.9 Hz*, CH_2), 2.64 (m, 2H, CH_2), 1.55-1.40 (m, 6H, CH_2 cycle). **^{13}C NMR (DMSO-d6, 100 MHz, 25 °C, δ(ppm)):** 121.4 (C2), 120.9 (C3), 57.3 (C6), 54.3 (C7), 45.9 (C5), 34.9 (C1), 25.4 (C8), 23.2 (C9), 9.2 (C10).

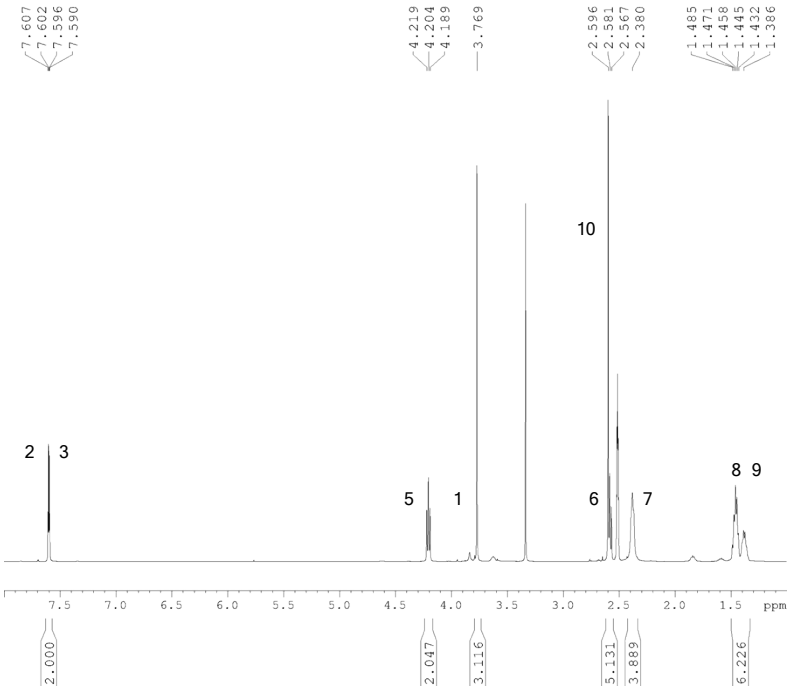

Figure S33. ^{1}H NMR spectrum of 1-(2-piperid-1-yl-ethyl)-2,3-dimethylimidazolium hexafluorophosphate **[PEDMim][PF_6]** (400 MHz, DMSO-d6, 25 °C)

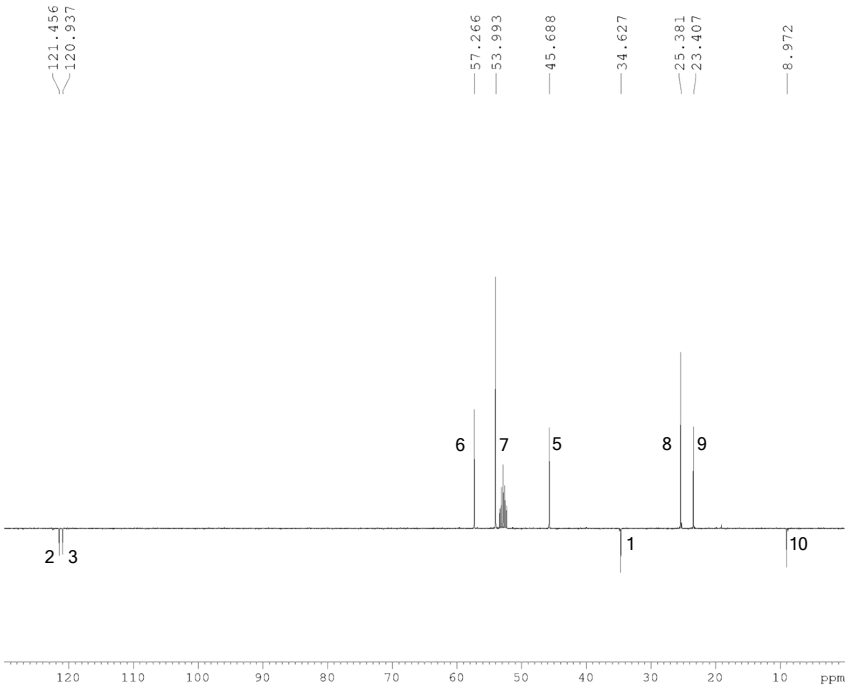

Figure S34. ^{13}C-JMOD NMR spectrum of 1-(2-piperid-1-yl-ethyl)-2,3-dimethylimidazolium hexafluorophosphate **[PEDMim][PF_6]** (100 MHz, DMSO-d6, 25 °C)

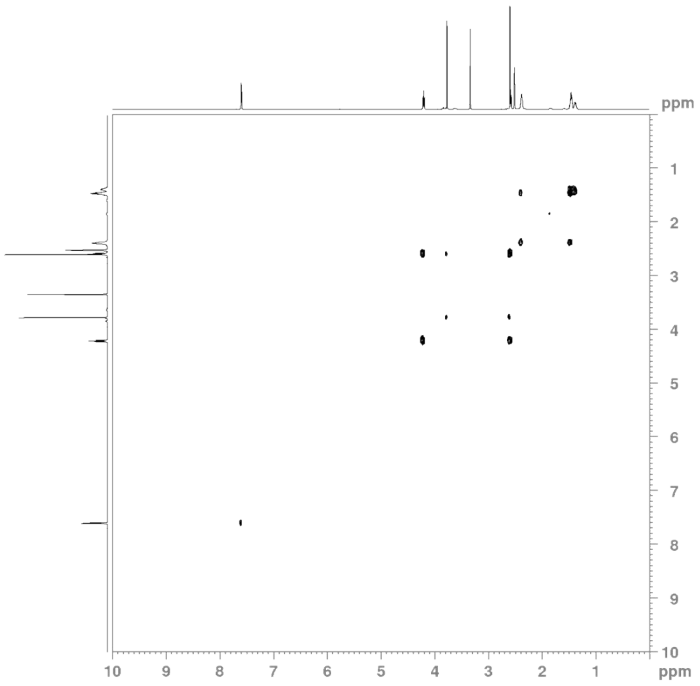

Figure S35. COSY NMR spectrum of 1-(2-piperid-1-yl-ethyl)-2,3-dimethylimidazolium hexafluorophosphate **[PEDMim][PF_6]** (400 MHz, DMSO-d6, 25 °C)

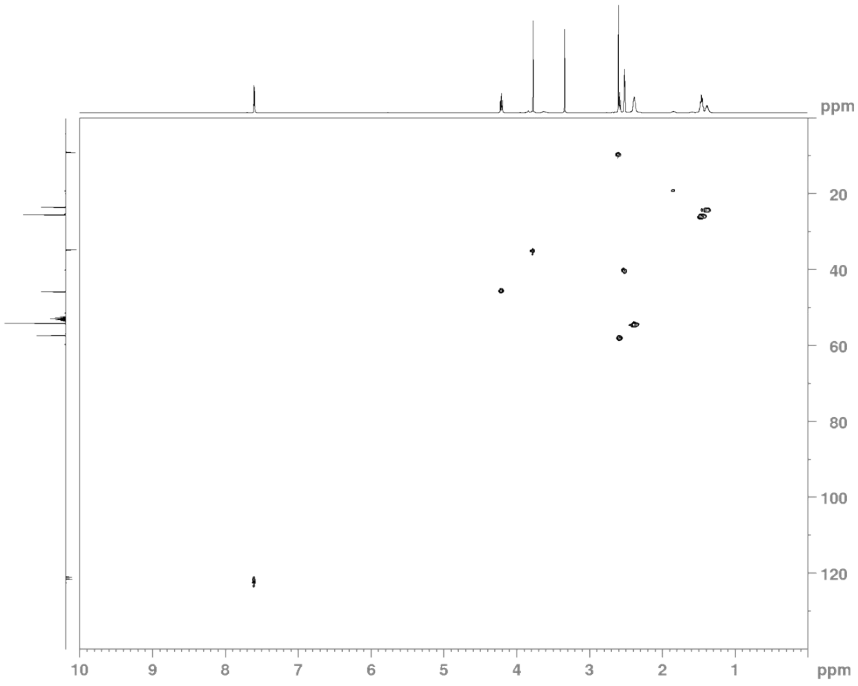

Figure S36. HSQC NMR spectrum of 1-(2-piperid-1-yl-ethyl)-2,3-dimethylimidazolium hexafluorophosphate **[PEDMim][PF_6]** (400 MHz, DMSO-d6, 25 °C)

10) 1-(2-(diethylamino)ethyl)-3-methylimidazolium chloride [Et_2NEMim][Cl]

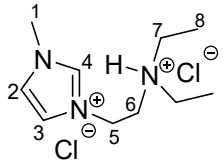

^{1}H NMR (DMSO-d6, 400 MHz, 25 °C, δ(ppm)): 11.48 (s, 1H, NH), 9.49 (s, 1H, N-CH-N), 8.02 (t, 1H, *J = 1,7 Hz,* CH), 7.77 (t, 1H, *J = 1,7 Hz,* CH), 4.75 (t, 2H, *J = 6,8* Hz, CH_2), 3.86 (s, 3H, CH_3), 3.62 (q, 2H, *J = 6,3 and 5,4 Hz*, CH_2), 3.18 (m, 4H, 2xCH_2), 1.24 (t, 6H, *J = 7,2 Hz*, 2xCH_3).
^{13}C NMR (DMSO-d6, 100 MHz, 25 °C, δ(ppm)): 138.3 (C4), 124.2 (C2), 122.7 (C3), 49.9 (C6), 47.2 (C7), 43.2 (C5), 36.3 (C1), 8.7 (C8).

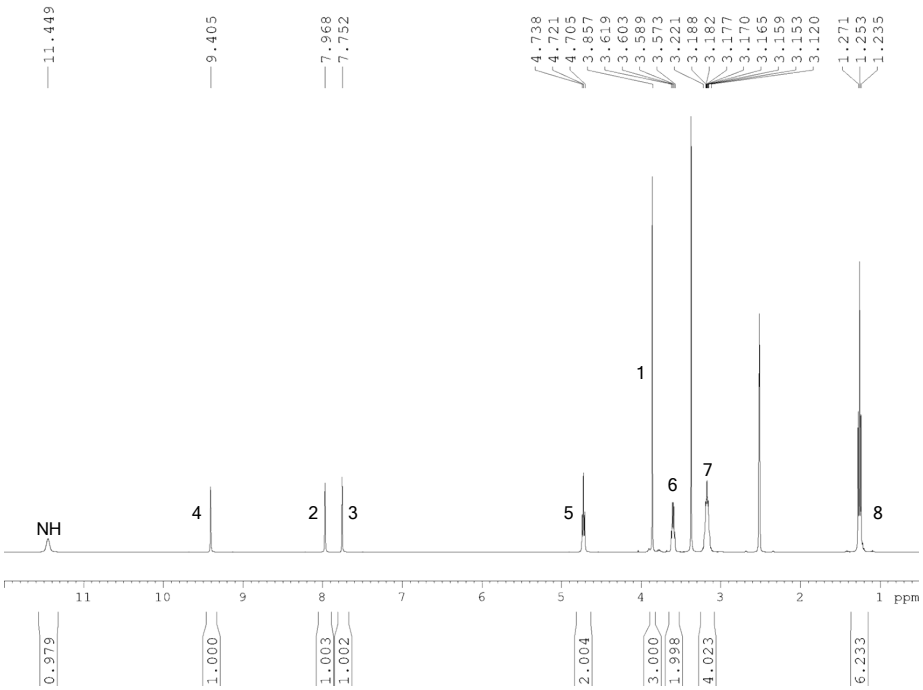

Figure S37. ^{1}H NMR spectrum of 1-(2-(diethylamino)ethyl)-3-methylimidazolium chloride **[Et_2NEMim][Cl]** (400 MHz, DMSO-d6, 25 °C)

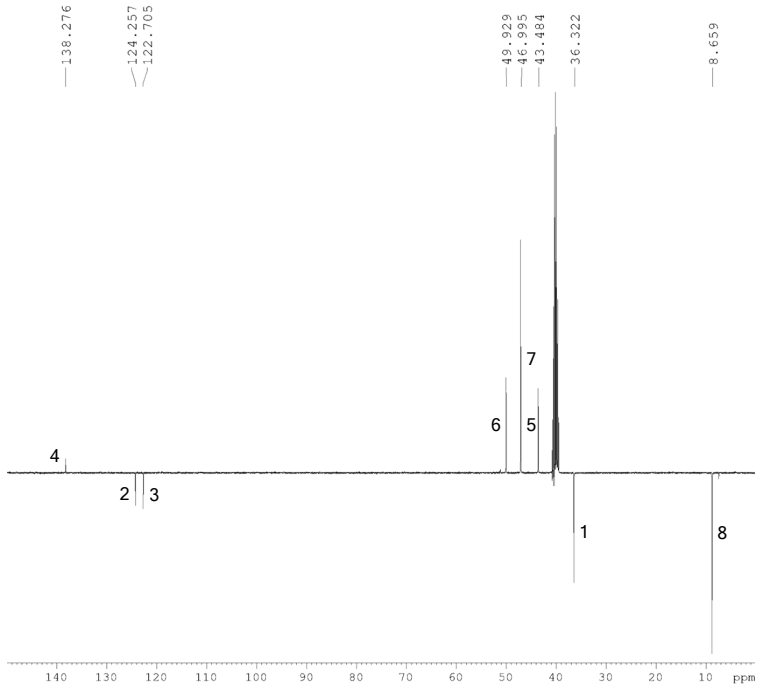

Figure S38. ^{13}C-JMOD NMR spectrum of 1-(2-(diethylamino)ethyl)-3-methylimidazolium chloride **[Et_2NEMim][Cl]** (100 MHz, DMSO-d6, 25 °C)

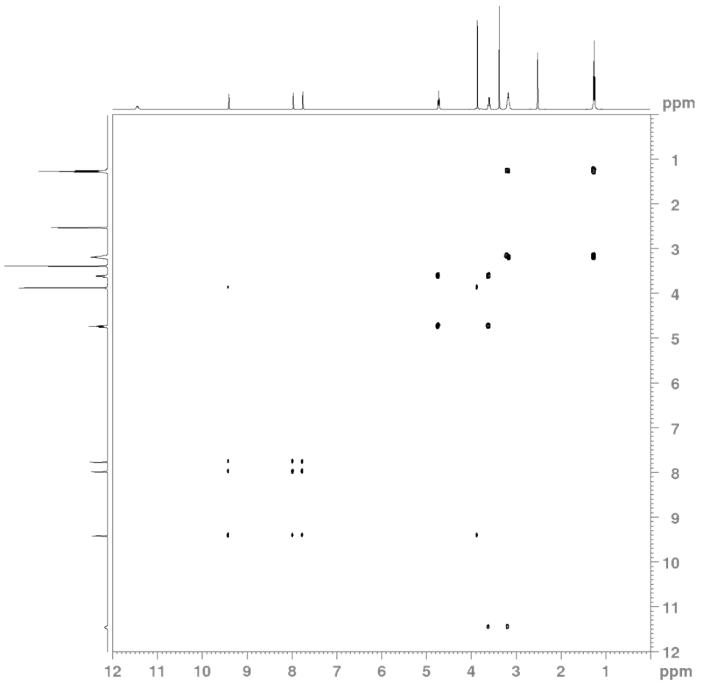

Figure S39. COSY NMR spectrum of 1-(2-(diethylamino)ethyl)-3-methylimidazolium chloride **[Et_2NEMim][Cl]** (400 MHz, DMSO-d6, 25 °C)

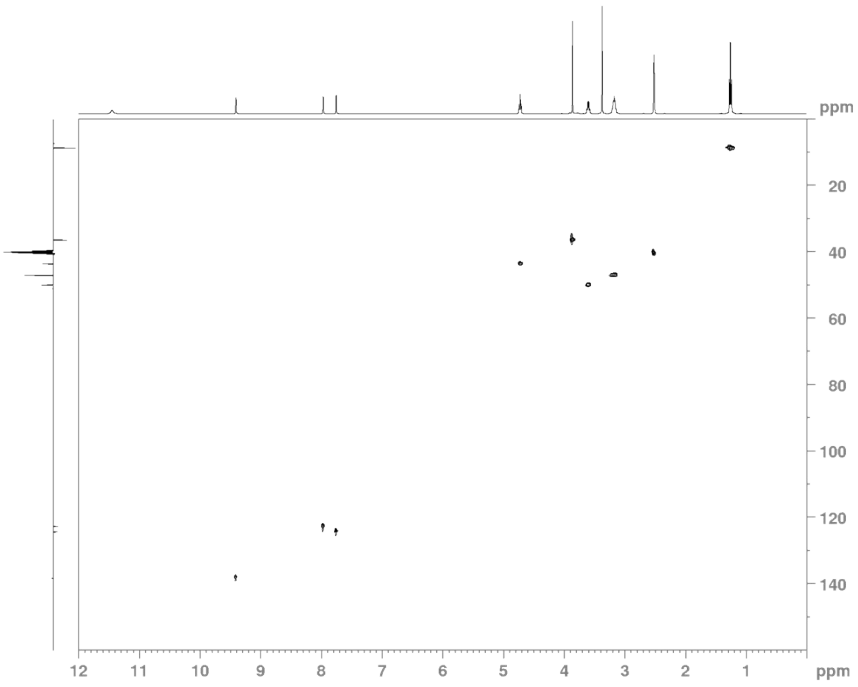

Figure S40. HSQC NMR spectrum of 1-(2-(diethylamino)ethyl)-3-methylimidazolium chloride **[Et_2NEMim][Cl]** (400 MHz, DMSO-d6, 25 °C)

11) 1-(2-(diethylamino)ethyl)-3-methylimidazolium hexafluorophosphate [Et_2NEMim][PF_6]

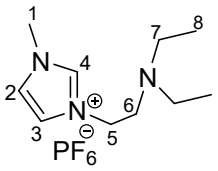

^{1}H NMR (DMSO, 400 MHz, 25 °C, δ(ppm)): 9.03 (s, 1H, N-CH-N), 7.74 (t, 1H, *J = 1,7 Hz,* CH), 7.66 (t, 1H, *J = 1,7 Hz,* CH), 4.19 (t, 2H, *J = 5.9 Hz*, CH_2), 3.87 (s, 3H, CH_3), 2.72 (t, 2H, *J = 5,9 Hz*, CH_2), 2.47 (q, 4H, *J = 7 Hz*, 2xCH_2), 0.86 (t, 6H, *J = 7 Hz*, 2xCH_3). **^{13}C NMR (DMSO, 100 MHz, 25 °C, δ(ppm)):** 137.2 (C4), 123.6 (C2), 123.1 (C3), 52.2 (C6), 47.9 (C5), 46.9 (C7), 36.3 (C1), 12.1 (C8).

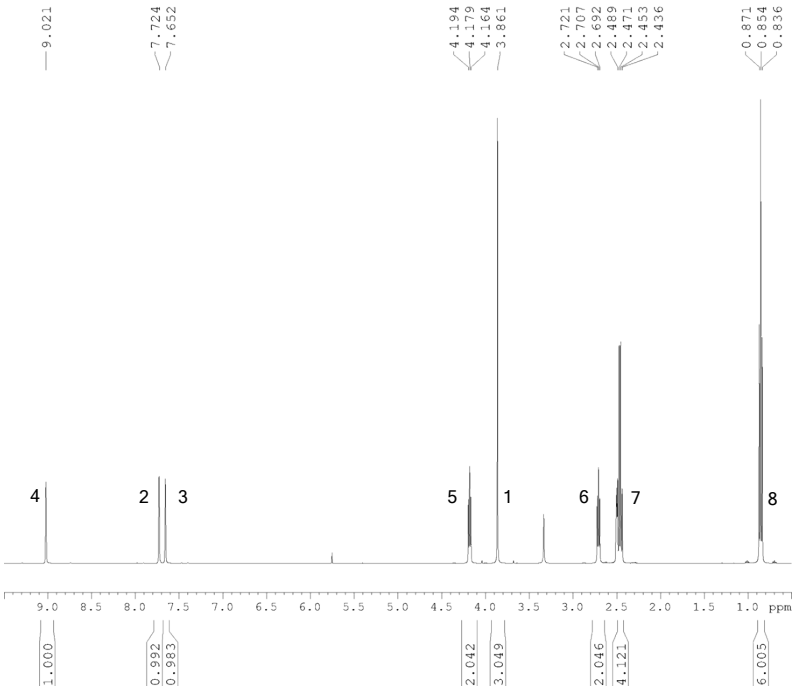

Figure S41. ^{1}H NMR spectrum of 1-(2-(diethylamino)ethyl)-3-methylimidazolium hexafluorophosphate **[Et_2NEMim][PF_6]** (400 MHz, DMSO-d6, 25 °C)

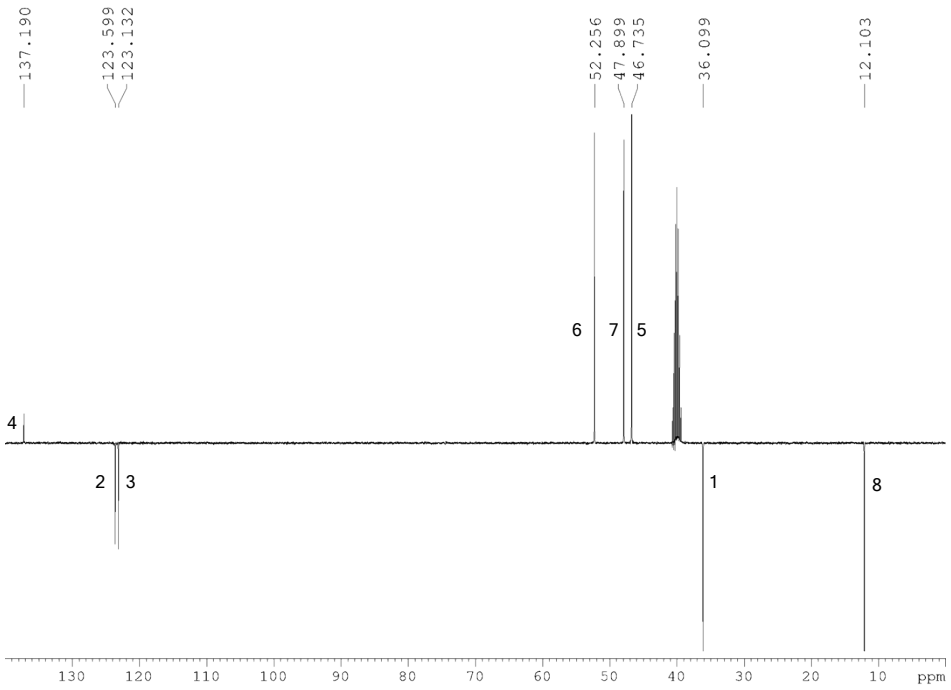

Figure S42. ^{13}C-JMOD NMR spectrum of 1-(2-(diethylamino)ethyl)-3-methylimidazolium hexafluorophosphate **[Et_2NEMim][PF_6]** (100 MHz, DMSO-d6, 25 °C)

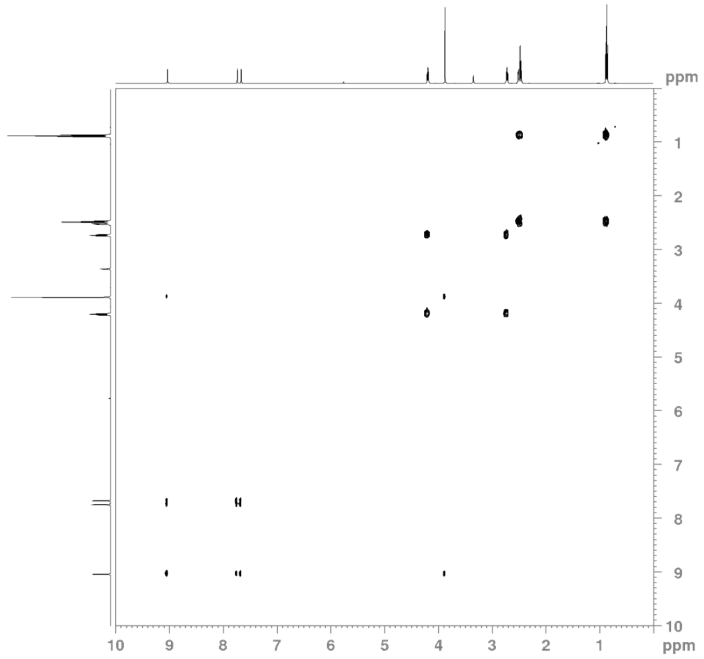

Figure S43. COSY spectrum of 1-(2-(diethylamino)ethyl)-3-methylimidazolium hexafluorophosphate **[Et_2NEMim][PF_6]** (400 MHz, DMSO-d6, 25 °C)

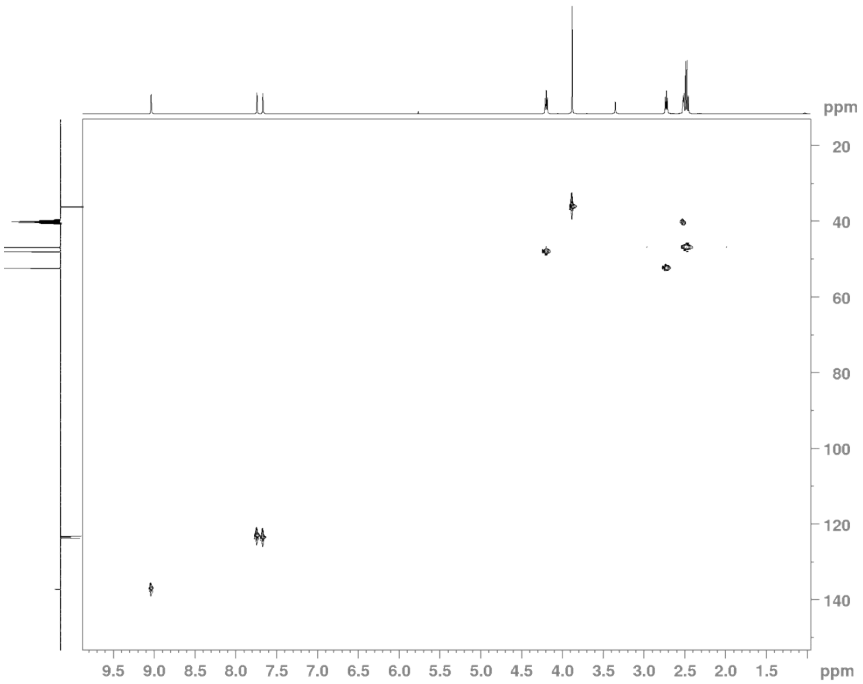

Figure S44. HSQC spectrum of 1-(2-(diethylamino)ethyl)-3-methylimidazolium hexafluorophosphate **[Et_2NEMim][PF_6]** (400 MHz, DMSO-d6, 25 °C)

12) 1-(2-(diethylamino)ethyl)-3-methylimidazolium bis(trifluoromethylsulfonyl)imide [Et_2NEMim][Tf_2N]

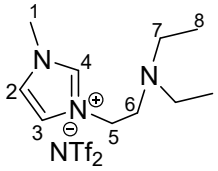

^{1}H NMR (DMSO-d6, 400 MHz, 25 °C, δ(ppm)): 9.04 (s, 1H, N-CH-N), 7.74 (t, 1H, *J = 1,7 Hz,* CH), 7.67 (t, 1H, *J = 1,7 Hz,* CH), 4.19 (t, 2H, *J = 5.8 Hz*, CH_2), 3.87 (s, 3H, CH_3), 2.71 (t, 2H, *J = 5,8 Hz*, CH_2), 2.47 (q, 4H, *J = 7,1 Hz*, 2xCH_2), 0.86 (t, 6H, *J = 7,1 Hz*, 2xCH_3). **^{13}C NMR (DMSO-d6, 100 MHz, 25 °C, δ(ppm)):** 137.2 (C4), 124.7 (CF_3), 123.6 (C3), 123.1 (C2), 121.6 (CF_3), 118.3 (CF_3), 115.1 (CF_3), 52.3 (C6), 48.1 (C7), 46.9 (C5), 36.1 (C1), 12.1 (C8).

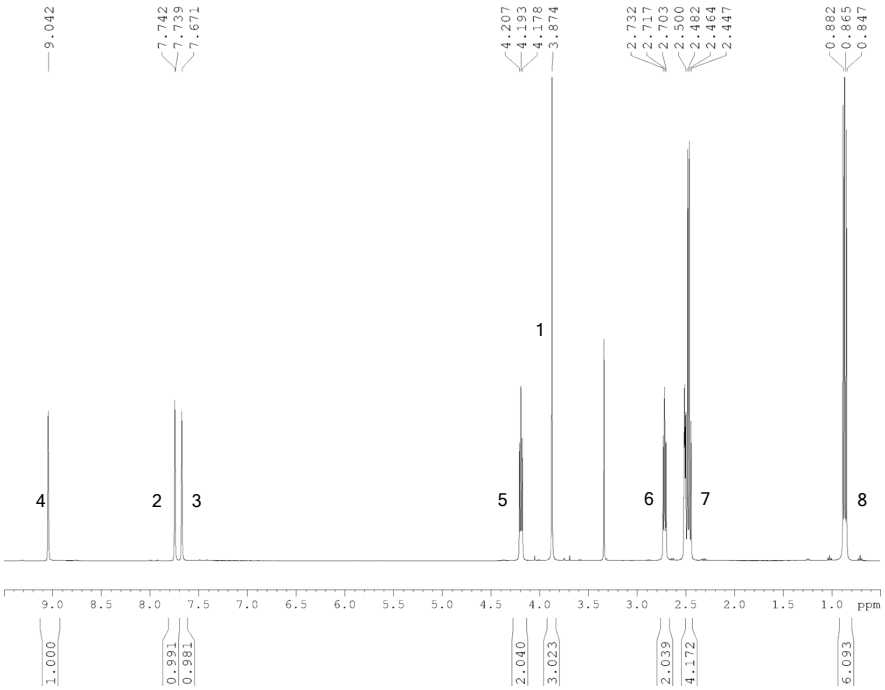

Figure S45. ^{1}H NMR spectrum of 1-(2-(diethylamino)ethyl)-3-methylimidazolium bis(trifluoromethylsulfonyl)imide **[Et$_2$NEMim][Tf$_2$N]** (400 MHz, DMSO-d6, 25 °C)

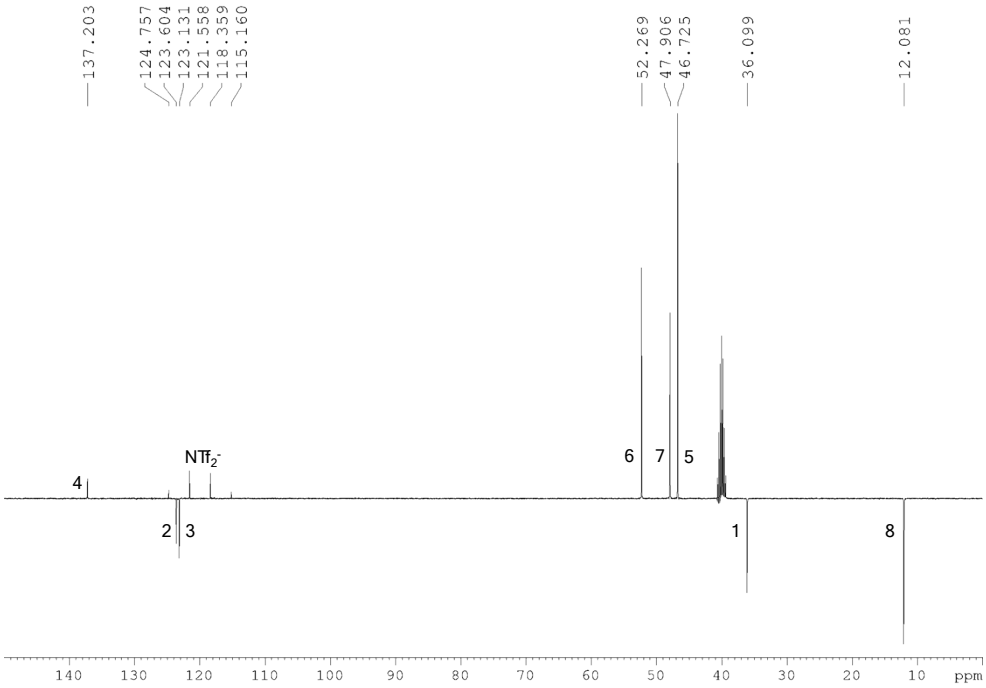

Figure S46. ^{13}C-JMOD NMR spectrum of 1-(2-(diethylamino)ethyl)-3-methylimidazolium bis(trifluoromethylsulfonyl)imide **[Et$_2$NEMim][Tf$_2$N]** (100 MHz, DMSO-d6, 25 °C)

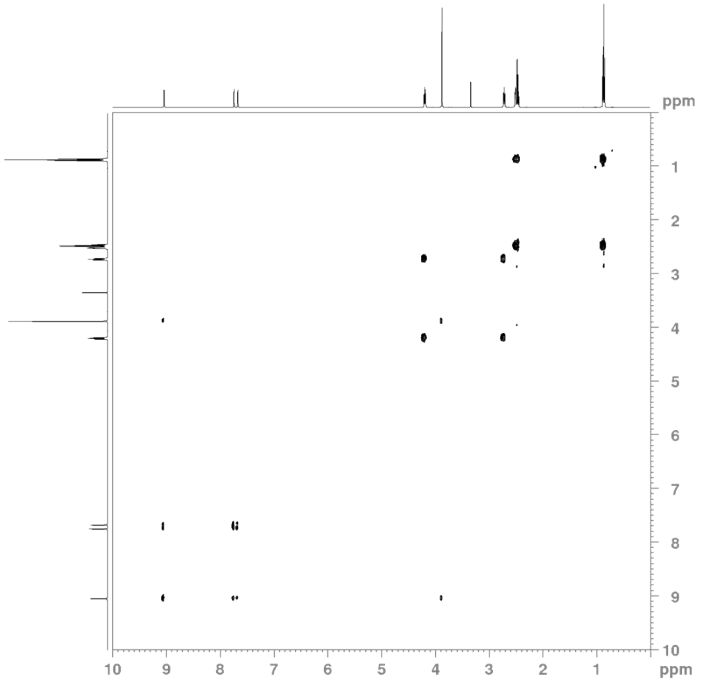

Figure S47. COSY spectrum of 1-(2-(diethylamino)ethyl)-3-methylimidazolium bis(trifluoromethylsulfonyl)imide **[Et_2NEMim][Tf_2N]** (400 MHz, DMSO-d6, 25 °C)

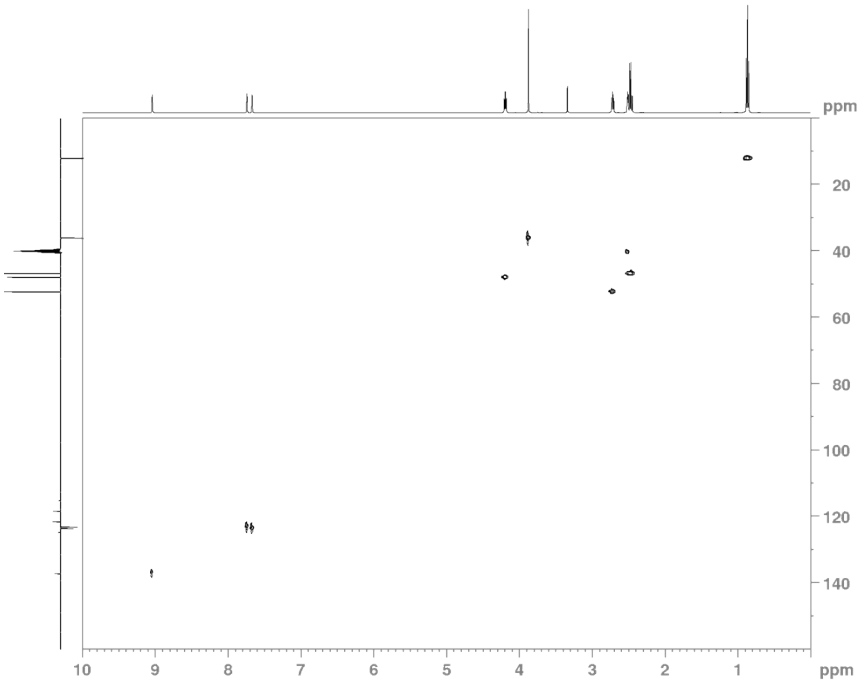

Figure S48. HSQC spectrum of 1-(2-(diethylamino)ethyl)-3-methylimidazolium bis(trifluoromethylsulfonyl)imide **[Et_2NEMim][Tf_2N]** (400 MHz, DMSO-d6, 25 °C)

13) 1-(2-(diethylamino)ethyl)-2,3-dimethylimidazolium hexafluorophosphate [Et_2NEDMim][PF_6]

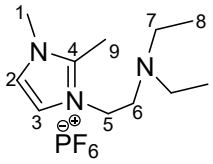

^{1}H NMR (DMSO-d6, 400 MHz, 25 °C, δ(ppm)): 7.63 (d, 1H, *J = 2,1 Hz,* CH), 7.60 (d, 1 H, *J = 2,1 Hz*, CH), 4.15 (t, 2H, *J = 5.9 Hz*, CH_2), 3.75 (s, 3H, CH_3), 2.66 (t, 2H, *J = 5,9 Hz*, CH_2), 2.59 (s, 3H, CH_3), 2.45 (q, 2H, *J = 7,2 Hz*, 2xCH_2), 0.83 (t, 6H, *J = 7 Hz*, 2xCH_3). **^{13}C NMR (DMSO-d6, 75 MHz, 25 °C, δ(ppm)):** 145.1 (C1), 122.5 (C2), 121.8 (C3), 54.8 (C4), 52.7 (C5), 46.9 (C6), 35.1 (C7), 12.4 (C8), 9.1 (C9).

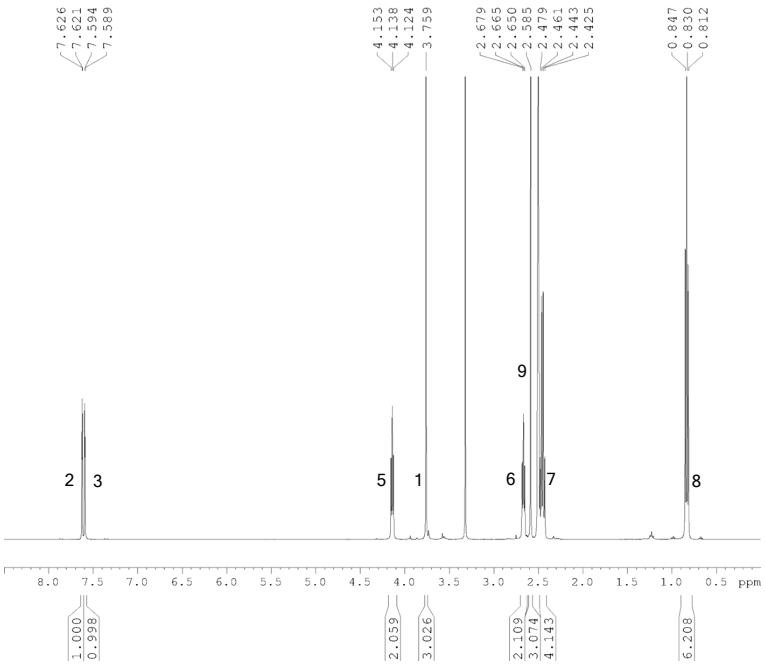

Figure S49. ^{1}H NMR spectrum of 1-(2-(diethylamino)ethyl)-2,3-dimethylimidazolium hexafluorophosphate **[Et_2NEDMim][PF_6]** (400 MHz, DMSO-d6, 25 °C)

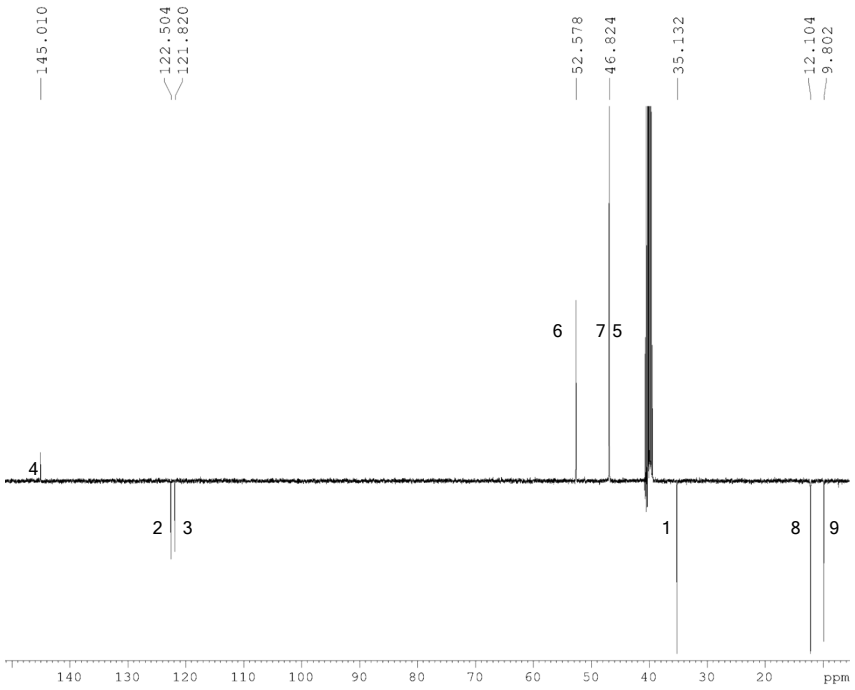

Figure S50. ^{13}C-JMOD NMR spectrum of 1-(2-(diethylamino)ethyl)-2,3-dimethylimidazolium hexafluorophosphate **[Et_2NEDMim][PF_6]** (100 MHz, DMSO-d6, 25 °C)

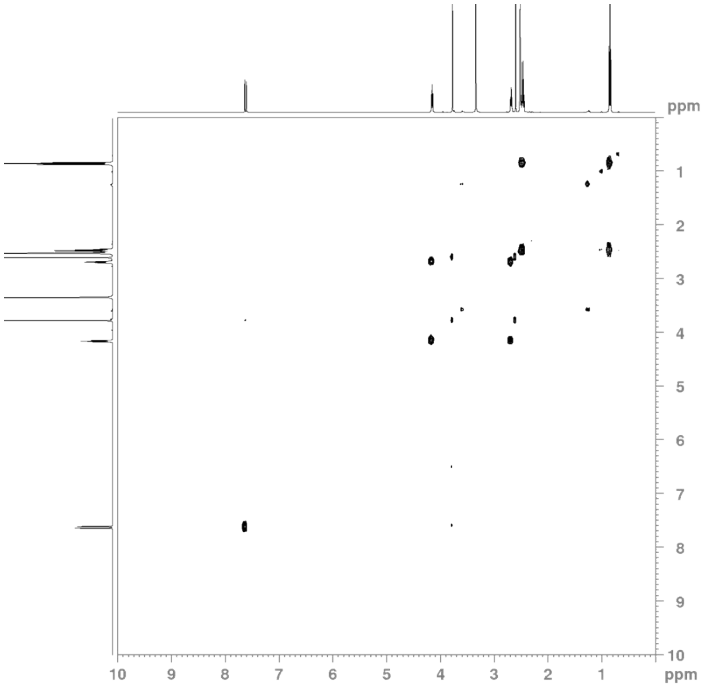

Figure S51. COSY spectrum of 1-(2-(diethylamino)ethyl)-2,3-dimethylimidazolium hexafluorophosphate [**[Et_2NEDMim][PF_6]** (400 MHz, DMSO-d6, 25 °C)

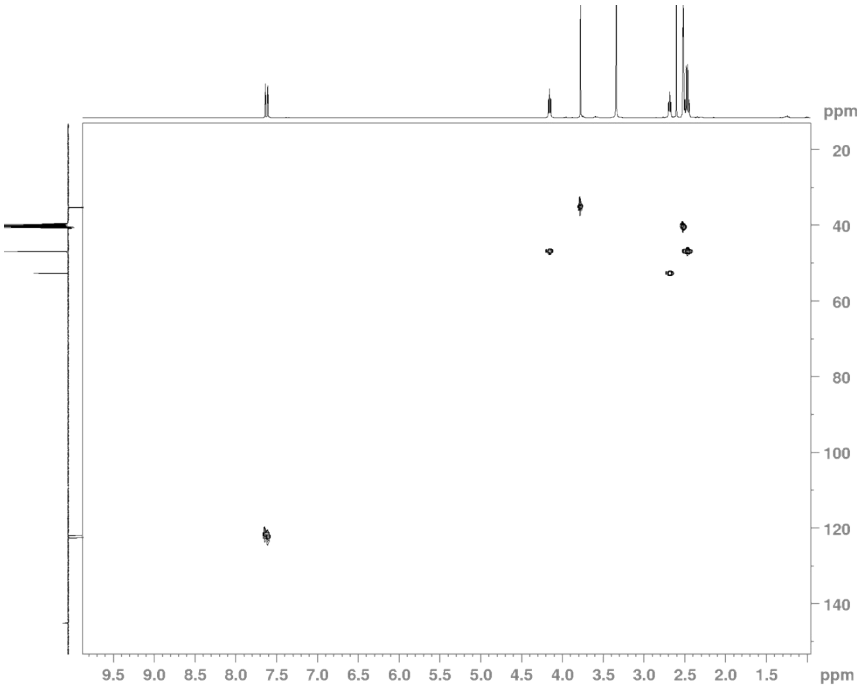

Figure S52. HSQC spectrum of 1-(2-(diethylamino)ethyl)-2,3-dimethylimidazolium hexafluorophosphate **[Et_2NEDMim][PF_6]** (400 MHz, DMSO-d6, 25 °C)

14) N-(butyl)-1,4-diazabicyclo[2.2.2]octane bis(trifluoromethylsulfonyl)imide [BuDABCO][Tf_2N]

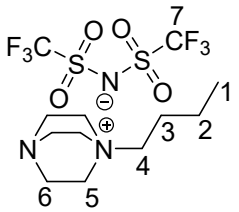

^{1}H NMR (DMSO-d6, 400 MHz, 25 °C, δ(ppm)): 3.25 (t, 6H, *J = 6.9 Hz*, 3xCH_2 cycle), 3.16 (m, 1 H, CH_2), 3.02 (t, 6H, *J = 7,8 Hz*, 3xCH_2 cycle), 1.63 (m, 2H, CH_2), 1.31 (m, 2H, *J = 7,5 Hz*, CH_2), 0.94 (t, 3H, *J = 7,3 Hz*, CH_3). **^{13}C NMR (DMSO-d6, 100 MHz, 25 °C, δ(ppm)):** 63.5 (C4), 52.0 (C6), 45.2 (C5), 23.5 (C3), 19.8 (C2), 14.0 (C1).

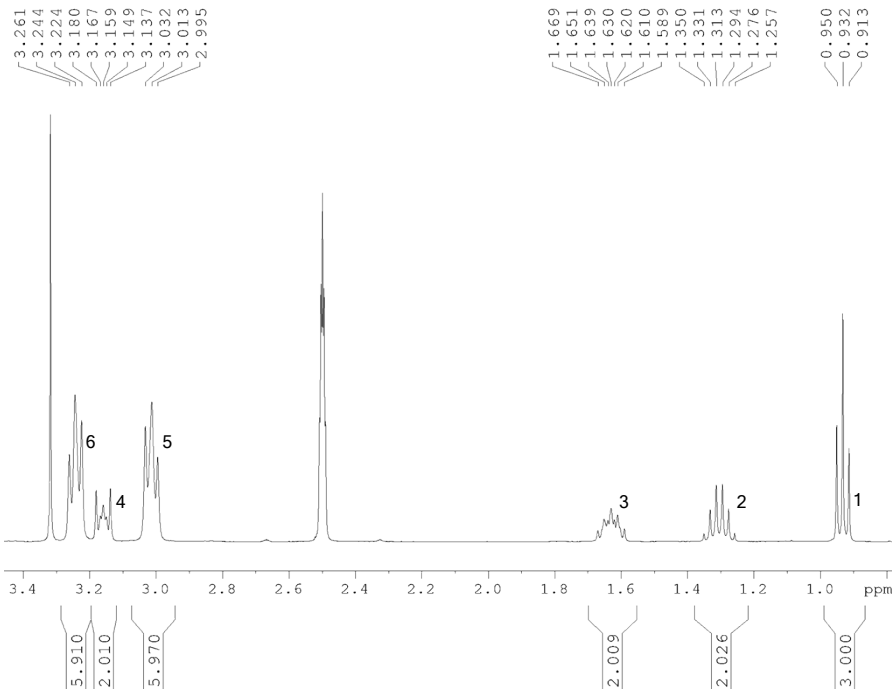

Figure S53. ^{1}H NMR spectrum of N-(butyl)-1,4-diazabicyclo[2.2.2]octane bis(trifluoromethylsulfonyl)imide **[BuDABCO][Tf$_2$N]** (400 MHz, DMSO-d6, 25 °C)

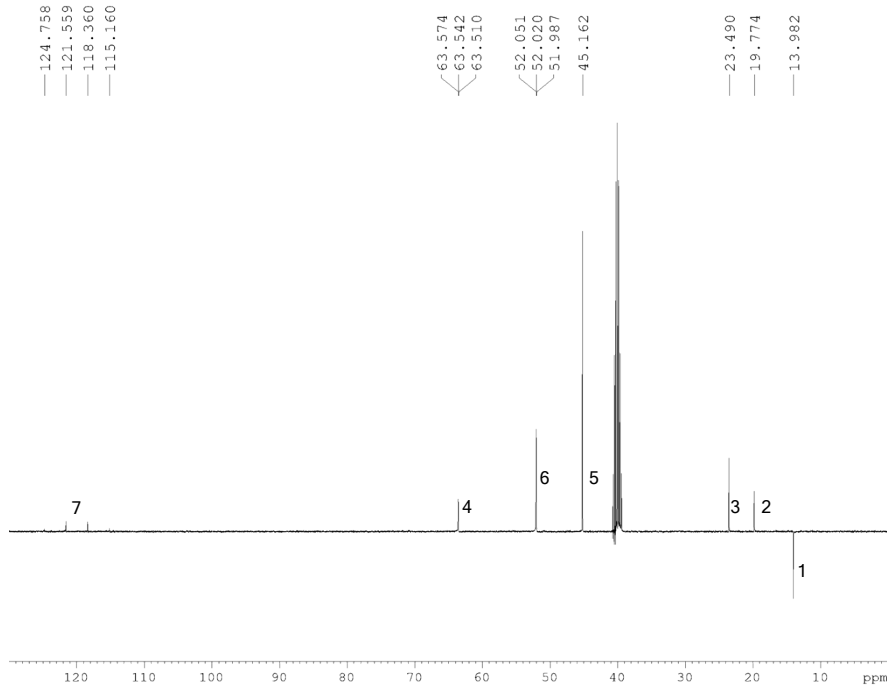

Figure S54. ^{13}C-JMOD NMR spectrum of N-(butyl)-1,4-diazabicyclo[2.2.2]octane bis(trifluoromethylsulfonyl)imide **[BuDABCO][Tf$_2$N]** (100 MHz, DMSO-d6, 25 °C)

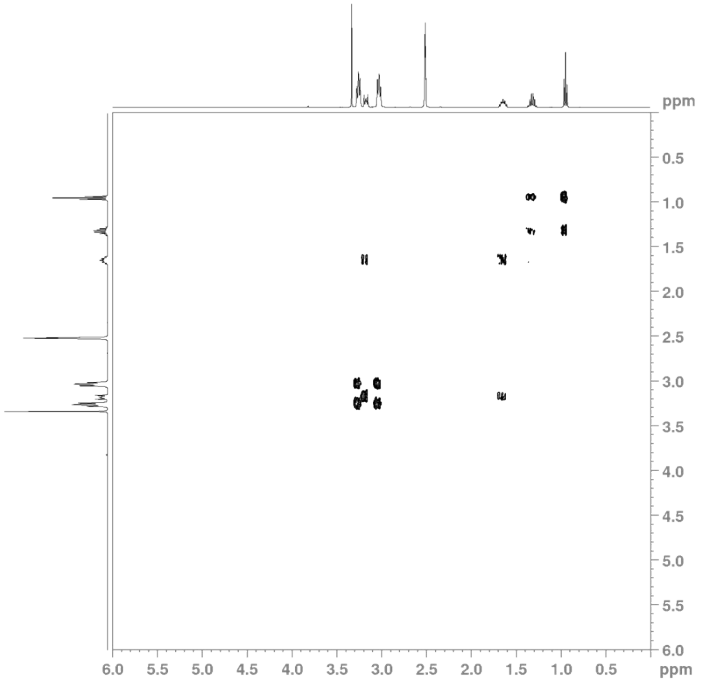

Figure S55. COSY spectrum of N-(butyl)-1,4-diazabicyclo[2.2.2]octane bis(trifluoromethylsulfonyl)imide **[BuDABCO][Tf_2N]** (400 MHz, DMSO-d6, 25 °C)

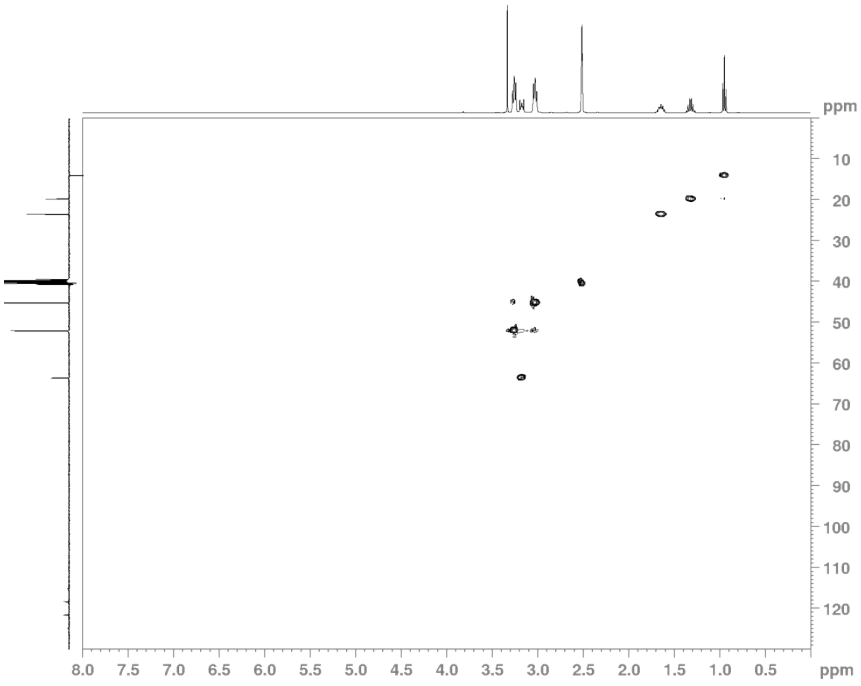

Figure S56. HSQC spectrum of N-(butyl)-1,4-diazabicyclo[2.2.2]octane bis(trifluoromethylsulfonyl)imide **[BuDABCO][Tf_2N]** (400 MHz, DMSO-d6, 25 °C)

15) 1-(2-Diethylaminoethyl)dimethylethylammonium Hexafluorophosphate $[Et_2NENMe_2Et][PF_6]$

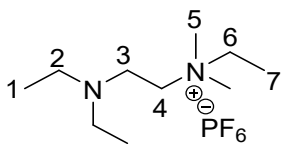

^{1}H NMR ($CDCl_3$, 400 MHz, 25 °C, δ(ppm)): 3.50 (q, 2H, *J = 7,4 Hz*, CH_2), 3.37 (t, 1 H, *J = 5,8 Hz,* CH_2), 3.14 (s, 6H, 2xCH_3), 2.77 (t, 2H, *J = 5,9 Hz,* CH_2), 2.59 (q, 4H, *J = 7,2 Hz*, 2xCH_2), 1.30 (t, 3H, *J = 7,3 Hz*, CH_3), 1.04 (t, 6H, *J = 7,2 Hz*, 2xCH_3). **^{13}C NMR ($CDCl_3$, 100 MHz, 25 °C, δ(ppm)):** 60.6 (C6), 60.2 (C3), 50.7 (C5), 47.6 (C4), 46.2 (C2), 11.1 (C1), 8.2 (C7).

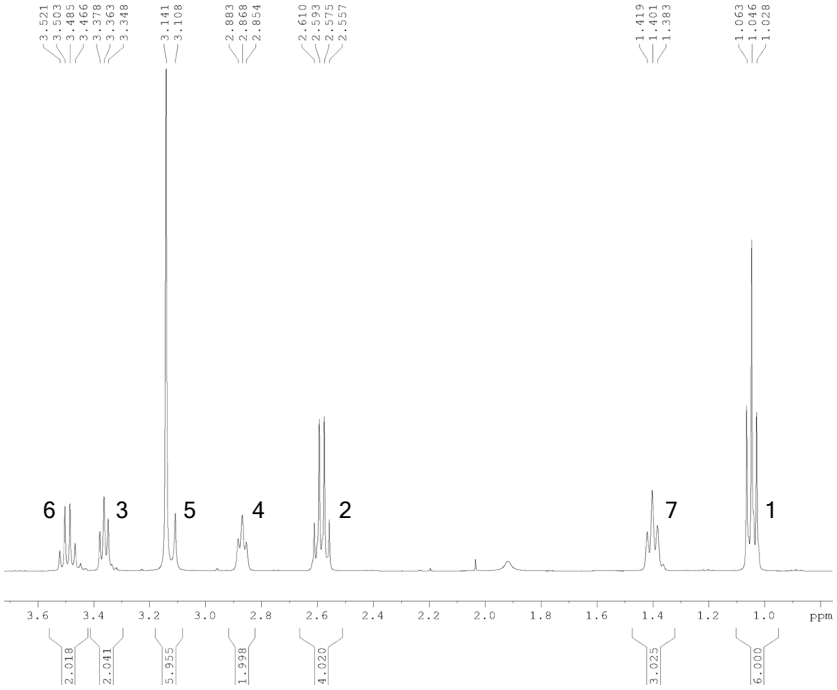

Figure S57. ^{1}H NMR spectrum of 1-(2-Diethylaminoethyl)dimethylethylammonium Hexafluorophosphate **[Et_2NENMe_2Et][PF_6]** (400 MHz, DMSO-d6, 25 °C)

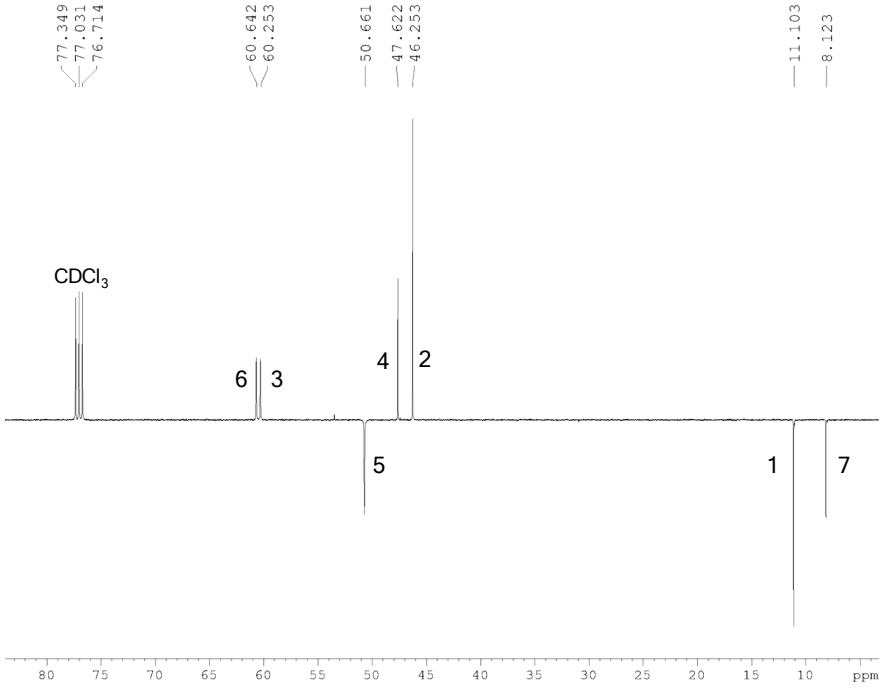

Figure S58. ^{13}C-JMOD NMR spectrum of 1-(2-Diethylaminoethyl)dimethylethylammonium Hexafluorophosphate **[Et_2NENMe_2Et][PF_6]** (100 MHz, DMSO-d6, 25 °C)

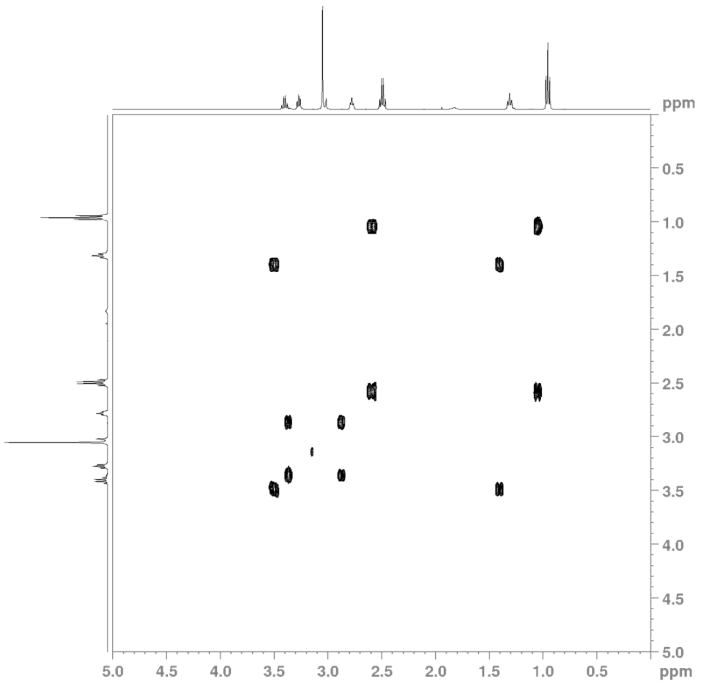

Figure S59. COSY spectrum of 1-(2-Diethylaminoethyl)dimethylethylammonium Hexafluorophosphate **[Et_2NENMe_2Et][PF_6]** (400 MHz, DMSO-d6, 25 °C)

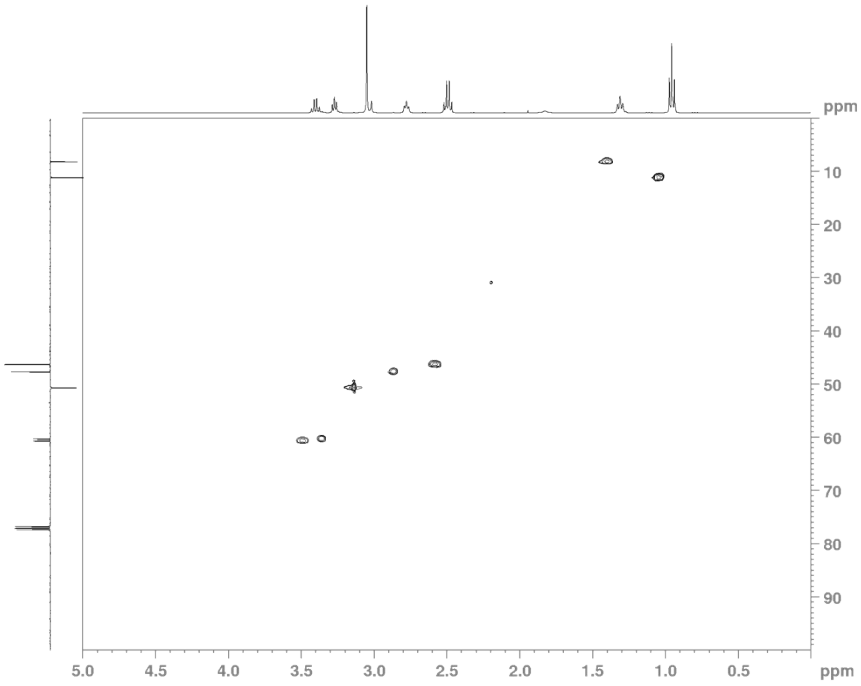

Figure S60. HSQC spectrum of 1-(2-Diethylaminoethyl)dimethylethylammonium Hexafluorophosphate **[Et_2NENMe_2Et][PF_6]** (400 MHz, DMSO-d6, 25 °C)

16) Stability of [PEEtOHim][PF_6], [PEMim][PF_6] and [PEMim][Tf_2N] under optimal conditions

The stability of the ionic liquid **[PEEtOHim][PF_6]** was investigated (**Figure S61**). The ^{1}H NMR spectrum of **[PEEtOHim][PF_6]** is shown **(a)**. Spectrum **(b)** shows that **[PEEtOHim][PF_6]**

remains stable under the reaction conditions, at 80 °C and 80 bar of CO/H_2 for 6 h in 10 mL of heptane. **[PEEtOHim][PF_6]** is equally stable upon the addition of the catalyst $Rh(acac)CO_2$ **(c)**. Finally, the NMR analysis **(d)** of **[PEEtOHim][PF_6]** after 8 recycling cycles demonstrates the robustness of the ionic liquid under these conditions.

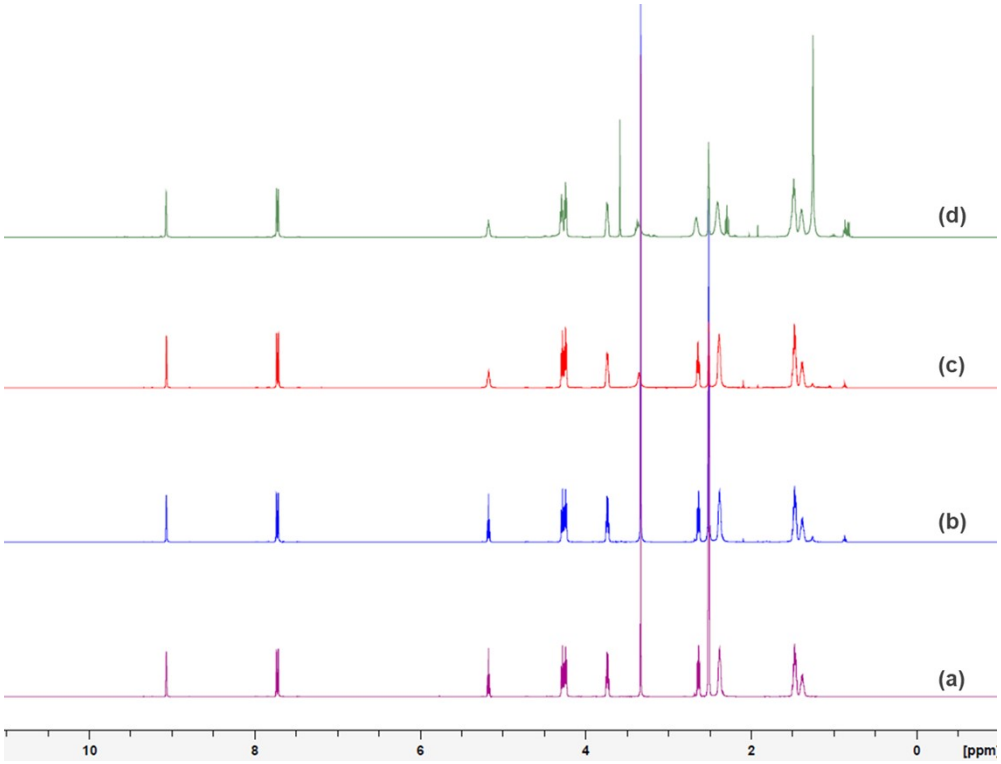

Figure S61. Superposition of ^1H NMR spectrum of (a) **[PEEtOHim][PF_6]**, (b) **[PEEtOHim][PF_6]** after 6 h at 80°C and 80 Bar of CO/H_2 pressure (ratio 1/1), (c) **[PEEtOHim][PF_6]** after 16 h at 80°C and 80 Bar of CO/H_2 pressure (ratio 1/1) in presence of $Rh(acac)(CO)_2$, (d) **[PEEtOHim][PF_6]** after 8 runs (400 MHz, DMSO-d6, 25 °C)

Control measurements by ^{19}F NMR were also carried out to assess the stability of the PF_6^- and Tf_2N^- anions under the various catalytic conditions.

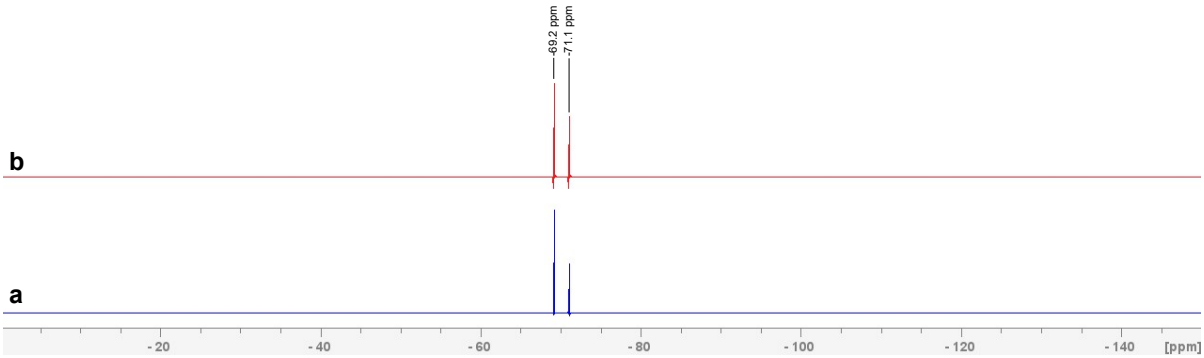

Figure S62. Superposition of ^{19}F NMR spectrum of (a) pure **[PEEtOHim][PF_6]** and (b) after recycling (5 run of 6h at 80°C and 80 Bar of CO/H_2 pressure (ratio 1/1)) followed by air storage for three months (376 MHz, DMSO-d_6, 25 °C).

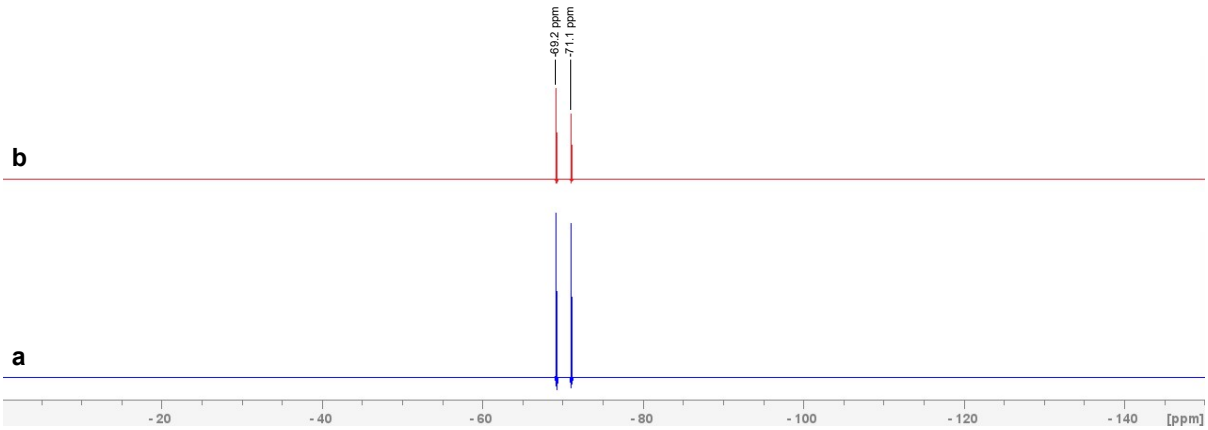

Figure S63. Superposition of ^{19}F NMR spectra of (a) pure **[PEMim][PF_6]** and (b) after reaction (6h at 80°C and 80 Bar of CO/H_2 pressure (ratio 1/1)) followed by air storage for one year (376 MHz, DMSO-d_6, 25 °C).

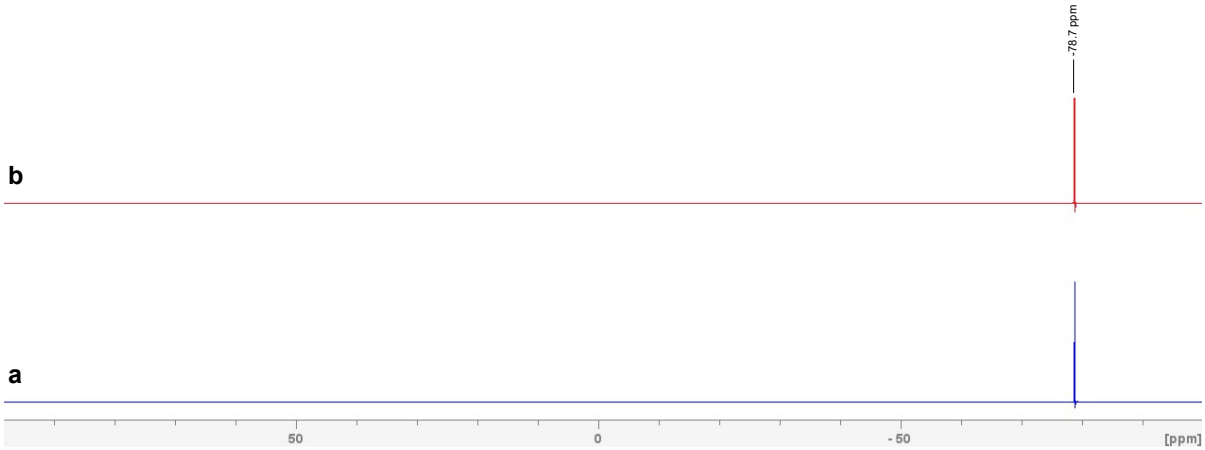

Figure S64. Superposition of ^{19}F NMR spectra of (a) pure **[PEMim][Tf_2N]** and (b) after reaction (6h at 80°C and 80 Bar of CO/H_2 pressure (ratio 1/1)) followed by air storage for one year (376 MHz, DMSO-d_6, 25 °C).

IV) IR-ATR and NMR characterization of anionic metallic species

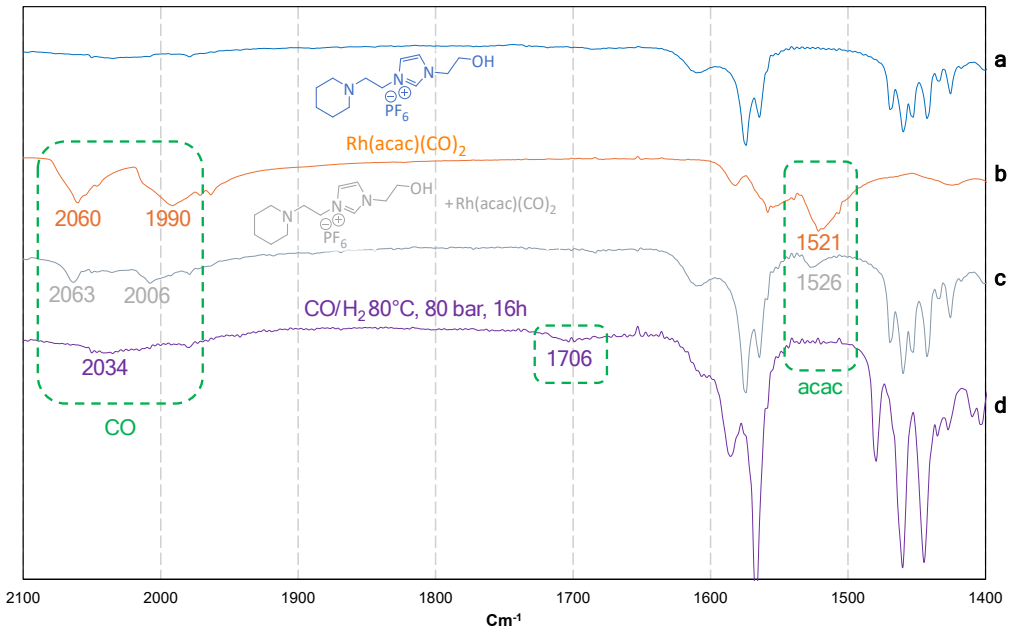

Figure S65. (a) **[PEEtOHim][PF$_6$]**, (b) Rh(acac)(CO)$_2$, (c) **[PEEtOHim][PF$_6$]** and Rh(acac)(CO)$_2$ after grinding, (d) **[PEEtOHim][PF$_6$]** and Rh(acac)(CO)$_2$ after 16 h at 80°C and 80 Bar of CO/H$_2$ pressure (ratio 1/1) in presence of Rh(acac)(CO)$_2$.

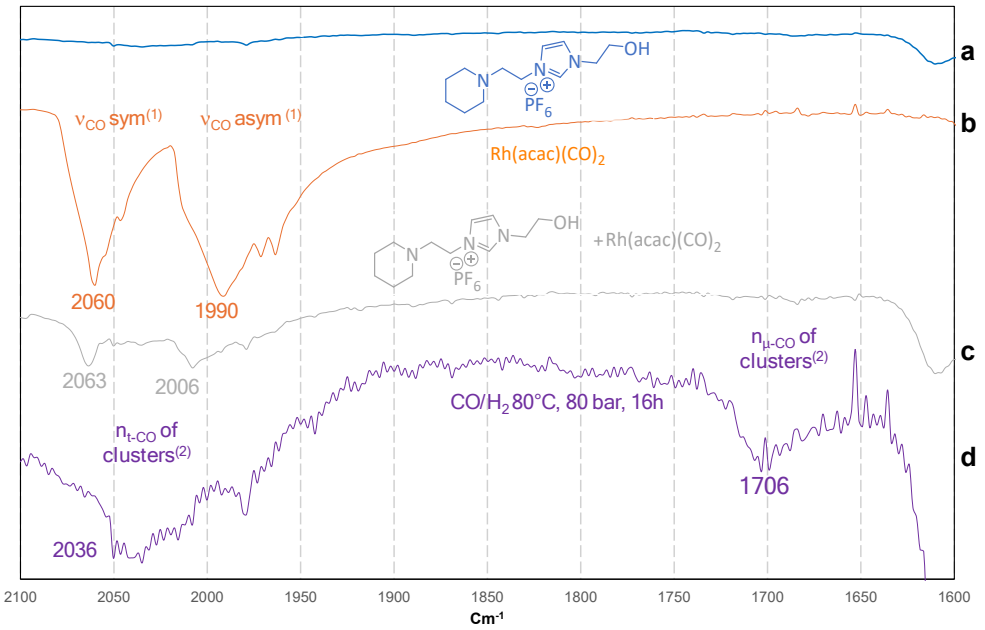

Figure S66. zoomed-in region highlighting key absorptions (a) **[PEEtOHim][PF$_6$]**, (b) Rh(acac)(CO)$_2$,(c) **[PEEtOHim][PF$_6$]** and Rh(acac)(CO)$_2$ after grinding, (d) **[PEEtOHim][PF$_6$]** and Rh(acac)(CO)$_2$ after 16 h at 80°C and 80 Bar of CO/H$_2$ pressure (ratio 1/1) in presence of Rh(acac)(CO)$_2$. (1) Symmetric and asymmetric stretching of the two CO ligands in Rh(acac)(CO)$_2$ (2060 and 1990 cm^{-1}, respectively). (2) Stretching of terminal CO ligands (t CO) and bridging CO ligands (μ-CO) in rhodium clusters (2036 and 1706 cm^{-1}, respectively).

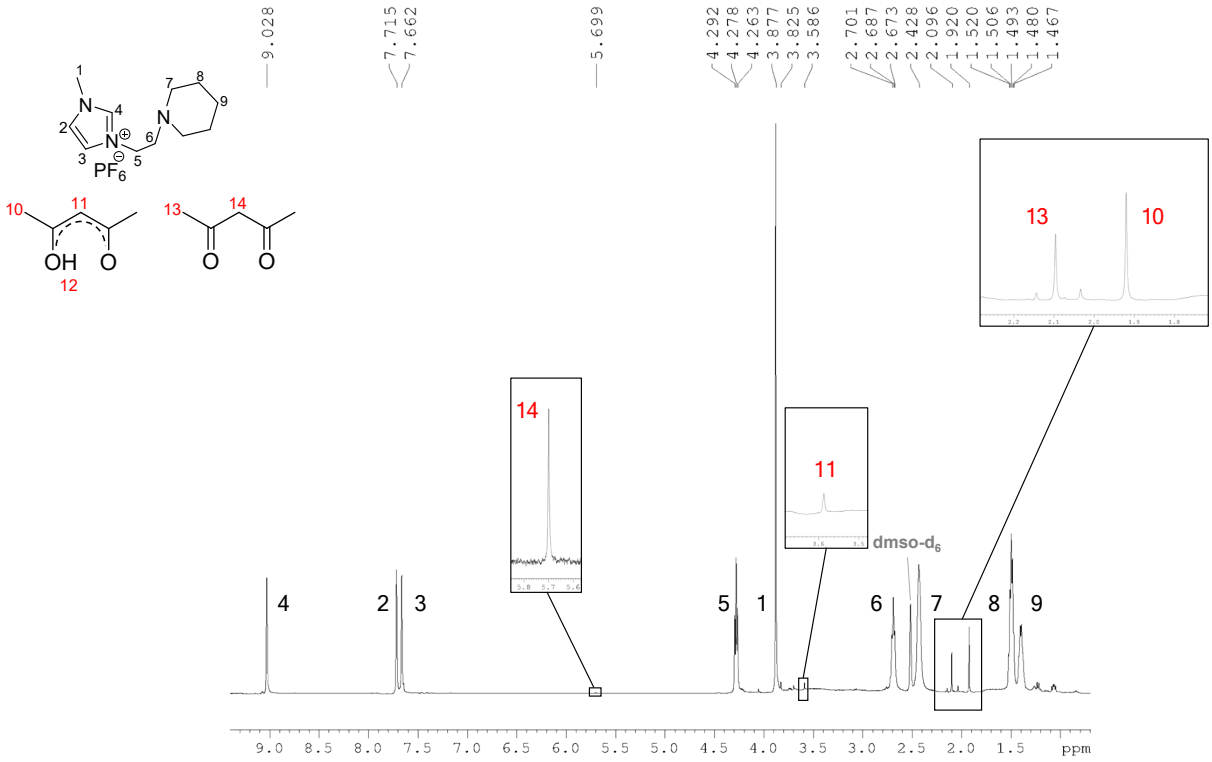

Figure S67. ^{1}H NMR spectrum of 1-(2-piperid-1-yl-ethyl)-3-methylimidazolium hexafluorophosphate **[PEMim][PF$_6$]** with Rh(acac)(CO)$_2$ (LI/Rh = 5), analysis following treatment under **1:1 CO/H$_2$** (3 h); tube sealed under **N$_2$** atmosphere. (400 MHz, DMSO-d6, 25 °C)

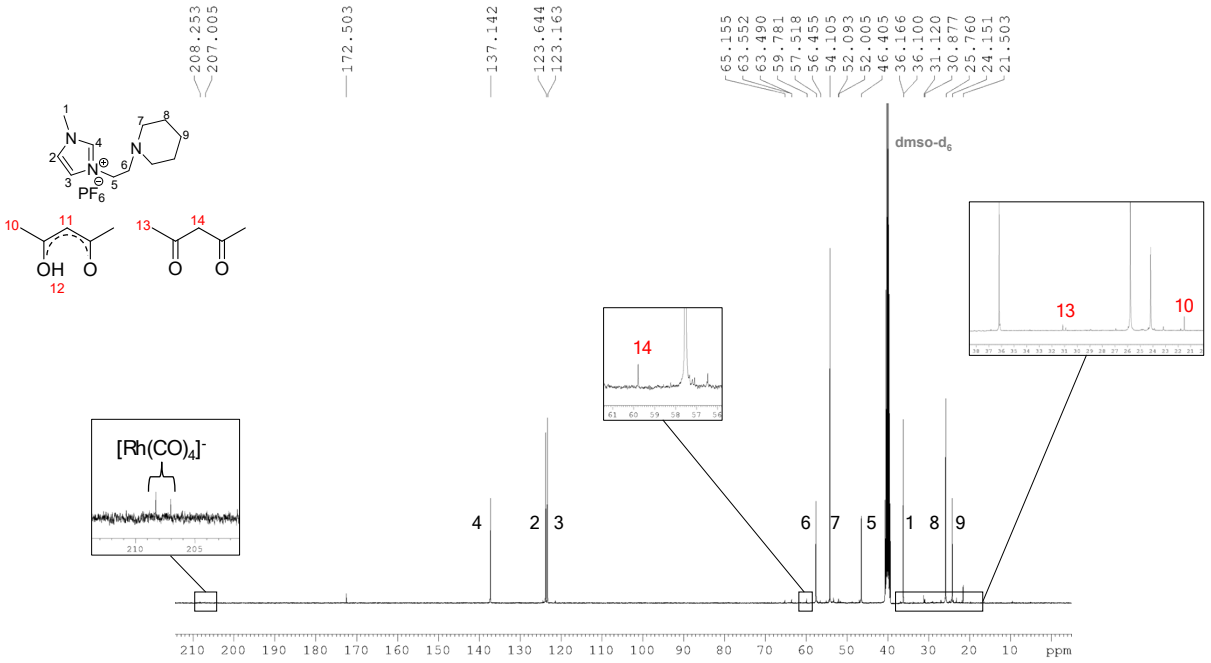

Figure S68. ^{13}C NMR spectrum of 1-(2-piperid-1-yl-ethyl)-3-methylimidazolium hexafluorophosphate **[PEMim][PF$_6$]** with Rh(acac)(CO)$_2$ (LI/Rh = 5), analysis following treatment under **1:1 CO/H$_2$** (3 h); tube sealed under **N$_2$** atmosphere. (100 MHz, DMSO-d6, 25 °C)

To gain mechanistic insight we raised the Rh concentration ([PEMim][PF$_6$]/Rh = 5) and acquired ^{13}C NMR of the IL phase following syngas exposure. The ^{1}H spectrum (Figure S64) illustrates that following syngas treatment, signals corresponding to free acetylacetone appear

at δ 1.9 ppm (s), 2.1 ppm (s), and 5.7 ppm (s). This indicates that the acac ligand is displaced from the rhodium coordination sphere and subsequently protonated. Additionally, the ^{13}C NMR spectrum (Figure S65) exhibits a characteristic doublet at δ 207.0 and 208.2 ppm, confirming the formation of the $[Rh(CO)_4]^-$ species.

V) Single-Crystal DRX characterization of ligands derivates

Table S1. Crystal data and structure refinement			
Compound Name	[PEDMim][PF_6]	[PEMim][PF_6]	[PEEtOHim][PF_6]
Empirical formula	$C_{12}H_{22}N_3 \cdot F_6P$	$C_{11}H_{20}N_3 \cdot F_6P$	$C_{12}H_{22}N_3O \cdot F_6P$
Formula weight	353.29	339.27	369.29
Temperature/K	120	120	100
Crystal system	Orthorhombic	Monoclinic	Monoclinic
Space group	$P2_12_12_1$	$P2_1/c$	$P2_1/n$
a/Å	7.1533 (3)	16.5378 (8)	7.1044 (2)
b/Å	9.2038 (3)	9.0955 (4)	26.2819 (6)
c/Å	24.3489 (10)	10.1158 (5)	c = 8.8053 (2)
α/°	90	90	90
β/°	90	95.695 (2)	103.780 (1)
γ/°	90	90	90
Volume/Å^3	1603.07 (11)	1514.10 (12)	1596.78 (7)
Z	4	4	4
ρ_{calc}Mg/m^3	1.464	1.488	1.536
μ/mm^{-1}	0.23	0.24	0.24
F(000)	736	704	768
Crystal size/mm^3	0.3 × 0.25 × 0.19	0.29 × 0.26 × 0.25	0.29 × 0.05 × 0.04
Radiation	Mo Kα	Mo Kα	Mo Kα
2Θ range for data collection/°	3.4 - 52.8	5.0 – 61.0	5.0 – 61.0
Index ranges	h = -8→8 k = -11→10 l = -30→30	h = -23→23 k = -12→12 l = -13→14	h = -10→10 k = -37→37 l = -12→12
Reflections collected	37557	52517	67947
Independent reflections	3275	4611	4866
R_{int}	0.025	0.027	0.048
Data/restraints/parameters	3275/18/238	4611/15/246	4866/0/211
Goodness-of-fit on F^2	1.06	1.05	1.06
$R_1(F^2 > 2\sigma(F^2)$ /all)	0.0248/0.0254	0.0319/0.0356	0.0336/0.0406
$wR_2(F^2 > 2\sigma(F^2)$ /all)	0.0664/0.0669	0.0915/0.0942	0.0916/0.0950
Largest diff. peak/hole / e Å^{-3}	0.18	0.30	0.47
Deepest diff. peak/hole / e Å^{-3}	-0.22	-0.40	-0.34

VI) Comparative assessment of ionic liquid basicity

The Hammett function measures basicity by evaluating the relative dissociation of acidic indicators in solution. When an acid is dissolved in an ionic liquid, changes in its degree of dissociation reflect whether the medium behaves as neutral, acidic, or basic. The basicity of an ionic liquid can therefore be estimated by UV-visible spectrophotometry using the reverse Hammett function (H_). However, this method has inherent limitations: it assumes complete dissociation of the indicator and requires dissolving the ionic liquid in a solvent, making the

measured values strongly solvent-dependent. In particular, methanol, used here as the solvent, is a protic medium capable of donating hydrogen bonds, which can attenuate the effective basicity of the amine compared to what would be expected in the aprotic IL phase; an effect that is partially mitigated in the protic [PEEtOHim][PF_6] ionic liquid. In the neat ionic liquid, the absence of such protic solvation and the higher local concentration of coordinating groups are therefore likely to enhance the effective electron-donating ability toward rhodium. For these reasons, the Hammett values should be interpreted as comparative indicators rather than absolute descriptors of basicity under catalytic conditions.

The indicators, their concentrations, and the ILs concentrations employed were: bromocresol green ($pK_{HI} = 9.8$; $[HI] = 5 \times 10^{-5}\,M$; $[IL] = 2{,}8 \times 10^{-3}\,M$) and bromophenol blue ($pK_{HI} = 8{,}9$; $[HI] = 5 \times 10^{-5}\,M$; $[IL] = 2{,}8 \times 10^{-3}\,M$). The results obtained from the UV/vis experiments are summarized in Table 2.

Table S2. H_ values

Ils	H_
Bromocresol Green	
[PEEtOHim][PF_6]	9.43
[PEMim][PF_6]	9.47
[Et_2NEMim][PF_6]	9.10
[Et_2NEDMim][PF_6]	9.30
Bromophenol Blue	
[Et_2NENMe_2Et][PF_6]	8.70
[BuDABCO][Tf_2N]	H_<8.70

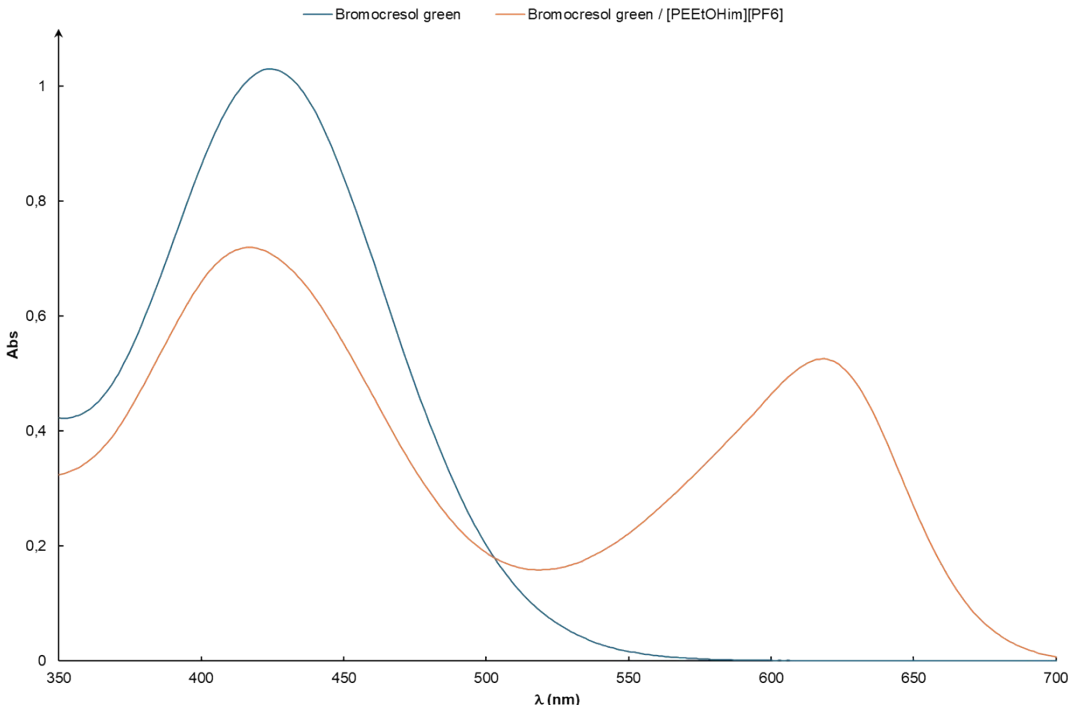

Figure S69. UV-vis spectra of bromocresol green collected in MeOH and at a fixed concentration of **[PEEtOHim][PF_6]**

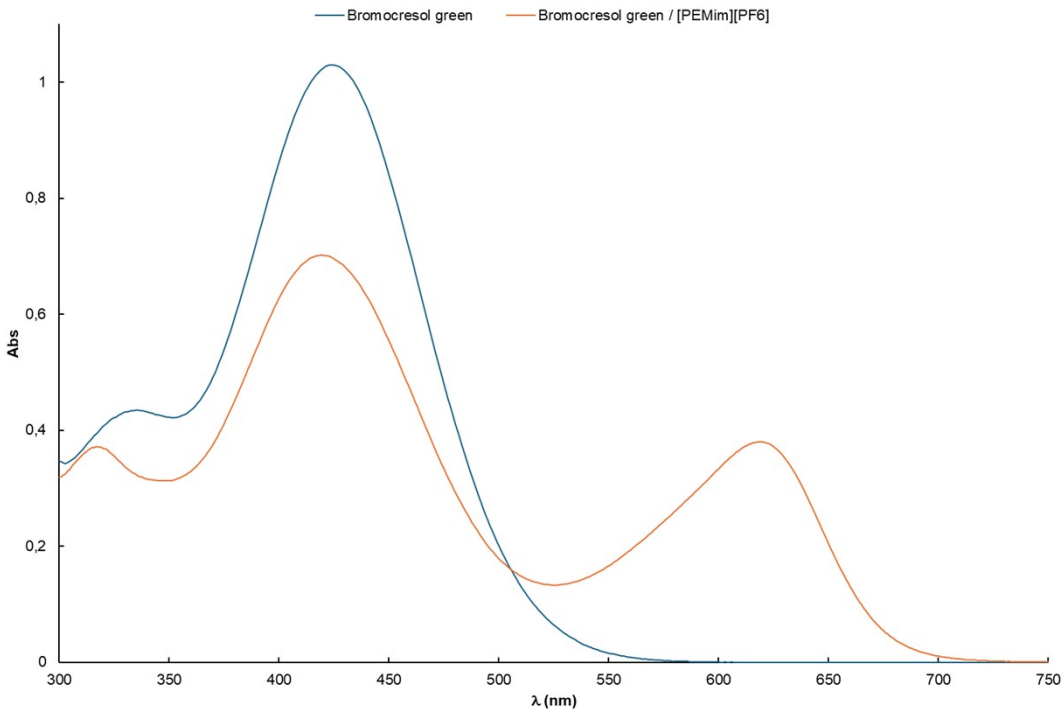

Figure S70. UV-vis spectra of bromocresol green collected in MeOH and at a fixed concentration of **[PEMim][PF_6]**

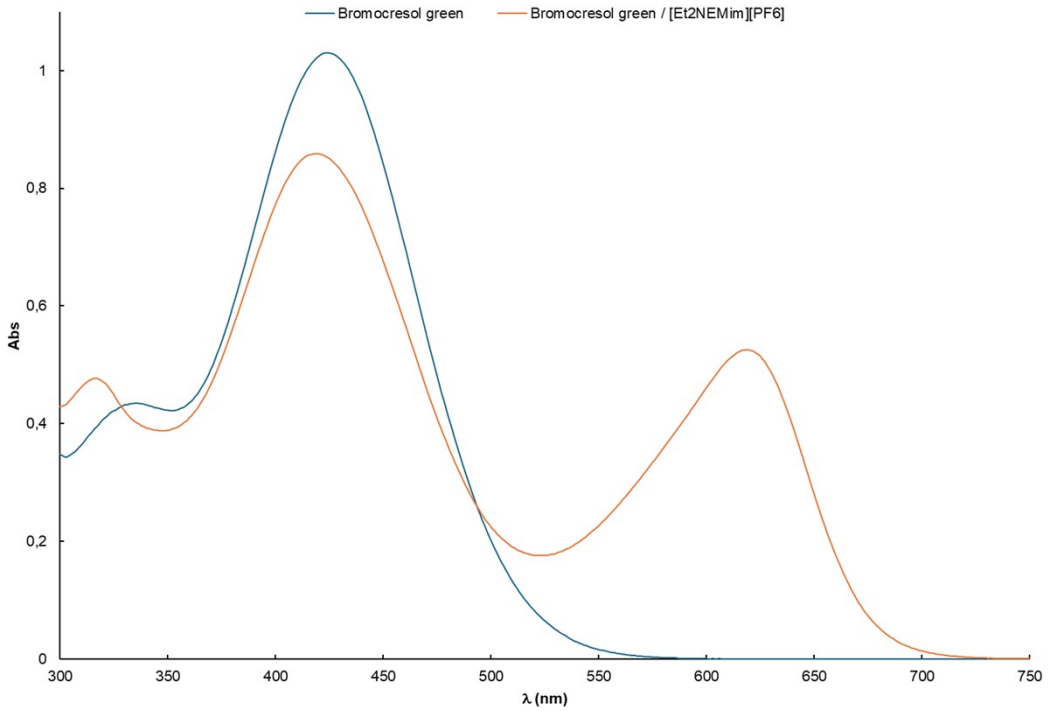

Figure S71. UV-vis spectra of bromocresol green collected in MeOH and at a fixed concentration of **[Et_2NEMim][PF_6]**

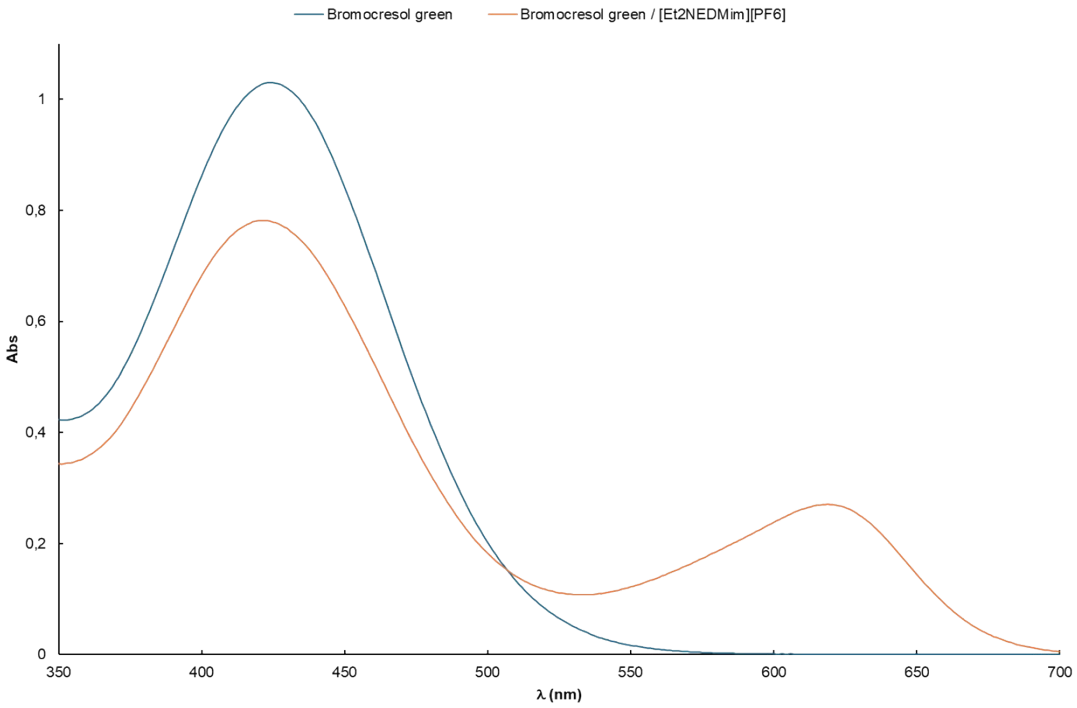

Figure S72. UV-vis spectra of bromocresol green collected in MeOH and at a fixed concentration of **[Et_2NEDMim][PF_6]**

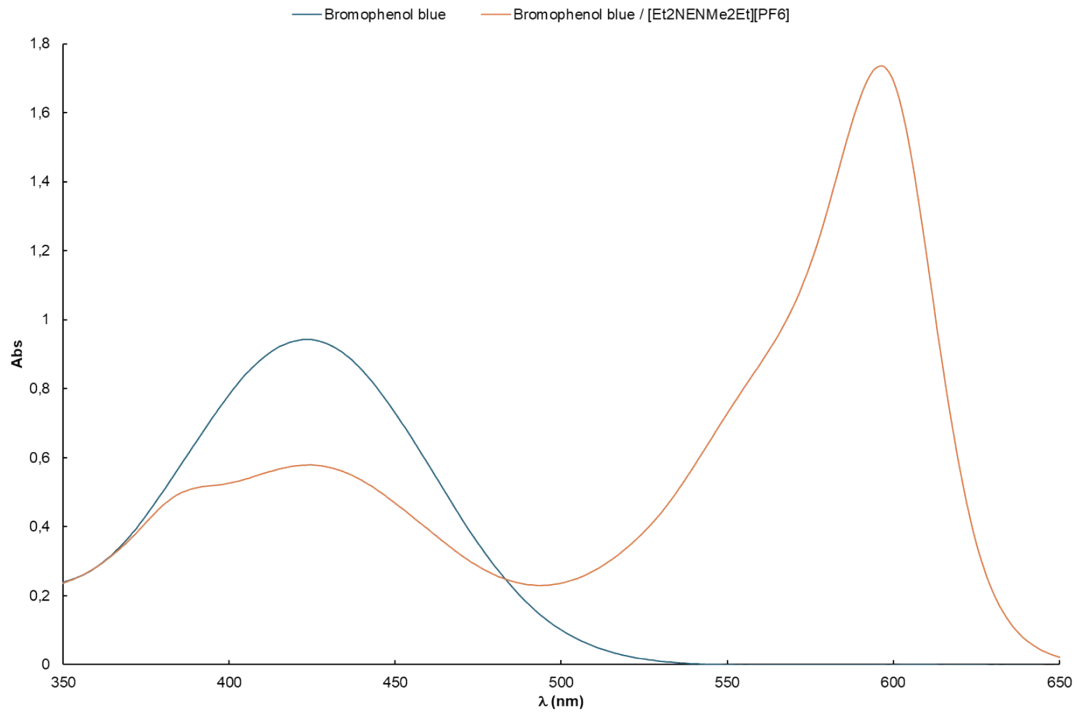

Figure S73. UV-vis spectra of bromocresol green collected in MeOH and at a fixed concentration of **[Et_2NENMe_2Et][PF_6]**

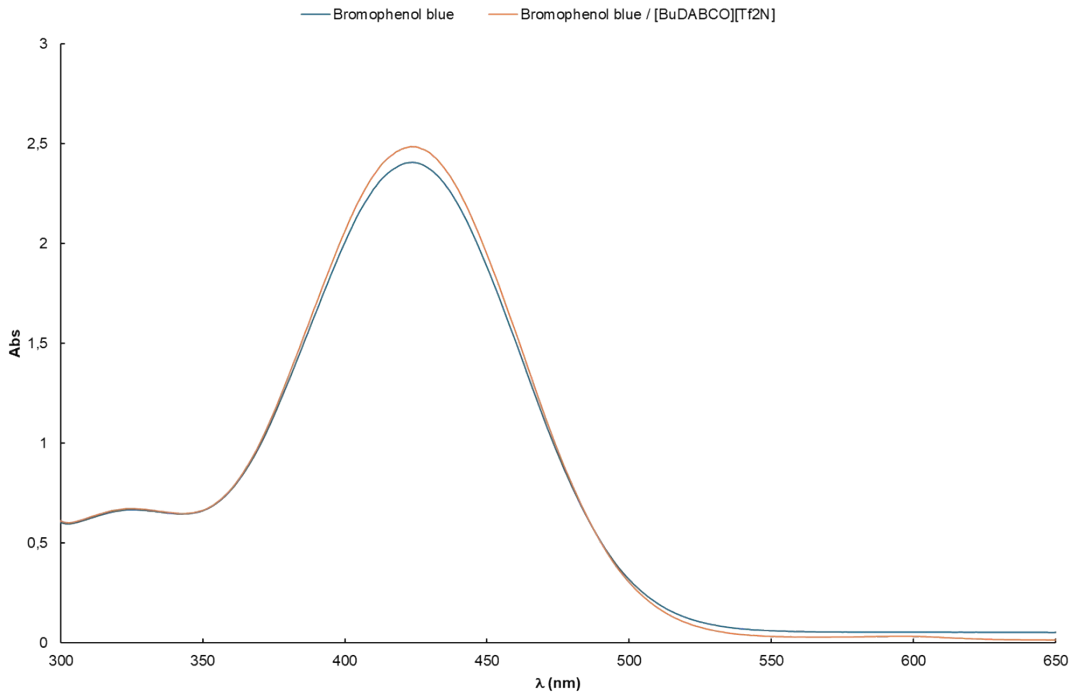

Figure S74. UV-vis spectra of bromophenol blue collected in MeOH and at a fixed concentration of **[BuDABCO][Tf_2N]**

VII) DSC and TGA characterization of ligands derivates

Table S3. Overview of Melting Points Obtained from DSC Onset Analysis

Ligands	Melting point (°C)
[PEEtOHim][PF_6]	62.1
[PEMim][PF_6]	33.0
[PEMim][BF_4]	< -20
[PEMim][Tf_2N]	< -20
[PEMim][$(CN)_2N$]	< -20
[PEDMim][PF_6]	125.4
[Et_2NEMim][PF_6]	< -20
[Et_2NEMim][Tf_2N]	< -20
[Et_2NEDMim][PF_6]	82.0
[BuDABCO][Tf_2N]	87.3
[Et_2NNMe_2Et][PF_6]	79.8

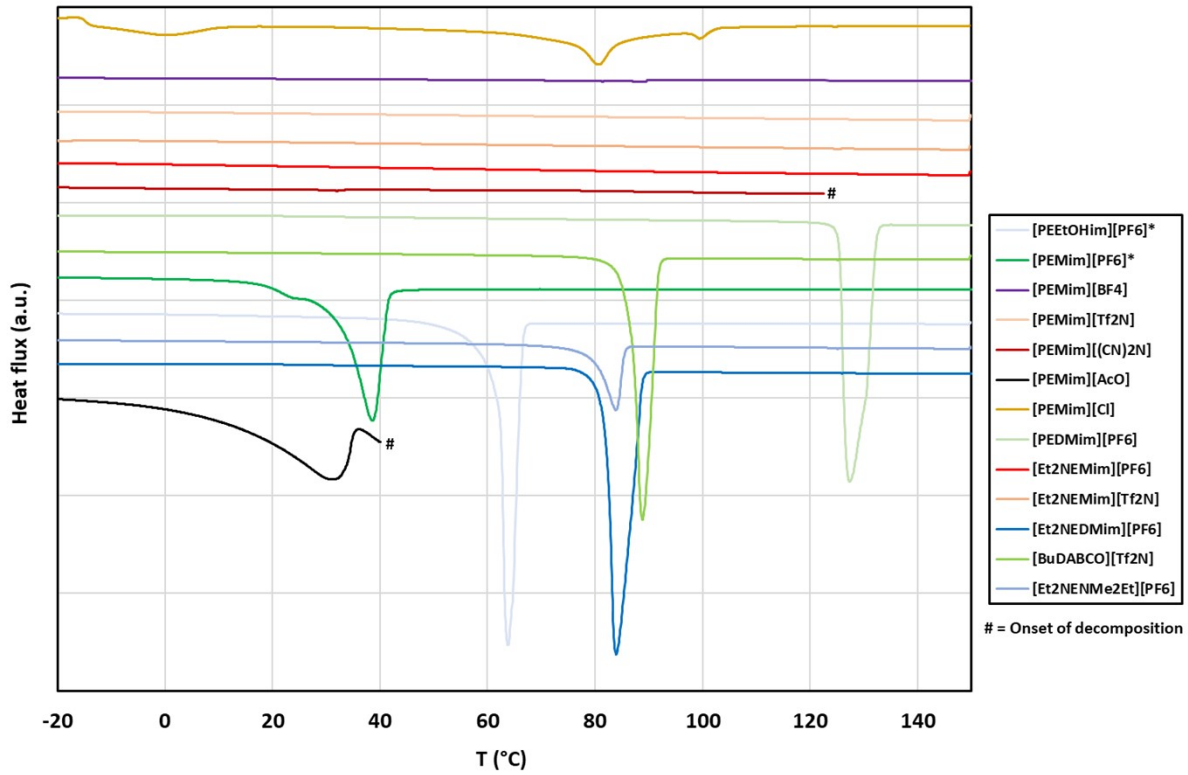

Figure S75. Differential Scanning Calorimetry Thermograms of the ligands
(*) melting was measured during the first heating run

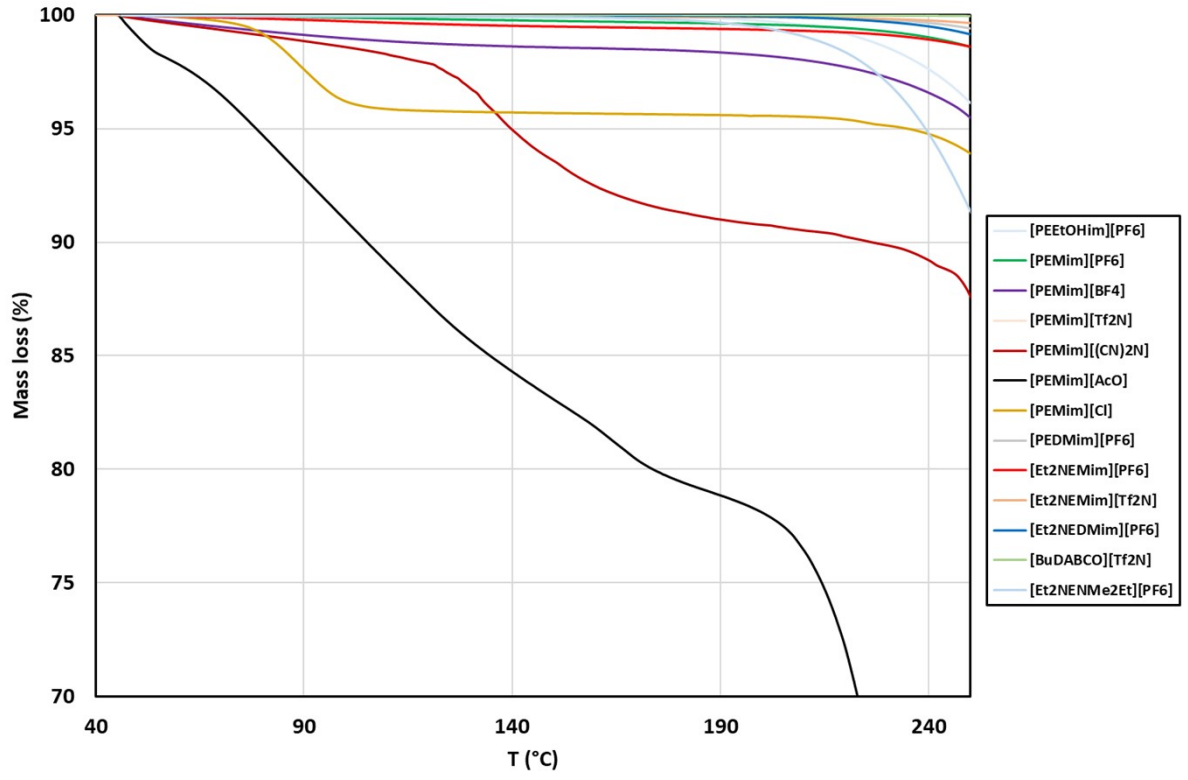

Figure S76. Thermogravimetric Analysis (TGA) Curves of the ligands

VIII) TEM of ionic liquids after reaction

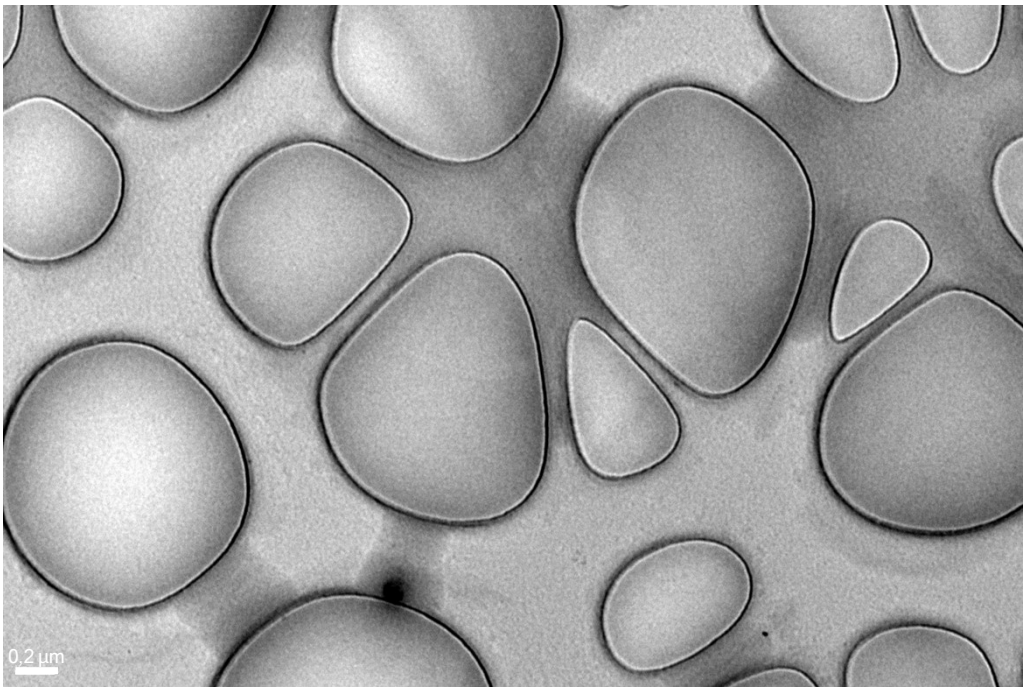

Figure S77. TEM image of **[PEMim][PF_6]** after reaction, condition reaction: Rh(acac)$(CO)_2$ (6.0 mg, 23.3 µmol, 1 equiv), **[PEMIM][PF_6]** (ratio N/Rh = 75), Methyl 10-undecenoate (1.325 mL, 5.9 mmol), heptane (10 mL), 80 bar CO/H_2 (1:1), 6 h

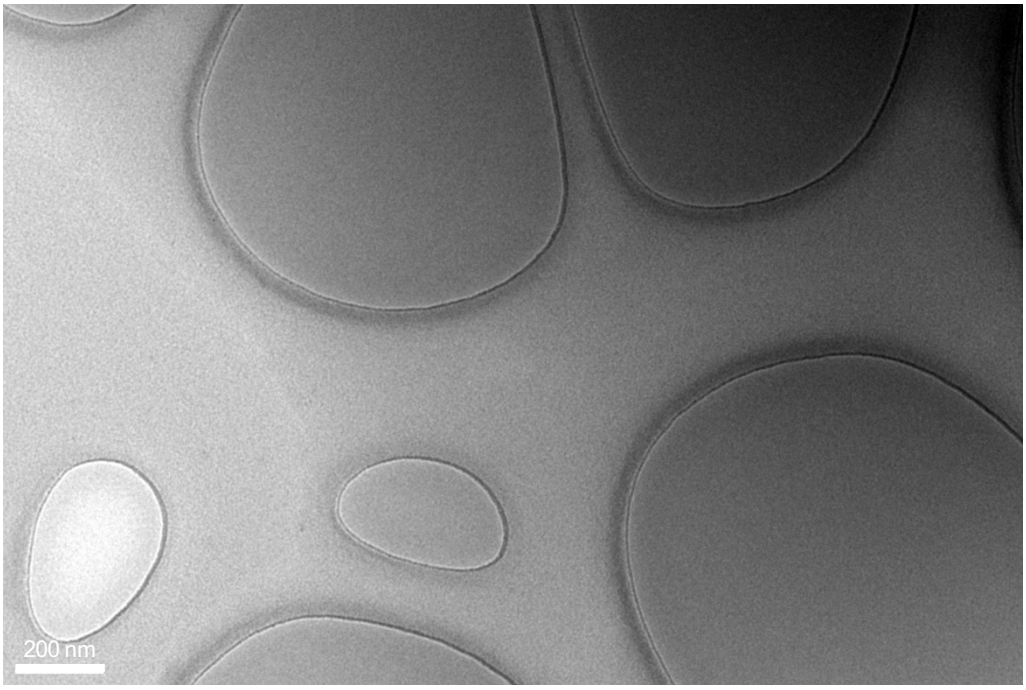

Figure S78. TEM image of **[PEMim][PF_6]** after reaction, condition reaction: Rh(acac)$(CO)_2$ (6.0 mg, 23.3 µmol, 1 equiv), **[PEMIM][PF_6]** (ratio N/Rh = 75), Methyl 10-undecenoate (1.325 mL, 5.9 mmol), heptane (10 mL), 80 bar CO/H_2 (1:1), 6 h

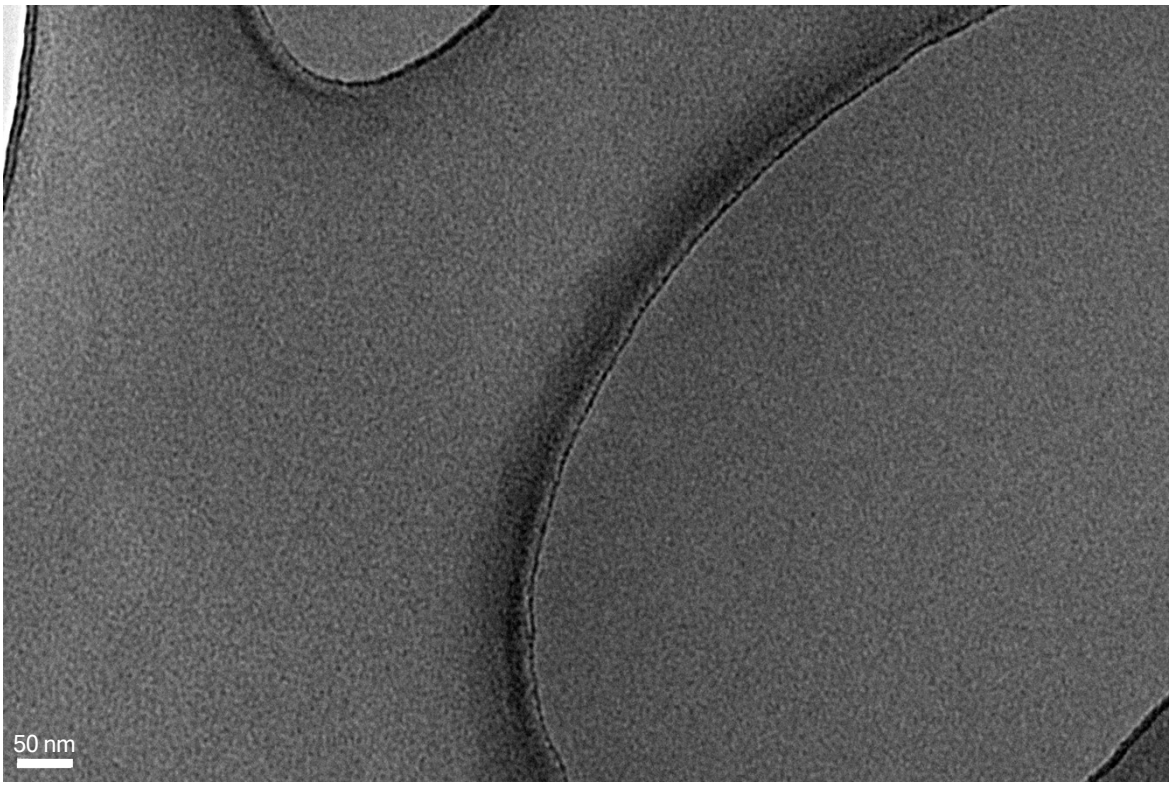

Figure S79. TEM image of **[PEMim][PF_6]** after reaction, condition reaction: Rh(acac)$(CO)_2$ (6.0 mg, 23.3 μmol, 1 equiv), **[PEMIM][PF_6]** (ratio N/Rh = 75), Methyl 10-undecenoate (1.325 mL, 5.9 mmol), heptane (10 mL), 80 bar CO/H_2 (1:1), 6 h

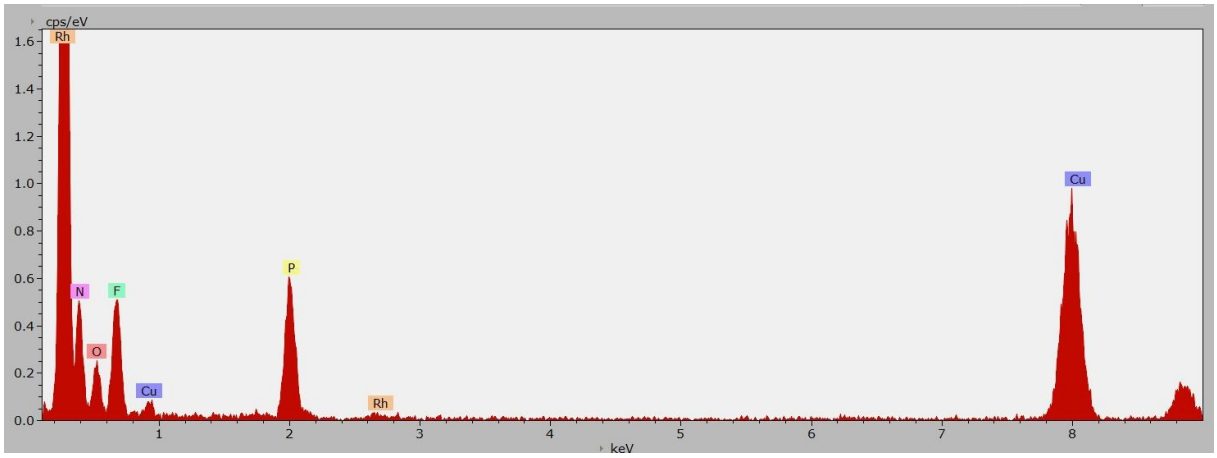

Figure S80. EDX spectrum of **[PEMIM][PF_6]** after reaction, condition reaction: Rh(acac)$(CO)_2$ (6.0 mg, 23.3 μmol, 1 equiv), **[PEMIM][PF_6]** (ratio N/Rh = 75), Methyl 10-undecenoate (1.325 mL, 5.9 mmol), heptane (10 mL), 80 bar CO/H_2 (1:1), 6 h

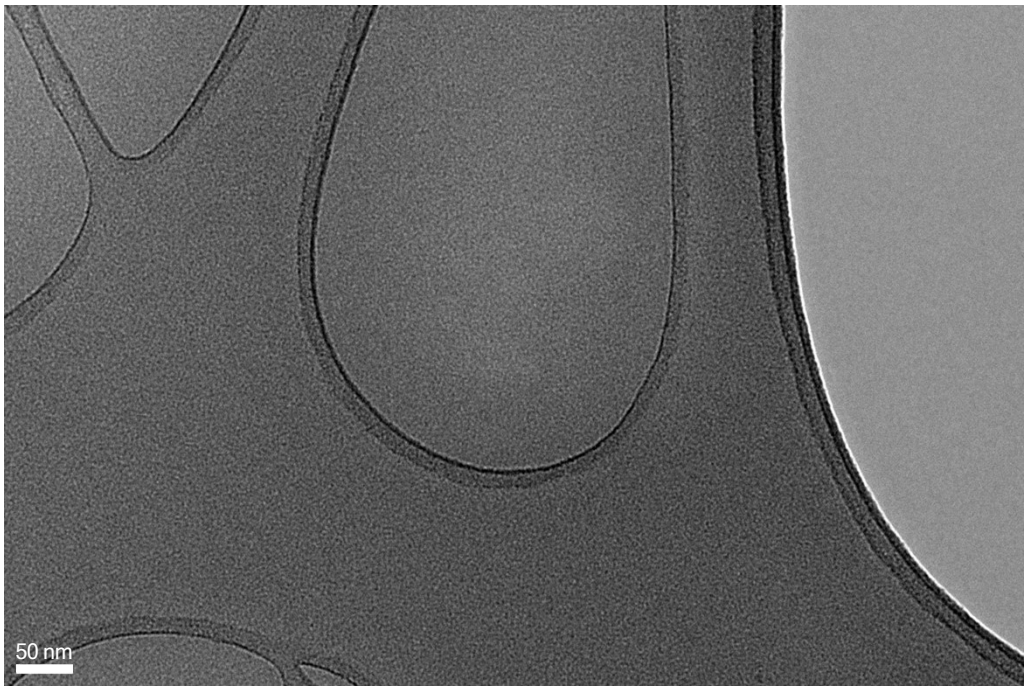

Figure S81. TEM image of **[PEMim][PF_6]** after reaction, 1 month in air, condition reaction: Rh(acac)$(CO)_2$ (6.0 mg, 23.3 µmol, 1 equiv), **[PEMIM][PF_6]** (ratio N/Rh = 75), Methyl 10-undecenoate (1.325 mL, 5.9 mmol), heptane (10 mL), 80 bar CO/H_2 (1:1), 6 h

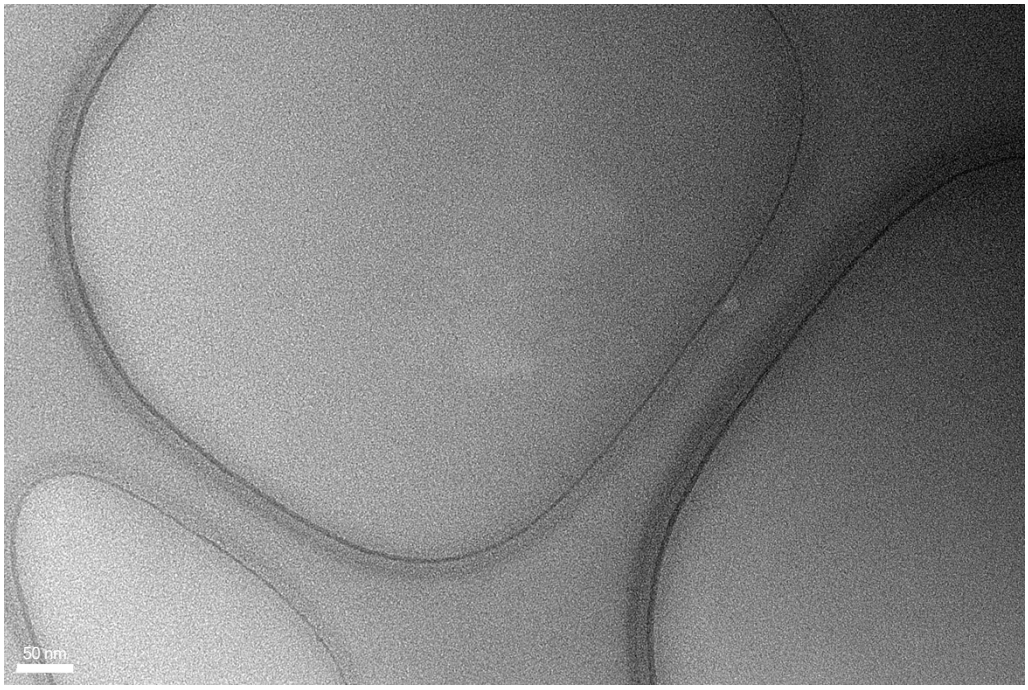

Figure S82. TEM image of **[PEMim][PF_6]** after reaction, 1 month in air, condition reaction: Rh(acac)$(CO)_2$ (6.0 mg, 23.3 µmol, 1 equiv), **[PEMIM][PF_6]** (ratio N/Rh = 75), Methyl 10-undecenoate (1.325 mL, 5.9 mmol), heptane (10 mL), 80 bar CO/H_2 (1:1), 6 h

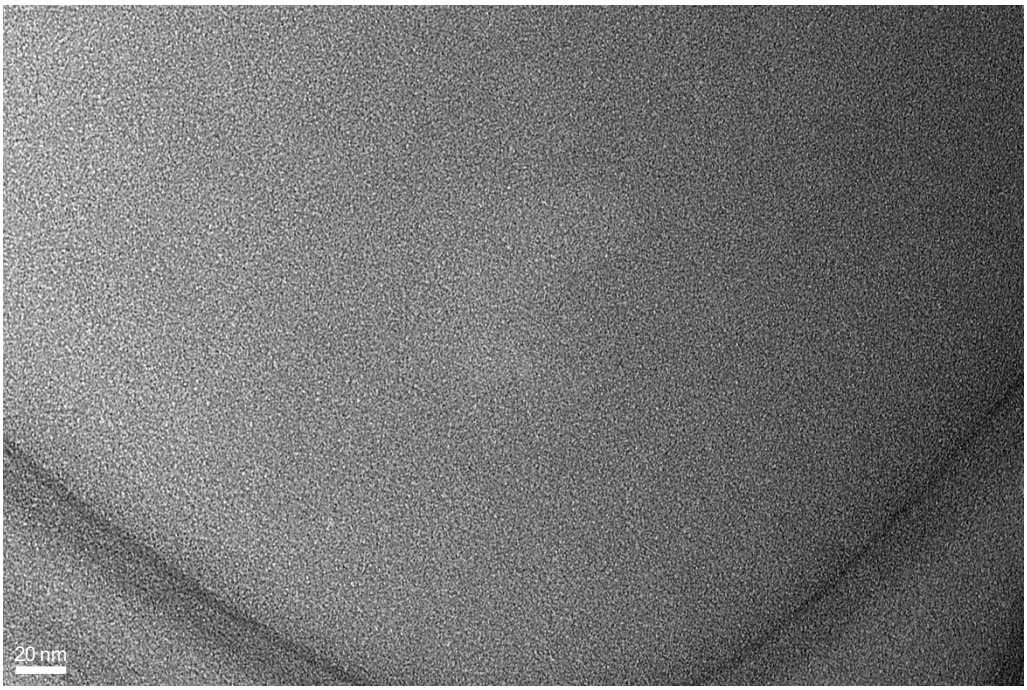

Figure S83. TEM image of **[PEMim][PF$_6$]** after reaction, 1 month in air, condition reaction: Rh(acac)(CO)$_2$ (6.0 mg, 23.3 µmol, 1 equiv), **[PEMIM][PF$_6$]** (ratio N/Rh = 75), Methyl 10-undecenoate (1.325 mL, 5.9 mmol), heptane (10 mL), 80 bar CO/H$_2$ (1:1), 6 h

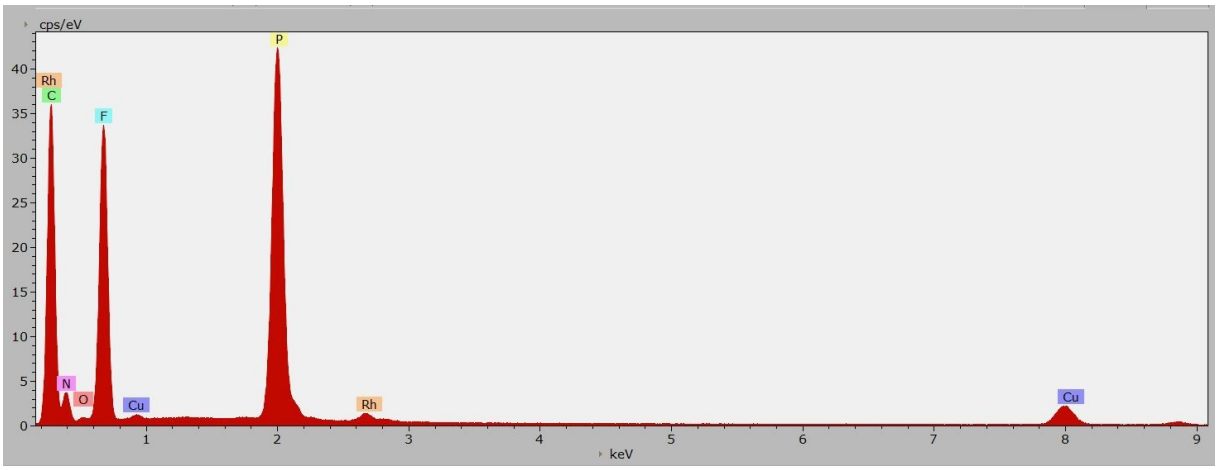

Figure S84. EDX spectrum of **[PEMIM][PF$_6$]** after reaction, 1 month in air, condition reaction: Rh(acac)(CO)$_2$ (6.0 mg, 23.3 µmol, 1 equiv), **[PEMIM][PF$_6$]** (ratio N/Rh = 75), Methyl 10-undecenoate (1.325 mL, 5.9 mmol), heptane (10 mL), 80 bar CO/H$_2$ (1:1), 6 h

IX) Optimization of the reaction conditions

Table S4. Effect of pressure[a]

Entry	Pressure (bar)	Conv.[b] (%)	$Y_{(Ald)}$[c] (%) [l/b][d]	$Y_{(Alc)}$[c] (%) [l/b][e]	$Y_{(Iso)}$[c] (%)	$Y_{(Sat)}$[c] (%)	Global [l/b][f]	Rh leaching (%)
1	**40**	99	32 [1.56]	23 [3.37]	39	5	2.10	2.9
2	**60**	100	27 [0.77]	50 [2.45]	20	3	1.84	3.5
3	**80**	99	20 [0.39]	71 [1.84]	6	2	1.26	5.0

4	**100**	100	19 [0.33]	79 [1.75]	0	2	1.28	2.7

[a] Experimental conditions: $Rh(acac)(CO)_2$ (6.0 mg, 23.3 µmol, 1 eq.), $[PEMIM][PF_6]$ (592 mg, 75 eq.), Methyl 10-undecenoate (1.325 mL, 5.9 mmol), heptane (10 mL), CO/H_2 (1:1), 80°C, 6 h. [b] Methyl 10-undecenoate conversion. [c] $Y_{(X)}$ = yield in (X); (Ald) = aldehydes; (Alc) = alcohols; (Iso) = methyl 10-undecenoate isomers; and (Sat) = saturated compound = methyl undecanoate. [d] Linear to branched ratio for aldehydes. [e] Linear to branched ratio for alcohols. [f] Global linear to branched ratio.

Table S5. Effect of temperature[a]

Entry	Temperature (°C)	Conv.[b] (%)	$Y_{(Ald)}$[c] (%) [l/b][d]	$Y_{(Alc)}$[c] (%) [l/b][e]	$Y_{(Iso)}$[c] (%)	$Y_{(Sat)}$[c] (%)	Global [l/b][f]	Rh leaching (%)
1	**60**	63	29 [1.14]	22 [2.08]	4	8	1.46	3.3
2	**80**	99	20 [0.39]	71 [1.84]	6	2	1.26	5.0
3	**100**	100	37 [0.30]	56 [1.60]	3	4	0.86	12.8
4	**120**	100	70 [0.38]	31 [1.33]	0	0	0.58	5.6
5	**140**	100	81 [0.26]	13 [0.66]	1	5	0.30	18.2

[a] Experimental conditions: $Rh(acac)(CO)_2$ (6.0 mg, 23.3 µmol, 1 equiv), $[PEMIM][PF_6]$ (592 mg, 75 eq.), Methyl 10-undecenoate (1.325 mL, 5.9 mmol), heptane (10 mL), 80 bar CO/H_2 (1:1), 6 h. [b] Methyl 10-undecenoate conversion. [c] $Y_{(X)}$ = yield in (X); (Ald) = aldehydes; (Alc) = alcohols; (Iso) = methyl 10-undecenoate isomers; and (Sat) = saturated compound = methyl undecanoate. [d] Linear to branched ratio for aldehydes. [e] Linear to branched ratio for alcohols. [f] Global linear to branched ratio.

Table S6. CO/H_2 ratio variation[a]

Entry	CO/H_2 Ratio	Conv.[b] (%)	$Y_{(Ald)}$[c] (%) [l/b][d]	$Y_{(Alc)}$[c] (%) [l/b][e]	$Y_{(Iso)}$[c] (%)	$Y_{(Sat)}$[c] (%)	Global [l/b][f]	Rh leaching (%)
1	**01:01**	99	20 [0.39]	71 [1.84]	6	2	1.26	5
2	**01:02**	100	19 [0.89]	61 [2.22]	14	6	1.76	5.6
3	**02 :01**	100	37 [0.82]	47 [2.50]	12	4	1.49	4.5

[a] Experimental conditions: $Rh(acac)(CO)_2$ (6.0 mg, 23.3 µmol, 1 equiv), $[PEMIM][PF_6]$ (592 mg, 75 eq.), Methyl 10-undecenoate (1.325 mL, 5.9 mmol), solvent (10 mL), 80 bar CO/H_2, 80°C, 6 h. [b] Methyl 10-undecenoate conversion. [c] $Y_{(X)}$ = yield in (X); (Ald) = aldehydes; (Alc) = alcohols; (Iso) = methyl 10-undecenoate isomers; and (Sat) = saturated compound = methyl undecanoate. [d] Linear to branched ratio for aldehydes. [e] Linear to branched ratio for alcohols. [f] Global linear to branched rati

Table S7. other variation of ionic liquids[a]

Entry	Ionic liquid	N/Rh	Conv.[b] (%)	$Y_{(Ald)}$[c] (%) [l/b][d]	$Y_{(Alc)}$[c] (%) [l/b][e]	$Y_{(Iso)}$[c] (%)	$Y_{(Sat)}$[c] (%)	Global [l/b][f]	Rh leaching (%)
1	**[PEMim][Tf_2N]**	25	100	61 [1.39]	16 [3.0]	11	12	1.61	10.5
2	**[PEMim][Tf_2N]**	75	95	53 [1.49]	16 [2 .86]	11	15	1.71	3.8
3	**[PEMim][Tf_2N]**	150	76	44 [1.55]	12 [3.30]	11	9	1.79	4.7
4	**[Et_2NEMim][Tf_2N]**	25	94	59 [1.54]	10 [3.25]	11	14	1.70	19.3
5	**[Et_2NEMim][Tf_2N]**	75	95	55 [1.48]	14 [3.10]	12	14	1.70	4.0
6	**[Et_2NEMim][Tf_2N]**	150	100	59 [1.12]	20 [2.80]	11	10	1.39	8.2

7	**[Et_2NEMim][PF_6]**	5	100	61 [1.15]	17 [2.46]	6	16	1.34	45.0
8	**[Et_2NEMim][PF_6]**	25	100	35 [0.58]	56 [1.90]	3	6	1.19	35.2
9	**[Et_2NEMim][PF_6]**	50	100	28 [0.53]	58 [2.14]	8	6	1.34	20.0
10	**[Et_2NEMim][PF_6]**	75	100	23 [0.42]	63 [2.11]	9	6	1.36	7.2
11	**[Et_2NEMim][PF_6]**	150	100	32 [0.63]	54 [2.27]	9	5	1.38	8.5
12	**[Et_2NEMim][PF_6]**	300	100	38 [0.83]	42 [2.55]	10	10	1.45	5.0

[a] Experimental conditions: Rh(acac)$(CO)_2$ (6.0 mg, 23.3 µmol, 1 equiv), ionic liquid (75 eq.), Methyl 10-undecenoate (1.325 mL, 5.9 mmol), heptane (10 mL), CO/H_2 (1:1), 100°C, 6 h. [b] Methyl 10-undecenoate conversion. [c] $Y_{(X)}$ = yield in (X); (Ald) = aldehydes; (Alc) = alcohols; (Iso) = methyl 10-undecenoate isomers; and (Sat) = saturated compound = methyl undecanoate. [d] Linear to branched ratio for aldehydes. [e] Linear to branched ratio for alcohols. [f] Global linear to branched ratio

Table S8. Comparison of ligands with methylated carbene positions[a]

Entry	Ligand	Pressure (Bar)	Conv.[b] (%)	$Y_{(Ald)}$[c] (%) [l/b][d]	$Y_{(Alc)}$[c] (%) [l/b][e]	$Y_{(Iso)}$[c] (%)	$Y_{(Sat)}$[c] (%)	Global [l/b][f]	Rh leaching (%)
1	**[PEMim][PF_6]**	60	100	44 [0.32]	41 [1.59]	7	8	0.73	26.0
2	**[PEMim][PF_6]**	80	100	37 [0.30]	56 [1.60]	3	4	0.86	12.8
3	**[Et_2NEMim][PF_6]**	60	97	31 [0.68]	39 [2.41]	19	8	1.34	8.2
4	**[Et_2NEMim][PF_6]**	80	100	41 [0.37]	49 [2.11]	3	7	1.4	13.0
5	**[Et_2NEDMim][PF_6]**	60	100	50 [0.77]	18 [2.34]	23	9	1.02	17.2
6	**[Et_2NEDMim][PF_6]**	80	100	26 [0.61]	50 [2.14]	14	10	1.37	2.1

[a] Experimental conditions: Rh(acac)$(CO)_2$ (6.0 mg, 23.3 µmol, 1 equiv), ionic liquid (75 eq.), Methyl 10-undecenoate (1.325 mL, 5.9 mmol), heptane (10 mL), CO/H_2 (1:1), 100°C, 6 h. [b] Methyl 10-undecenoate conversion. [c] $Y_{(X)}$ = yield in (X); (Ald) = aldehydes; (Alc) = alcohols; (Iso) = methyl 10-undecenoate isomers; and (Sat) = saturated compound = methyl undecanoate. [d] Linear to branched ratio for aldehydes. [e] Linear to branched ratio for alcohols. [f] Global linear to branched ratio

Table S9. Ionic Liquid Phase Composed of BMIM and [PEMim][PF_6][a]

Entry	[PEMim][PF_6] (eq)	BMIM (eq)	Conv.[b] (%)	$Y_{(Ald)}$[c] (%) [l/b][d]	$Y_{(Alc)}$[c] (%) [l/b][e]	$Y_{(Iso)}$[c] (%)	$Y_{(Sat)}$[c] (%)	Global [l/b][f]	Rh leaching (%)
1	**(-)**	**(-)**	100	96 [1.16]	0 [/]	1	19	1.16	/
2	**(-)**	**75**	99	96 [1.11]	0 [/]	2	1	1.11	72.0
3	**5**	**75**	100	73 [0.89]	22 [2.43]	0	5	1.11	14.1
4	**25**	**75**	100	54 [0.80]	39 [2.46]	3	4	1.25	5.9
5	**75**	**75**	99	42 [0.75]	48 [2.28]	3	6	1.33	5.2
6	**300**	**75**	99	43 [0.88]	43 [2.50]	8	5	1.45	3.7

[a] Experimental conditions: Rh(acac)$(CO)_2$ (6.0 mg, 23.3 µmol, 1 equiv), Methyl 10-undecenoate (1.325 mL, 5.9 mmol), heptane (10 mL), CO/H_2 (1:1), 80°C, 6 h. [b] Methyl 10-undecenoate conversion. [c] $Y_{(X)}$ = yield in (X); (Ald) = aldehydes; (Alc) = alcohols; (Iso) = methyl 10-undecenoate isomers; and (Sat) = saturated compound = methyl undecanoate. [d] Linear to branched ratio for aldehydes. [e] Linear to branched ratio for alcohols. [f] Global linear to branched ratio

To compare our results with those reported in our previous study on rhodium catalyst immobilization using a taurinate salt solubilized in an ionic liquid phase, [1] we investigated the catalytic consequences of diluting [PEMim][PF_6] in [BMIM][PF_6]. Alcohol yield increased with [PEMim][PF_6] loading, reaching a plateau at 75 equivalents towards rhodium, similar to pure IL conditions. Moreover, dilution of the nitrogen-functionalized ionic liquid in [BMIM][PF_6] failed to reduce rhodium leaching, highlighting the limited benefit of IL blending.

Table S10. substrate variation[a]

Entry	Substrate	Conv.[b] (%)	$Y_{(Ald)}$[c] (%)	$Y_{(Alc)}$[c] (%)	$Y_{(Iso)}$[c] (%)	$Y_{(Sat)}$[c] (%)	TOF_{alc} h^{-1}
1	**Methyl 10-undecenoate**	99	20	71	6	2	29
2	**1-decene**	100	70	25	4	0	11
3	**Methyl oleate**	54	44	4	x	6	2
4	**VHOSO**	35	31	0	0	3	/

[a]Experimental conditions: $Rh(acac)(CO)_2$ (6.0 mg, 23.3 µmol, 1 equiv), [PEMIM][PF_6] (592 mg, 75 eq.), substrate (250 equiv.), heptane (10 mL), 80 bar CO/H_2, 80°C, 6 h. [b]substrate conversion. [c]Y(X) = yield in (X); (Ald) = aldehydes; (Alc) = alcohols; (Iso) = isomers; and (Sat) = saturated compound.